

ACTA AGROPHYSICA MONOGRAPHIAE



SURFACE SOIL MOISTURE SATELLITE AND GROUND-BASED MEASUREMENTS

Mateusz Łukowski, Bogusław Usowicz

**Instytut Agrofizyki
im. Bohdana Dobrzańskiego PAN
w Lublinie**

2014 (1)

Redaktor Naczelny – Józef Horabik
Zastępca Redaktora Naczelnego – Grzegorz Józefaciuk
Sekretarz Redakcji – Wanda Woźniak
Redaktor Tematyczny – Jerzy Lipiec
Redaktor Statystyczny – Stanisława Roczkowska-Chmaj
Redaktor Języka Polskiego – Barbara Pietrasiewicz
Redaktor Języka Angielskiego – Tomasz Bylica

Rada Redakcyjna

Dorota Witrowa-Rajchert – Przewodnicząca

Andrey Alekseev, Rosja	Viliam Novák, Słowacja
Tadeusz Filipek, Polska	Josef Pecen, Czechy
Jarosław Frączek, Polska	Pedro Aguado Rodriguez, Hiszpania
Werner Herppich, Niemcy	István Seres, Węgry
Andrzej Lenart, Polska	Stanisław Skonecki, Polska
Janusz Olejnik, Polska	Jerzy Weres, Polska
Leonid Muravsky, Ukraina	Gerd Wessolek, Niemcy

Opiniował do druku:

Bogdan Chojnicki

Adres redakcji

Instytut Agrofizyki im. Bohdana Dobrzańskiego PAN, Wydawnictwo
ul. Doświadczalna 4, 20-290 Lublin, tel. (81) 744-50-61, www.ipan.lublin.pl

Streszczenia i pełne teksty prac dostępne są na stronie internetowej czasopisma
www.acta-agrophysica-monographiae.org

Wersja pierwotna wszystkich zeszytów to wersja drukowana

©Copyright by Instytut Agrofizyki im. Bohdana Dobrzańskiego PAN, Lublin 2014

ISSN 2084-3429, ISBN 978-83-89969-24-8

Acta Agrophysica są do nabycia w dziale Wydawnictw Instytutu Agrofizyki PAN w Lublinie.
Prenumeratę instytucjonalną można zamawiać w dziale Wydawnictw Instytutu Agrofizyki PAN w Lublinie
oraz w oddziałach firmy Kolporter S.A. na terenie całego kraju. Informacje pod numerem infolinii 0801-
205-555 lub na stronie internetowej <http://www.kolporter-spolka-akcyjna.com.pl/prenumerata.asp>

Wydanie I. Nakład 150 egz., ark. 8,2
Skład komputerowy: Wanda Woźniak
Druk: *ALF-GRAF*, ul. Abramowicka 6, 20-391 Lublin

ACKNOWLEDGMENTS

The authors would like to thank Wojciech Marczewski and Jerzy Usowicz for inspirational conversations, valuable advice and comments.

The publication material is based upon research funded by:

1. The National Science Centre (grant No. N N310 734640),
2. The Government of Poland through ESA Contracts under the PECS

(Plan for European Cooperating States):

- 2.1. No. 4000107897/13/NL/KML
“ELBARA_PD (Penetration Depth)”
- 2.2. No.98084 „SWEX-R, Soil Water and
Energy Exchange/Research”



CONTENTS

1. INTRODUCTION	5
2. STUDIED AREAS AND METHODS	8
2.1. Description of spatial phenomena	8
2.2. Semivariogram	10
2.3. Anisotropy	14
2.4. Trend	14
2.5. Cross-semivariogram	16
2.6. Kriging	17
2.7. Co-kriging	19
2.8. Inverse distance weighting	21
2.9. Examined objects, their properties and methods for their determination	22
2.10. Satellite data	25
3. RESULTS AND DISCUSSION	29
3.1. Comparison of soil moisture measured by gravimetric and TDR methods	29
3.2. Analysis of soil moisture and soil parameters in a commune scale	30
3.3. Evaluation of the impact of topography on soil moisture	39
3.4. Temporal analysis of soil moisture from satellite and ground-based measurements	43
3.5. Surface soil moisture assessment using ASAR	68
3.6. Soil moisture assessment using ground measurements and ASAR	75
3.7. The distributions of soil moisture for selected days	79
3.8. Soil moisture assessment using ground-based and SMOS measurements	95
4. CONCLUSIONS	98
5. REFERENCES	99
6. SUMMARY	103
7. SUMMARY IN POLISH (STRESZCZENIE)	105

1. INTRODUCTION

The water contained in the soil is one of the most important components of the environment. Without it any growth or development of plants on land surface would be impossible. Soil moisture is defined as the ratio of the weight of water contained in the soil to the weight of the solid phase or as the ratio of the volume of water in the soil to the total sample volume. Soil moisture governs the partitioning of incoming energy (sun radiation) into the sensible, latent and soil heat fluxes and precipitation, supplying the Earth's surface with water, to infiltrating and running downstreams. The recognition and understanding of temporal changes and spatial distributions of soil moisture are essential to answer many fundamental scientific questions, and then to use this knowledge practically. The application of knowledge about soil moisture is very broad and refers to (Houser 1996):

1. atmosphere dynamics – the moisture content in the soil affects macro-, meso- and micro scale movement of water and air masses in the atmosphere;
2. water resources – soil moisture is an important variable to be considered in the management of water reservoirs, drought assessment, flood forecasting and determination of water balance;
3. agriculture, because crop production, the need for irrigation, and even the presence of plant diseases and parasites are strongly related to the amount of water in the soil where the plants grow;
4. forestry, because the production capacity of tree stand depends on soil moisture, as does the likelihood of fires;
5. civil engineering, due to the effect of water on soil mechanics and assessment of the risk of flooding, which is obligatory before the construction of new real estate;
6. ecosystems modelling, because soil moisture affects many physical, biological and chemical processes;
7. studies of adverse and potentially dangerous phenomena such as erosion, landslides and floods.

Soil moisture affects the dynamics of the circulation of matter and energy in the atmosphere for a very wide range of spatial and temporal scales (Eastman *et al.* 1998, McCumber and Pielke 1981, Ookouchi *et al.* 1984, Zhang and Anthes 1982). A typical spatial dimension termed “large scale”, “global scale” or “macroscale” is 1000 km and a time period longer than one day. In such scale models of the atmosphere dynamics, soil moisture is used as a parameter in the equations describing evapotranspiration and convection (Koster *et al.* 2000). The large variability of soil moisture may increase the volume and duration of energy and mass fluxes fluctuations in the part of the atmosphere nearest to the Earth's surface

(Delworth and Manaba 1993) and also has an impact on the processes of formation of fronts (Castelli and Rodriguez-Iturbe 1995) and cyclones in tropical regions (Dastoor and Krishnamurti 1991).

“The average scale”, “regional scale” or “mesoscale” is a spatial dimension that ranges from 2 to 400 km and the time period shorter than one day. Results from mesoscale numerical models revealed that the uneven spatial distributions of moisture and granulometric composition of soil can cause horizontal movement of mass and energy in the atmosphere (Eastman *et al.* 1998) and even affect the formation of tornados (Chang and Wetzel 1991).

The term “microscale” refers to phenomena described in the spatial scale of less than 3 km and a time period of about an hour. In this scale the effect of soil moisture on the division of the energy flux into the sensible, latent and soil heat fluxes (Kędziora 1995, Stull 1988) becomes apparent. The water content in the soil significantly affects the albedo and the thermal properties of the soil (Usowicz *et al.* 2009). Higher surface soil moisture causes a decrease in albedo that determines the increase of the amount of absorbed solar radiation. Simultaneously, wet soil has a lower temperature than dry soil, which reduces the sensible heat flux, so latent heat flux is increased. These two effects result in a faster transport of water vapour to the atmosphere, which increases the probability of precipitation (Zheng and Eltahir 1998).

Knowledge about soil moisture is very important in the management of water resources, assessment of droughts, and prediction of floods and surface runoffs. Measurements of soil moisture has become the basis for the development of optimal irrigation systems (Connell *et al.* 1999). Soil moisture may determine the probability, frequency, scale and dynamics of flooding (Smith and Karr 1986). Maps of surface soil moisture distribution are used for planning the construction of water reservoirs (Mehrotra 1999), prediction of flood events (Pietroniro *et al.* 1994) and surface runoffs (Mehrotra 1999).

Deficit or excess of water in the soil strongly influence the spatial and temporal dynamics of plants health and development. For this reason, information on soil moisture is important for applications in agriculture, such as determining the time of sowing, irrigation management, crop forecasting and identification of areas exposed to drought or flooding (Green and Erskine 2004, Jaynes *et al.* 2003, McGinn and Shepherd 2003, Odhiambo and Bomke 2007). Intensive crop production is dependent on the availability of water which largely determines the quality of yield through better use of nutrients from the soil. Therefore, information about soil moisture is a very important factor to be taken into account in making decisions, including the most important, global ones (Vermeulen *et al.* 2010).

Although soil moisture is such a significant and desired parameter, its measurement raises many difficulties, especially if it is to be carried out frequently and in macro- or meso scale. Methods for soil moisture measurement can be divided into two categories: direct and indirect methods. The direct methods are based on determining the weight of a given volume of soil sample before and after drying. The drying is usually done at a temperature of 105°C for 48 hours. This is called the gravimetric method and because of its accuracy is treated as a reference for other methods (Usowicz and Kossowski 1996).

Indirect methods, which often are more rapid, are much more numerous. They are based on the measurement of other, easily measurable physical parameters of examined soil, related to the amount of retained water. Such measurements are divided into those carried out *in situ* (ground-based measurements) and contactless, from a distance (remote sensing). *In situ* measurements can be carried out by examining neutron or gamma radiation scattering, and also by determining electrical, dielectric and thermal properties of soils (Robinson *et al.* 2008). Due to the fact that soil moisture can be spatially variable, the ground-based measurements in the meso- or macroscale are often very time-consuming and costly, but relatively precise. Remote sensing of soil moisture is also an indirect method. This type of observation may be carried out from towers, aircraft or from Earth's orbit, using satellites. Those measurements can be passive (receiving natural electromagnetic noise incoming from the soil), active (sending electromagnetic waves in the direction of the Earth's surface and observing their backscattering), or taking into account the Earth's gravity field whose changes follow the movement of huge masses of the water in soil (Robinson *et al.* 2008). The latter method is very accurate, but due to the poor spatial resolution suitable only for the global scale. In contrast, the two methods mentioned first allow one to obtain better spatial resolution and, starting from the eighties of the twentieth century, are still being developed thanks to technological progress and evolution in signal theory (Baup *et al.* 2007, Jackson and Le Vine 1996, Jackson *et al.* 1999, Kerr *et al.* 2001, Schmugge *et al.* 1994). The value of remote sensing methods, superior to the ground techniques, is its spatial continuity. Furthermore, when observations are carried out from satellites or aircraft, the measurements are fast and cover large areas so that consistent results are obtained even when conditions during examination are changing (this may be caused by heavy rain or intensive evaporation). The costs of sending satellites into space are indeed very large, but compensated by the huge amount of systematically delivered data. Therefore, mainly the observations conducted from the Earth's orbit are hoped to be the source of high-quality, spatially and temporally continuous data on soil moisture. But, so far, it is

not possible to obtain soil moisture data from remote sensing electromagnetic methods in a layer thicker than the first 10 cm of the soil surface (Escorihuela *et al.* 2010). It is also still not well explained how to compare data collected at single *in situ* point on the ground with remote sensing measurements covering a whole area. One can perform remote sensing data disaggregation down to point scale or act contrariwise: upscale information obtained from points to the area seen from remote sensing measurements (Hu *et al.* 1998). This raises the scaling problem which can be solved using statistical and geostatistical methods (Pan 2002, Webster and Oliver 1990, Vauclin *et al.* 1983). Going from higher spatial resolution data to a smaller one (and *vice versa*), as well as the interpolation of missing data, may only be performed when the information about the changes in time and the type of spatial distribution of the researched soil moisture field is sufficient. In reality, due to the limited set of data, the needed knowledge is rarely complete. Minimal size of dataset at a given soil moisture estimation error can be determined by means of geostatistical methods, i.e. semivariograms, cross-semivariograms, kriging, co-kriging and cross-validation (Brus 1993, McBratney and Webster 1983, Papritz 1993, Trangmar *et al.* 1985, Webster 1985). These methods also allow one to describe the relationship between the easily-measurable and not-easily-measurable variables. Moreover, they are useful to determine the parameters of spatial dependence and inter-dependence. They are used to acquire maps of the spatial distribution of each examined variable characterising the soil in an optimal manner and at a given estimation error (Griffith 1987, Isaaks and Srivastava 1989, Usowicz *et al.* 1995, Webster and Oliver 1990, Vieira *et al.* 1983).

The main objectives of the study were:

1. Development of a methodology for determining the soil moisture content of the surface layer of soil with the help of satellite data and ground-based measurements.
2. Determination of spatial variability of soil moisture at different scales.
3. Evaluation of the impact of topography, land cover type and soil granulometric composition on the spatial distribution of soil moisture.

2. STUDIED AREAS AND METHODS

2.1. Description of spatial phenomena

Classical statistical methods assume that the analysed observations are independent. Since the majority of the processes observed in the nature are continuous, this assumption introduces a significant limitation for understanding the true nature of the phenomena. Assuming that the tested dataset consists only of ran-

dom values, valuable information about the location of occurrence of examined features is completely lost and wasted. However, there is a branch of statistics, called geostatistics, which is the study of random events, but taking into account the place in space which they occur. Geostatistics uses the idea of so-called regionalised variable, on which the mathematical apparatus of this tool is built (Brus 1993, Matheron 1971, McBratney and Webster 1983, Papritz 1993, Zawadzki 2011). This type of variable combines (local) random aspects, while taking into account the correlations associated with the spatial distribution of the data (globally). That is why it is said that regionalised variables have properties intermediate between random variables and deterministic variables (Zawadzki 2011). Geostatistics improves the interpretation of the spatial distribution of examined data by determining how much of the variability comes from the error or the imperfection of chosen method of analysis, and how much from the existence of spatial correlation between the measuring points. It also defines the spatial correlation length and allows modelling mathematically the variability of the tested feature.

In the natural environment, the spatial distributions of examined features are continuous. But for technical and mathematical reasons, it is not possible to study these characteristics by taking samples in an infinitely dense measuring grid. Sometimes, for various reasons, the individual measurements are far from one another. Hence, knowledge about the processes and properties of studied objects is inherently fragmented and limited to specific areas or sites from which samples were taken. It is not known what happens between the measuring points, but by using geostatistical methods it is possible to estimate the point data to continuous distributions and inference of the areas that are not represented by any measurement (David 1977, Haan 1977, Isaaks and Srivastava 1989, Matheron 1971, Trangmar *et al.* 1985). Another very valuable advantage of this method is the ability to capture precise designation of the estimation error, together with its spatial distribution. Such information can be used for effective planning of measurement grid, through a kind of feedback, generally shown in the Pannatier diagram (Fig.1) (Pannatier 1994). This diagram shows the general relationship between the observations and the process of modeling of semivariogram (fundamental function calculated in geostatistics) and the impact of the models on the way to measure reality, all assuming a stationary process.

Geostatistics, due to its unique properties, has been used in a wide range of fields in which it is necessary to study spatial phenomena: crisis management, meteorology, mining, geology, hydrology, agriculture, forestry, soil studies, biology, civil engineering, power industry, and even economics and sociology.

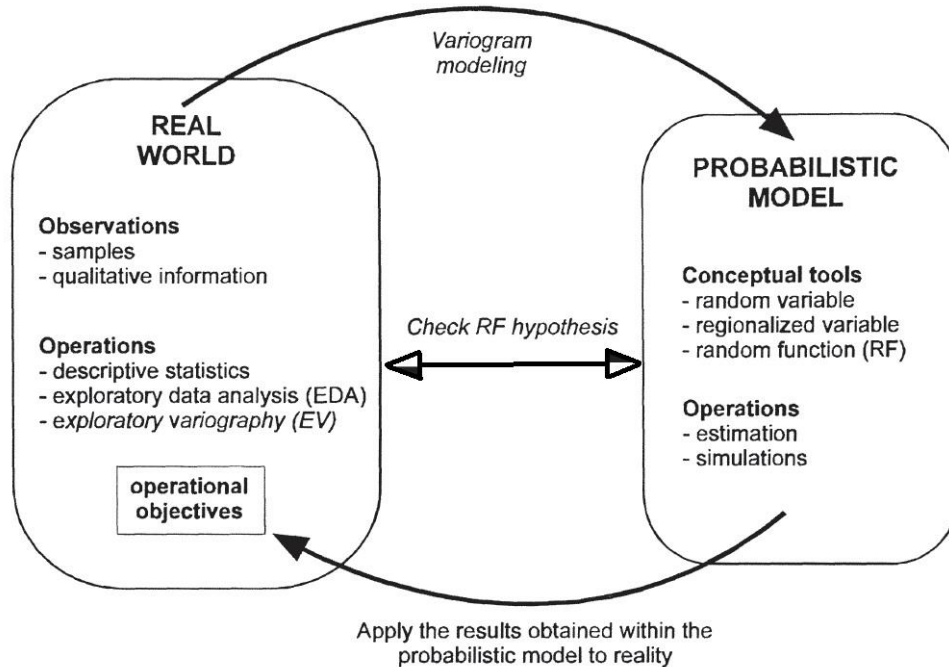


Fig. 1. Concept of geostatistical modelling introduced by Pannatier (Pannatier 1994)

The basic statistical concepts used during the data examination in this research are described below.

2.2. Semivariogram

The fundamental principle of geostatistics is the theorem that next to the point in space, to which a specified value of the tested feature is assigned, there exist other, similar points, i.e. with similar values of that feature, and therefore correlated (Webster and Oliver 1990). This theorem has been confirmed by many observations of the natural environment. The basic function which allows to describe this phenomenon is the semivariogram function which is equal to a half of the expected difference of the value of the regionalised variable $Z(x)$ in point x and value $Z(x+h)$ at a point distant from it by separation vector h . Semivariogram (sometimes abbreviated “variogram”) shows the behaviour of the regionalised variable in space or time. Regionalised variable variogram analyses are conducted to give the measure and the structure identification of its variability. There are three phases of analysis:

1. Studies on collected dataset and calculation of descriptive statistics.
2. Calculation of the empirical variogram of regionalised variable.
3. Adjusting mathematical model to the empirical variogram.

The analysis requires information of the first two statistical moments of random functions assigned to the examined phenomena (Brus 1993, Pannatier 1994, Papritz 1993, Vieira *et al.* 1983):

- mean value $m(x)$

$$E[Z(x)] = m(x), \quad (1)$$

- variance

$$Var\{Z(x)\} = E\{[Z(x) - m(x)]^2\}. \quad (2)$$

If regionalised variables $Z(x_1)$, $Z(x_2)$ have variance, they also have covariance which is a function of locations x_1 , x_2 :

$$C(x_1, x_2) = E\{[Z(x_1) - m(x_1)] \cdot [Z(x_2) - m(x_2)]\} = E\{Z(x_1) \cdot Z(x_2)\} - m(x_1) \cdot m(x_2) \quad (3)$$

Semivariogram $\gamma(x_1, x_2)$ is defined as a half of the variance of the two regionalised variables difference (Pannatier 1994, Webster 1985):

$$\gamma(x_1, x_2) = \frac{1}{2} Var\{Z(x_1) - Z(x_2)\}. \quad (4)$$

In geostatistical analysis, it is expected that the tested process is ergodic, i.e. expected value of regionalised variable is equal to its average value calculated over the area whose surface tends to infinity. It is also required for the examined process to be stationary, i.e. invariant with respect to any vector displacement. In the case of fulfillment of the condition of ergodicity and stationarity, random function $Z(x)$ is defined as a second-order stationary. Furthermore, it is expected that (Pannatier 1994):

- mean value exists and does not depend on the location x

$$E[Z(x)] = m, \quad \forall x; \quad (5)$$

- for each pair of random variables $\{Z(x), Z(x+h)\}$ covariance exists and depends only on the separation vector h , is independent on the location x

$$C(h) = E\{Z(x+h) \cdot Z(x)\} - m^2, \quad \forall x; \quad (6)$$

– covariance stationarity implies stationarity of variance and semivariogram:

$$\text{Var}\{Z(x)\} = E\{[Z(x) - m]^2\} = C(0) \quad \forall x. \quad (7)$$

It can be shown that there is a link between the covariance and semivariogram (Pannatier 1994):

$$\begin{aligned} 2C(h) &= 2E\{Z(x+h) \cdot Z(x)\} - 2m^2 = [E\{Z(x+h)^2\} - m^2] + [E\{Z(x)^2\} - m^2] \\ &\quad - [E\{Z(x+h)^2\} - 2E\{Z(x+h) \cdot Z(x)\} + E\{Z(x)^2\}] \\ 2C(h) &= 2C(0) - 2\gamma(h) \\ C(h) &= C(0) - \gamma(h) \end{aligned} \quad (8)$$

and for all separation vectors h difference $Z(x+h) - Z(x)$ has a finite variance, and does not depend on x :

$$\gamma(h) = \frac{1}{2} \text{Var}\{Z(x+h) - Z(x)\} = \frac{1}{2} E\{[Z(x+h) - Z(x)]^2\}, \quad \forall x. \quad (9)$$

When the length of the separation vector h is zero, the value of semivariance is also equal to zero.

Semivariogram is symmetrical, independent of the direction of separation vector h :

$$\gamma(h) = \gamma(-h). \quad (10)$$

The experimental semivariogram $\gamma(h)$ for the separation vector h is calculated according to the formula (Pannatier 1994, Webster 1985):

$$\gamma(h) = \frac{1}{2N(h)} \sum_{i=1}^{N(h)} [z(x_i) - z(x_i + h)]^2 \quad (11)$$

where $N(h)$ is the number of pairs of points distant from each other by $|h|$. Equation (11) expresses the differentiation of deviations of the analysed variable, depending on the distance between points $z(x_i+h)$ and $z(x_i)$. There are three characteristic parameters of the semivariogram: nugget C_0 , sill $C+C_0$ and range A_0 . C is the so-called “structural variance”, determining the variability associated with the location of the sample. If semivariogram is a function increasing not from zero

but from a certain value, this value is called “nugget”. It expresses the existing variability of the tested feature in a scale smaller than the sampling interval. Nugget effect may appear also due to measurement uncertainty or too sparse sampling. Semivariogram value at which there is no further function increase (“saturation”) is called “sill”, and is approximately equal to the variance of the sample. The length of separation vector at which the semivariogram reaches a sill is called “range”. Range is equal to the longest distance at which the samples are correlated together.

To semivariograms determined from empirical data, mathematical models can be adjusted (Gamma Design 2008, Pannatier 1994, Zawadzki 2011), for example:

1. Model of pure nugget effect, where the empirical semivariogram is described by the equation

$$\gamma(h) = C_0. \quad (12)$$

In this model, the spatial relationship between the values of the samples does not exist because the sill is equal to the nugget. Next models also take into account the value of the nugget.

2. The linear model, in which the empirical semivariogram is approximated by the equation

$$\gamma(h) = C_0 + \left[|h| \left(\frac{C}{A_0} \right) \right] \quad (13)$$

In the linear model semivariogram never saturates, so it is assumed that the range of spatial correlations of the investigated variables is equal to the maximum distance between samples.

3. The spherical model, described by the equation:

$$\gamma(h) = \begin{cases} C_0 + C \cdot \left[1.5 \frac{|h|}{A_0} - 0.5 \left(\frac{|h|}{A_0} \right)^3 \right] & |h| \leq A_0 \\ C_0 + C & |h| > A_0 \end{cases} \quad (14)$$

The range of spatial relationships is equal to the distance beyond which the samples are no longer correlated.

4. The exponential model:

$$\gamma(h) = C_0 + C \cdot \left[1 - e^{-\frac{|h|}{A_0}} \right] \quad |h| > 0 \quad (15)$$

In the exponential model, the semivariance reaches the sill asymptotically in infinity. Therefore, in determining the length of spatial relationships the so-called “apparent range” is applied, $A = 3A_0$. It is the distance for which the semivariogram reaches 95% of asymptotical sill in infinity.

5. The Gaussian model is the only one whose chart has the inflection point. It is expressed by the formula:

$$\gamma(h) = C_0 + C \cdot \left[1 - e^{-\frac{|h|^2}{A_0^2}} \right] \quad |h| > 0 \quad (16)$$

Gaussian model has an apparent range $A = 3^{0.5}A_0$.

Adjusting the models to empirical data is done by minimising the sum of squared deviations, so-called “residual variance”:

$$RSS = \frac{\sum_{i=1}^n [\gamma_{\text{exp}}(h) - \gamma_{\text{mod}}(h)]^2}{n - k} \quad (17)$$

where $\gamma_{\text{exp}}(h)$ is the experimental semivariance for the separation vector h , $\gamma_{\text{mod}}(h)$ is semivariance obtained from the model, n is the number of samples and k is the number of estimated parameters.

2.3. Anisotropy

In the two-dimensional data field it is often the case that the shape of semivariogram depends on the selected spatial direction of analysis (Isaaks and Srivastava 1989). This is because the distribution of tested feature is generally non-homogeneous, anisotropic. The sill, range and even model that describe the directional empirical semivariogram may depend on chosen direction (Zawadzki 2011). Description of the studied phenomena by a series of direction-dependent semivariograms is impractical and it is better to replace it with a single model which takes into account the anisotropy. The easiest way to do this is selecting the primary axis of analysis along the direction of the smallest anisotropy i.e. the line along which the average semivariance is the smallest (Gamma Design 2008).

2.4. Trend

Sometimes the regionalised variable does not fulfil the assumption of stationarity. This may be because of phenomenon called “trend” (sometimes used inter-

changeably with the term “drift”) which reflects the fundamental characteristics of the physical environment. This may be a systematic change with altitude, vegetation or soil type. Regionalised variable can then be represented as the sum of the two components:

$$z(x) = \varepsilon(x) + m(x), \quad (18)$$

where $\varepsilon(x)$ is a random component which includes also the error, while $m(x)$ is an essential structural component which is supposed to reflect large-scale variability of the examined phenomenon – the trend. The individual components, random and trend, need to undergo decomposition, be identified and separated (Gotway and Hergert 1997, Webster 1985). For the one-dimensional case the equations of trend may be as follows:

$$\begin{aligned} m(x) &= a_0 \\ m(x) &= a_0 + a_1x \\ m(x) &= a_0 + a_1x + a_2x^2 \end{aligned} \quad (19)$$

If there is a surface (x, y) trend, its equations may be as follows:

$$\begin{aligned} m(x, y) &= a_0 \\ m(x, y) &= ax + by + c \\ m(x, y) &= ax^2 + by^2 + cxy + dx + ey + f \end{aligned} \quad (20)$$

Separation of trend is a non-trivial task, because it is often difficult to distinguish how much of the variance comes from the random component and how much from the trend. Therefore, the equations of trend are polynomials rarely higher than the third degree. After separation of the trend only random component should remain, with zero mean value and finite variance, satisfying the condition of ergodicity and stationarity, for which the calculated semivariogram is:

$$\gamma(h) = \frac{1}{2N(h)} \sum_{i=1}^{N(h)} [\varepsilon(x_i) - \varepsilon(x_i + h)]^2, \quad (21)$$

where $N(h)$ is the number of pairs of points distant from each other by $|h|$. Equation (21) expresses differentiation of deviations of the variable $\varepsilon(x_i)$ from trend, depending on the distance equal to $|h|$ between the measurement points.

2.5. Cross-semivariogram

Regionalised variables can be assigned to different physical properties, and if the samples were taken from the same area it is often found that their features are correlated. The assumption of the second order stationarity allows one to characterise the values of variables Z_1 and Z_2 by means of cross-covariance defined as (Webster 1985, Vieira *et al.* 1983):

$$C_{12}(h) = E\{Z_1(x) \cdot Z_2(x+h)\} - m_1 m_2 \quad (22)$$

and by

$$C_{21}(h) = E\{Z_2(x) \cdot Z_1(x+h)\} - m_1 m_2 \quad (23)$$

and cross-semivariogram defined as:

$$\gamma_{12}(h) = \gamma_{21}(h) = \frac{1}{2} E\{[Z_1(x+h) - Z_1(x)] \cdot [Z_2(x+h) - Z_2(x)]\}, \quad \forall x \quad (24)$$

where m_1 and m_2 are the expected values of $E\{Z_1(x)\}$ and $E\{Z_2(x)\}$. Then the cross-semivariogram can be written as:

$$2\gamma_{12}(h) = 2\gamma_{21}(h) = 2C_{12}(0) - C_{12}(h) - C_{21}(h). \quad (25)$$

Empirical cross-semivariogram for the separation vector h is calculated from the equation:

$$\gamma_{12}(h) = \frac{1}{2N(h)} \sum_{i=1}^{N(h)} [z_1(x_i) - z_1(x_i+h)] \cdot [z_2(x_i) - z_2(x_i+h)], \quad (26)$$

where $N(h)$ is the number of pairs of points distant by $|h|$ for the first and second variable – $[z_1(x_i), z_1(x_i+h)]$ and $[z_2(x_i), z_2(x_i+h)]$. Calculation of the cross-semivariogram does not require an equal number of z_1 and z_2 variables. Similarly as in the semivariogram, there are three basic parameters of the cross-semivariogram: nugget, sill and range of the correlation. For the empirical cross-semivariograms also the mathematical models are fitted and then the quality of fitting is checked.

Obtained semivariograms and cross-semivariogram functions are used for spatial and temporal autocorrelation analysis or to visualise regionalised variable by estimation, e.g. by means of kriging or co-kriging methods (Englund and Sparks 1988, Gamma Design 2008, Pannatier 1994).

2.6. Kriging

Spatial phenomena occurring in the natural environment often have continuous distributions. On the other hand, for practical reasons the field measurements carried out in order to know the studied features are discrete point measurements, and therefore do not cover the entire studied area. Because of that, to obtain reliable spatial distributions of the investigated features interpolation methods are often used. The information gathered at the measuring points is used to estimate the value of a given feature in areas where no measurement was made, and at the same time the approximation error is minimised. Such estimation can be carried out by the method of kriging. This method gives the best, unbiased estimator of the tested regionalised variable $Z(x)$. Using this method one also obtains the minimum variance of the deviations of estimated values from measured values. Kriging variance depends on the position of samples versus the location in which values are to be estimated, weights assigned to samples and the semivariogram model parameters. Kriging estimator is a linear equation expressed by formula (Webster 1985):

$$z^{\bullet}(x_o) = \sum_{i=1}^N \lambda_i z(x_i), \quad (27)$$

where $z^{\bullet}(x_o)$ is the estimated value at the point of estimation x_o , N is the number of measurements, $z(x_i)$ is value measured at a point x_i and λ_i are weights. If $z(x_i)$ is a realisation of the random function $Z(x_i)$ then the estimator of random function can be written as:

$$Z^{\bullet}(x_o) = \sum_{i=1}^N \lambda_i Z(x_i). \quad (28)$$

Weights λ_i assigned to corresponding points x_i are called ‘‘coefficients of kriging’’. Their values change according to the nature of the phenomena spatial variations, which is expressed by values of estimated feature. Weights are chosen so that the mean squared error is minimal. This error is called the kriging variance σ_k^2 and can be calculated for each sampling method and each configuration of the estimation area. The main problem in determining the random function is to find weights λ_i . They are determined from the system of equations containing the condition of unbiasedness of the estimator:

$$E\{Z^{\bullet}(x_o) - Z(x_o)\} = 0 \quad (29)$$

and its effectiveness:

$$\sigma_k^2(x_o) = \text{Var}\{Z^{\bullet}(x_o) - Z(x_o)\} = \min . \quad (30)$$

$Z(x_o)$ is the realization of the random function at the point x_o .

From the condition of unbiasedness of the estimator it can be obtained:

$$E\{Z^*(x_o) - Z(x_o)\} = \sum_i \lambda_i E\{Z(x_i)\} - E\{Z(x_o)\} = m \sum_i \lambda_i - m = 0. \quad (31)$$

As can be seen from the above equation, the expected value is equal to zero if:

$$\sum_{i=1}^N \lambda_i = 1. \quad (32)$$

Substituting the variance with the estimator of the random function it can be shown that:

$$\sigma_k^2(x_o) = \sum_i \sum_j \lambda_i \lambda_j C(x_i, x_j) + C(0) - 2 \sum_i \lambda_i C(x_i, x_o) \quad (33)$$

or (through the semivariance):

$$\sigma_k^2(x_o) = - \sum_i \sum_j \lambda_i \lambda_j \gamma(x_i, x_j) + 2 \sum_i \lambda_i \gamma(x_i, x_o). \quad (34)$$

Variance minimisation can be performed using the technique of Lagrange multipliers. Then the N partial derivatives are equal to zero:

$$\frac{\partial \left[\sigma_k^2(x_o) - 2\mu \sum_i \lambda_i \right]}{\partial \lambda_i} = 0, \quad (35)$$

where μ is Lagrange multiplier. After differentiating and simplifying:

$$-2 \sum_j \lambda_j \gamma(x_i, x_j) + 2\gamma(x_i, x_o) - 2\mu = 0. \quad (36)$$

Taking into account the condition of the sum of the kriging weights one gets the system of equations:

$$\begin{cases} \sum_{j=1}^N \lambda_j \gamma(x_i, x_j) + \mu = \gamma(x_i, x_o) & i=1 \dots N \\ \sum_{i=1}^N \lambda_i = 1 \end{cases} \quad (37)$$

After solving the above system of equations a set of kriging weights $\{\lambda_i\}$ is obtained. These weights allow one to determine the estimated random function Z^* and its variance from the formula:

$$\sigma_k^2(x_o) = \mu + \sum_{i=1}^N \lambda_i \gamma(x_i, x_o). \quad (38)$$

2.7. Co-kriging

Areas of the natural environment can be described by sets of variables related to the individual characteristics of examined features. It often happens that these variables are correlated. Using the information about the mutual relation of examined features one can improve the quality of one variable interpolation using data from measurements of another variable. This is especially useful if one wants to estimate a rarely sampled feature (e.g. due to high cost of analysis) with the aid of a correlated, densely sampled, easily measurable parameter. One of the methods allowing achieving it is the co-kriging method (Webster 1985, Vauclin *et al.* 1983). It involves determining, for certain sets of parameters Z_1 and Z_2 : covariance, cross-covariance and the function of so-called cross-semivariogram. The mathematical basis for co-kriging is the claim of a linear relationship between unknown estimator $Z_2^*(x_o)$ and correlated Z_1 and Z_2 (Webster 1985, Vauclin *et al.* 1983):

$$Z_2^*(x_o) = \sum_{i=1}^{N_1} \lambda_{1i} Z_1(x_{1i}) + \sum_{j=1}^{N_2} \lambda_{2j} Z_2(x_{2ij}), \quad (39)$$

where λ_{1i} and λ_{2j} are weights corresponding to Z_1 and Z_2 , respectively, N_1 and N_2 are numbers of neighbours included in the estimation at the point x_o . As before, the co-kriging weights are determined from the system of equations taking into account the condition of unbiasedness of the estimator:

$$E\{Z_2^*(x_o) - Z_2(x_o)\} = 0 \quad (40)$$

and its effectiveness:

$$\sigma_k^2(x_o) = \text{Var}\{Z_2^*(x_o) - Z_2(x_o)\} = \min. \quad (41)$$

Substituting expected value with the estimate of the weighted average it can be obtained:

$$\begin{aligned}
E\{Z_2^*(x_o) - Z_2(x_o)\} &= \sum_{i=1}^{N_1} \lambda_{1i} E\{Z_1(x_{1i})\} + \sum_{j=1}^{N_2} \lambda_{2j} E\{Z_2(x_{2ij})\} - E\{Z_2(x_o)\} \\
&= m_1 \sum_i \lambda_{1i} + m_2 \sum_j \lambda_{2j} - m_2 = 0
\end{aligned} \quad (42)$$

From the above equation it can be concluded that the expected value is zero when:

$$\sum_{i=1}^{N_1} \lambda_{1i} = 0 \text{ and } \sum_{j=1}^{N_2} \lambda_{2j} = 1. \quad (43)$$

After substituting to the variance:

$$\sigma_{ck}^2(x_o) = E\{Z_2^{*2}(x_o)\} + E\{Z_2^2(x_o)\} - 2E\{Z_2^*(x_o)Z_2(x_o)\}. \quad (44)$$

Substituting the variance with the random function estimator it can be shown (Vauclin *et al.* 1983) that

$$\begin{aligned}
\sigma_{ck}^2(x_o) &= \sum_i \sum_k \lambda_{1i} \lambda_{1k} C_{11}(x_{1i}, x_{1k}) + \sum_i \sum_l \lambda_{1i} \lambda_{2l} C_{12}(x_{1i}, x_{2l}) \\
&+ \sum_j \sum_k \lambda_{2j} \lambda_{1k} C_{21}(x_{2j}, x_{1k}) + \sum_j \sum_l \lambda_{2j} \lambda_{2l} C_{22}(x_{2j}, x_{2l}) \\
&- 2 \sum_k \lambda_{1k} C_{21}(x_o, x_{1k}) - 2 \sum_l \lambda_{2l} C_{22}(x_o, x_{2l}) + C_{22}(0)
\end{aligned} \quad (45)$$

Variance minimisation can be performed using the technique of Lagrange multipliers, in a similar way as previously:

$$\frac{\partial \left[\sigma_{ck}^2(x_o) - 2\mu_2 \sum_l \lambda_{2l} \right]}{\partial \lambda_{2l}} = 0, \quad (46)$$

$$\frac{\partial \left[\sigma_{ck}^2(x_o) - 2\mu_1 \sum_k \lambda_{1k} \right]}{\partial \lambda_{1k}} = 0, \quad (47)$$

where μ_1 and μ_2 are the Lagrange multipliers. After differentiating and simplifying the equations and taking into account the condition on the sum of the co-kriging weights, the system of equations is as follows:

$$\begin{cases} \sum_{i=1}^{N_1} \lambda_{1i} C_{11}(x_{1i}, x_{1k}) + \sum_{j=1}^{N_2} \lambda_{2j} C_{12}(x_{1k}, x_{2j}) - \mu_1 = C_{21}(x_o, x_{1k}) & k = 1, N_1 \\ \sum_{i=1}^{N_1} \lambda_{1i} C_{21}(x_{2l}, x_{1i}) + \sum_{j=1}^{N_2} \lambda_{2j} C_{22}(x_{2j}, x_{2l}) - \mu_2 = C_{22}(x_o, x_{2l}) & l = 1, N_2 \\ \sum_{i=1}^{N_1} \lambda_{1i} = 0 \\ \sum_{j=1}^{N_2} \lambda_{2j} = 1 \end{cases} \quad (48)$$

Solving the above system of equations it is possible to determine the co-kriging weights λ_i . These weights also allow one to determine the estimated random function Z_2^* and its variance:

$$\sigma_{ck}^2(x_o) = C_{22}(0) + \mu - \sum_{i=1}^{N_1} \lambda_{1i} C_{21}(x_o, x_{1i}) - \sum_{j=1}^{N_2} \lambda_{2j} C_{22}(x_{2j}, x_o). \quad (49)$$

2.8. Inverse distance weighting

Estimating the value of tested feature in places where no samples were taken can be also performed using the inverse distance weighting method (IDW). The method is based on interpolation using the weighted average. A limited number of neighbours around the interpolated point is included. The average includes data with weights inversely proportional to the distance from the interpolated point, raised to the appropriate power. IDW interpolation method is given as (Zawadzki 2011):

$$z^*(x_0) = \frac{\sum_{i=1}^N \frac{z(x_i)}{(h_{i0} + s)^p}}{\sum_{i=1}^N \frac{1}{(h_{i0} + s)^p}}, \quad (50)$$

where $z^{\bullet}(x_0)$ – the value estimated at point x_0 , N is the number of measurements, $z(x_i)$ – the measured value at point x_i , h_{i0} – distance from point x_i to point x_0 , s – “smoothing” factor, p – weight exponent. Smoothing coefficient is greater than 0, and the weight exponent takes the values from 1 to 5. Inverse distance method may be a good estimator for the case where the kriging equations become unstable.

2.9. Examined objects, their properties and methods for their determination

The main study of soil parameters was focused on two areas of approximately 140 km² each. The first area covers mineral soils of Southern Podlasie region and was located in the Trzebieszów commune (N 51°59' E 22°33'). The second area was located in the West Polesie region (N 51°23' E 23°11') in Urszulin commune and Hańsk commune. It covers humid, organo-mineral soils. Measurements of soil moisture on these objects (in the 0-10 cm layer) was performed using a moisture, salinity and temperature meter (TDR) produced by Easy Test Lublin. The principle of TDR (Malicki 1990) is based on the measurement of propagation velocity of electromagnetic wave in the tested medium (soil). The velocity is equal to the ratio of the speed of light in vacuum to the square root of the dielectric constant of tested medium. The dielectric constant of the soil depends mainly on the water content per unit volume of soil, and can be described with sufficient accuracy by third order polynomial (Topp *et al.* 1980). In practice, the measurement of soil moisture using TDR comes down to measuring the time required for the passage of an electromagnetic wave from the moment it enters the soil (where first reflection of wave occurs) along the needle probe immersed in the soil, on the end of which the wave is reflected a second time. Then the measured propagation time of the wave is converted to the volume of water per unit volume of soil (soil moisture). TDR probe consists of two steel rods with a length of 10 cm and spacing of 1.6 cm. The device measures the moisture content in the (theoretical) range of 0-100% with an accuracy $\pm 2\%$ and resolution 0.1%. Time of measurement is less than 10 seconds.

Measurements of soil moisture and soil bulk density of the examined areas were also conducted using the gravimetric method. Moreover, from the depth of 0-10 cm, soil samples were collected into plastic bags for the determination of soil particle size distribution.

The number of measurements and density of sampling were chosen depending on the size of the tested areas, the spatial variability of the analysed properties, the difficulty of measurements and the requirements of geostatistical analysis.

All the spatial coordinates were determined using the Global Positioning System (GPS) according to WGS-84 datum, with an accuracy of 1 to 5 m. Because of the diversity, the exact position of the measurement points is shown in the discussion of particular studies in the section “Results and Discussion” of this work.

To determine the surface soil moisture for the years 2010 and 2011 data from a network of agrometeorological automatic stations belonging to the Institute of Agrophysics, Polish Academy of Sciences (IA PAS), were used. The network was established in 2007-2010 and covers the eastern part of Poland (Fig. 2). All stations are located on small, experimental fields with systematically mowed grass. The wider surroundings of stations are very diverse: Białowieża and Janów stations are located in the direct proximity of large forest complexes. Biebrza station is located on a small sandy hill, surrounded by one of the largest wetland areas in Europe. Around the Urszulin station soil also contains a lot of sand, and like the Biebrza station is located in a swamp. Stations Cicibór, Trzebieszów and Majdanek are surrounded by cultivated fields and meadows, but the area around the station Majdanek is distinctly pleated. Felin station is located near the Institute of Agrophysics PAS, close to a cultivated field, on land administratively belonging to the city of Lublin. Wigry station is located on a hill with sandy soil in the direct vicinity of large forests and lakes. The stations measure air temperature and relative humidity, solar radiation balance components, evaporation, wind speed and direction, soil moisture, soil temperature, rainfall, soil water potential and photosynthetic radiation. In the study data from the shallowest soil moisture sensors were used. Stations Białowieża, Biebrza, Trzebieszów and Wigry have such sensors placed at a depth of 10 cm, the other stations closer to the surface, at a depth of 5 cm. The measuring instruments come from companies Easy Test (TDR in station Felin) and Delta-T (Theta Probe and PR2 instruments on other stations). From the depth of 0-10cm, in the nearest neighbourhood the stations' soil moisture sensors, soil samples were taken for the determination of the content of each of the particle size fractions of the soil. Rainfall data collected by rain gauges, installed in the majority of the stations, were also used.

The exact geographical locations of the stations, as well as more detailed information about the particle size distributions of the soils in which the moisture sensors are placed, are shown in the section "Results and Discussion" of the work.

Particle size distribution of the soils for examined areas in Polesie, Podlasie and around the automatic stations was determined by sieving and sedimentation methods. In the research the Bouyoucos sedimentation method with the modification of Casagrande and Prószyński was used. Taking into account the sieve analysis and division into the specific granulometric fractions of soil grains, the particle size distribution of the examined soils was shown according to recommended standards (listed in "References: Norms and standards"). Literature data on the distribution of sand and clay fractions for the whole area of Poland were also used (Marczewski *et al.* 2010).



Fig. 2. Network of automatic agrometeorological stations (top panel) belonging to the Institute of Agrophysics in Lublin (background: Zumi Map (Zumi 2012)) and exemplary station in Janów (bottom panel)

All data used in the study are limited to the surface layer of soil (0-10 cm) because, as described in literature (ASAR 2007, Escorihuela *et al.* 2010, McNairn and Brisco 2004), also devices installed on satellites are not able to perform the measurement deeper in the soil.

2.10. Satellite data

In the research data from the ENVISAT satellite and SMOS satellite were used. Depending on the context, fragments of satellite images covering a single cultivated field, commune, district, part or all of Polish territory were examined. The exact locations of the analysed areas are described in the discussion of particular studies in the section “Results and Discussion”.

The ENVISAT satellite was launched in 2002 by the European Space Agency. It is very large and weighs about 8 tons. It is equipped with 10 measuring instruments:

1. ASAR – Advanced Synthetic Aperture Radar,
2. MERIS – MEdium Resolution Imaging Spectrometer,
3. AATSR – Advanced Along Track Scanning Radiometer,
4. RA-2 – Radar Altimeter,
5. MWR – MicroWave Radiometer,
6. GOMOS – Global Ozone Monitoring by Occultation of Stars,
7. MIPAS – Michelson Interferometer for Passive Atmospheric Sounding,
8. SCIAMACHY – SCanning Imaging Absorption spectroMETER for Atmospheric CHartographY,
9. DORIS – Doppler Orbitography and Radiopositioning Integrated by Satellite,
10. LRR – Laser Retro-Reflector.

Such a broad spectrum of applications for environmental studies influenced the name of the satellite: ENVIronmental SATellite. In this research data from ASAR and MERIS instruments were used.

ASAR (Advanced Synthetic Aperture Radar) operates in the C-band (ENVISAT-ASAR 2007). Radar sends towards the Earth's surface a polarised electromagnetic wave with a frequency of 5.331 GHz and receives its reflection and/or scattering. The measure of the returning wave power is called backscatter coefficient σ° , most often expressed in units of decibel. Thanks to properly selected frequency, this coefficient is sensitive to the surface soil moisture up to a depth of 5 cm (McNairn and Brisco 2004) and to tiny changes of the surface called micro-relief or roughness. At the same time, the impact of the vegetation layer, often present on the tested area, is minimised (Ulaby *et al.* 1978, Ulaby *et al.* 1979). The electromagnetic wave sent by the radar can be polarised in the vertical (V) or

horizontal (H) direction. The received wave is also divided into horizontal (H) and vertical (V) polarisation components. This way of operating is reflected by the convention of backscatter coefficient marking. σ_{HH}^0 is a coefficient for waves sent and received horizontally. σ_{VV}^0 is a coefficient for waves sent and received vertically, while σ_{HV}^0 is a backscatter coefficient for waves sent vertically and received in horizontal polarisation. Unfortunately, ASAR never measures all three coefficients at the same time. Its maximum resolution is 30 m, i.e. readings from the radar antenna are placed on a grid consisting of homogeneous areas called pixels with dimensions of approximately 30×30 meters. The radar beam is not transmitted vertically down towards the Earth's surface, but at an acute angle. Among others, because of this, radar data requires geographic coordinates correction. This process is called geolocation. Radar measurements are not sensitive to the lack of solar lighting, clouds or fog. This independence from the weather and time of day enables to observe Earth's surface as often as it is allowed by the presence of the satellite over a given area. Over Polish latitudes ASAR measurements can be made about every five days.

MERIS (Medium Resolution Imaging Spectrometer) is an imaging spectrometer with a moderate spectral resolution (ENVISAT-MERIS 2009). This device scans the Earth's surface across satellite track and at the same time ENVISAT's orbit motion causes the collection of information along the flight path. MERIS uses natural sunlight which, after reflection from the surface of the Earth, hits the CCD matrix with 15 spectral channels. This range is from visible to infrared light, therefore electromagnetic wavelength range from 390 nm to 1040 nm. The maximum resolution of images is 260×300 m. MERIS images are sensitive to solar lighting conditions, the presence of aerosols and clouds in the atmosphere. For this reason, prior to the start of analysis it is necessary to calculate the probability of occurrence of clouds in the study area. If it is more than 0.2, there is a high risk of receiving incorrect values and those pixels should be excluded from analysis. Such procedures are standard and can be found in the software programs used for processing satellite images (BEAM 2007). Information contained in MERIS fifteen spectral channels can be used for many purposes such as vegetation layer analysis, assessment of surface water cleanliness, soil properties determination and evaluation of water vapour in the atmosphere. Green dye of plants, the chlorophyll, during photosynthesis strongly absorbs incident solar radiation in the band 420-460 nm (blue and violet light) and the band 640-670 nm (red light) (Gitelson *et al.* 1999). In contrast, the surface layer of leaves strongly reflects the infrared band (700-1100 nm). Because of that, in MERIS pictures green plants will be bright in infrared bands (NIR) and dark for the red bands (RED). This principle is used in the construction of NDVI (Normalised Difference Vegetation Index). The normalised differential vegetation index is given by the equation: $NDVI = (NIR - RED) / (NIR + RED)$. NDVI

values are in the range from -1 to 1 and show the condition of the vegetation layer on the surface of the Earth. Negative and slightly positive values are assigned to inanimate objects such as snow, rocks or bare soil. Higher values (0.1-0.5) indicate sparse vegetation or low chlorophyll content. NDVI above 0.6 means areas covered with dense vegetation (Mynemi *et al.* 1995).

Unfortunately, on April 8th, 2012, after 10 years of operation, the ENVI-SAT suddenly lost contact with its ground base. It ceased to transmit collected information.

After years of preparation and nearly two-year launch delay, at the end of 2009, the European Space Agency placed in orbit the SMOS satellite (Kerr *et al.* 2001). It measures the moisture content of the soil surface layer with an accuracy of approximately $0.04 \text{ m}^3 \text{ m}^{-3}$, by measuring the so-called brightness temperature via radiometric interferometer. SMOS provides data covering the Earth's surface on a 1000 km wide swath, with resolution of approximately $45 \times 45 \text{ km}$, placed on the geo-located DGG (DiscreteGlobalGrid) in the ISEA4H9 (Kotarba 2010) system. SMOS observation periods were selected so that the conditions for energy exchange between the ground and the atmosphere were stabilised, i.e. approximately at 6:00 am local time, in the same way every time, every 3-4 days. At this time of day the soil temperature is stable, because the process of energy exchange is not yet developed. Also the brightness temperature is close to the expected daily values and slowly varying then. At mid-latitudes the dusk time exhibits a faster rate of disappearance of the energy exchange processes and is therefore less suitable for measurements. SMOS antennas receive signals from different depths below the soil surface because all the layers of the soil radiate. Radiation from the deeper layers, however, is damped by subsurface layers and has a smaller contribution to the received signal. The exact depth to which SMOS "sees" depends on many factors, such as moisture and the type of soil. So far, this has not been carefully examined, but it is assumed that this depth is less than 5 cm (Escorihuela *et al.* 2010). SMOS measures brightness temperature at L-band (1.4 GHz). This frequency corresponds to a wavelength of approximately 21 cm, and is almost insensitive to the layer of plants growing on the soil. Brightness temperature is a radiometric measure and determines the intensity of the natural noise emission from the soil. This temperature has a close relationship with the thermodynamic temperature of the object. Its relationship with water content lies in the fact that water and its transport are the most influential factors in the thermodynamic temperature determination. Moreover, soil is not a blackbody and its brightness temperature depends not only on the thermodynamic temperature but also on many other factors such as the dielectric constant. Since water has a very high dielectric

constant compared to dry soil, the dielectric constant of the soil is strongly correlated with the water content. For the purpose of converting brightness temperature to soil moisture, the SMOS mission prepared, together with a research group ECMWF (ECMWF 2007), a software tool called CMEM (CMEM 2007). Input for the CMEM model is a number of environment variables, called in brief ECV (Environmental Climate related Variables). ECV includes, among others: soil temperature, land cover type, soil roughness, air temperature and soil moisture. CMEM model requires also an assessment of the spatial distributions of soil grain size composition, divided roughly into sand, silt and clay. There are not many sources of such data in Poland, and sometimes they are not developed digitally. However, maps adequately prepared for the Polish territory are available (Usowicz *et al.* 2009). In modelling, the data on the type of land cover is derived from ECOCLIMAP (ECOCLIMAP 2010) which is a universal database of archival environmental data, allowing differentiation between 216 classes of ecosystems. CMEM transforms many spatially ordered environmental variables into a variable instrumentally observed by SMOS – brightness temperature. In contrast, the objective of SMOS observation requires the use of inverse model, transforming the result of the instrument observation to the property of Earth's surface – the soil moisture. This transformation is performed by an iterative adjustment method: the soil moisture entering CMEM model is changed iteratively until the brightness temperature coming out from the model will equal the brightness temperature measured by SMOS. Microwave satellite measurements (including SMOS) are almost insensitive to precipitation, clouds or aerosols presence. However, they are susceptible to other factors. SMOS satellite measures the weak, natural noise of the soil in the range of 1.4 GHz, so it is very sensitive to artificial emissions of that frequency from the Earth's surface. Because it is a reserved frequency, the emission of such comes mostly from illegal sources and is called RFI (Radio Frequency Interference) (Oliva *et al.* 2011). In SMOS images RFIs appear as flares which very intensively increase in the registered brightness temperature, not only in the pixel where the source of emission lies, but often also in wide neighbouring areas. This results in artificial boosting of soil moisture and is filtered out by the data provider, the Brockmann Consult company. However, because SMOS is an interferometer, the error in any pixel propagates also to the other pixels. Work on improving the filtering algorithm and mitigation of the illegal radio emissions is underway (Oliva *et al.* 2011). Current information about the RFI is posted on the website dedicated to SMOS satellite (SMOS Blog 2012).

For each satellite and ground-based dataset basic statistical parameters were computed, i.e. the mean value, standard deviation, variance, coefficient of varia-

tion (CV), the maximum and minimum values, and parameters that characterise the variable distribution i.e. skewness and kurtosis. The spatial characteristics of examined data were analysed using geostatistical methods. Statistics, histograms, data transformations, semivariograms, cross-semivariograms, estimation of studied soil characteristics by kriging and co-kriging and their spatial distribution were obtained using computer programs: GS+9, Statistica 8 and Surfer 10 (Gamma Design 2008, StatSoft 2008, Golden Software 2011).

3. RESULTS AND DISCUSSION

3.1. Comparison of soil moisture measured by gravimetric and TDR methods

Surface soil moisture in the examined objects was measured using a TDR device. Simultaneously, at the same points, soil samples were taken into cylinders of 100 cm^3 in volume and a height of 5 cm, in order to determine soil density and soil moisture gravimetrically.

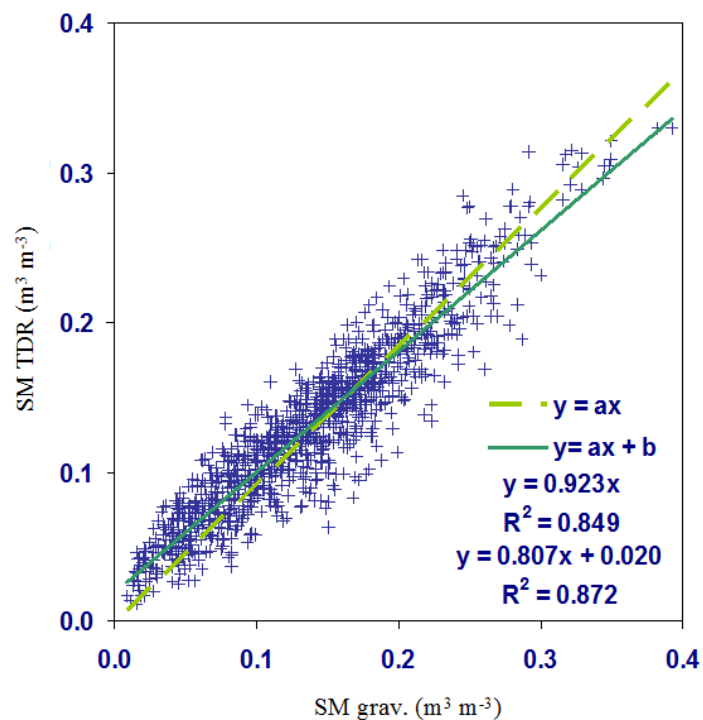


Fig. 3. Soil moisture measured by gravimetric (SM grav.) vs. TDR (SM TDR) methods

Soil moisture data obtained from the gravimetric method was used to verify the data obtained from the TDR (Usowicz and Kossowski 1996). There were 1240 data pairs in total.

Comparison of soil moisture from various test sites derived from the TDR and gravimetric method is shown in Figure 3. To the scatter plot of measurement points a linear regression model was fitted. Its coefficient of determination (R^2) was 0.872. The value of the slope of the linear equation was 0.807, and the intercept was equal to $0.02 \text{ m}^3 \text{ m}^{-3}$. Mean square error was $0.025 \text{ m}^3 \text{ m}^{-3}$. It can therefore be concluded that the TDR method gives satisfactory results and can be used for routine measurements of soil moisture. It should be taken into account that the TDR method overestimates the measurements at lower moisture contents and underestimates the values obtained at higher soil moisture contents.

3.2. Analysis of soil moisture and soil parameters in a commune scale

In July and August 2007 in Trzebieszów and Urszulin communes measurement campaigns were carried out to investigate moisture content and particle size distribution of the surface soil layer (0-10cm). Moisture content was measured using TDR probe. At the same time soil samples were taken into cylinders in order to investigate the moisture content and bulk density of soil by the gravimetric method. Soil was also collected into plastic bags. A total of 86 data were collected for commune Urszulin and 464 data in Trzebieszów commune.

Spatial distributions of measurement points in the areas of both communes were irregular (Fig. 4).

The analysis of particle size distribution of the 0-10 cm soil layer from the area of commune Trzebieszów showed that, on average, it was the highest in sand content (72%), followed by silt (26%) and the least in clay (2%). The minimum contents of these fractions in the collected data were 45, 4 and 0%, respectively and the maximum 95, 54 and 8%, respectively.

Analyses of data from commune Urszulin related to soil particle size distribution showed that in the 0-10 cm layer the soil was also the highest in sand (average 83%), and thus 11% more than in commune Trzebieszów. Silt was significantly less (15%) and, just like in Trzebieszów, the least was silt (2%). The minimum content of these fractions was 58, 3 and 0%, respectively, and the maximum 96, 31 and 15%, respectively.

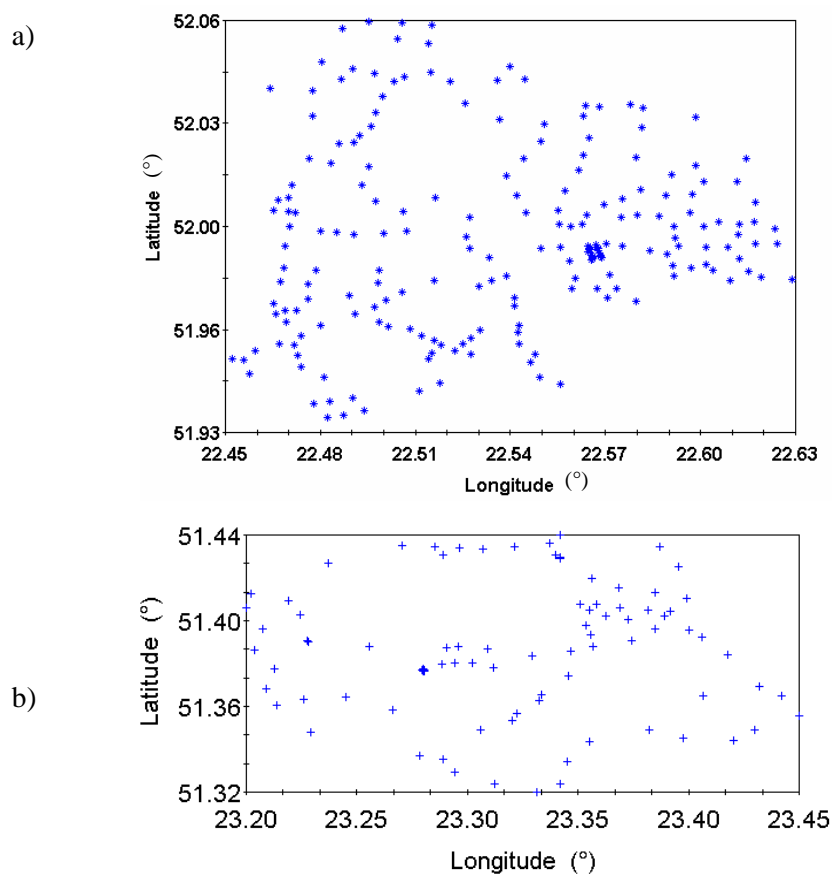


Fig. 4. Spatial distribution of measurement points in Trzebieszów (a) and Urszulin (b) communes

The largest variation, characterised by the coefficient of variation (CV), was observed for the clay fraction content in Urszulin commune – 105%. In Trzebieszów commune CV for clay was much lower and reached 67%. For both communes the lowest variability was observed for the sand fraction.

Skewness, which characterises the degree of asymmetry of a statistical distribution around its mean, in the case of sand and silt, for the two communes, was considered low, close to zero. In contrast, the distribution of clay content in the surface soil layer of both communes was characterised by a significant right-skewed asymmetry.

Differences between mean values and median values for each considered variable and the values of the asymmetry and kurtosis indicate that a majority of the studied variables can be described with fairly good accuracy by a normal distribu-

tion. In cases where differences were significant, the data were transformed using a logarithmic or square root transform in order to bring them closer to normal distribution, as required by geostatistical analysis (Gotway and Hergert 1997).

Within the geostatistical analysis, all the measurement data collected from the two communes were tested for the detection of trends in the spatial distributions of the examined soil characteristics. In the event of a trend, it was included in further analysis (Golden Software 2011). For the studied areas of Trzebieszów and Urszulin communes it can be assumed that examined parameters satisfied the condition of stationarity or quasi-stationarity of process, required for geostatistical analysis (Gotway and Hergert 1997). Spatial variation of each variable under consideration was tested with semivariograms and cross-semivariograms. Semivariance analysis was carried out to detect surface anisotropy in the spatial distribution of studied variables. If it was found, the direction along which it was the smallest was chosen and taken into account during further analysis.

The values of nuggets, sills and ranges of spatial autocorrelation were determined and semivariogram and cross-semivariogram models were fitted to empirical values, together with an indication of fitting of these models by the coefficient of determination r^2 . Efforts were made to choose sampling step, method of semivariance and cross-semivariance calculation, in a way that the quality of fit of theoretical models of semivariograms and cross-semivariograms to empirical data was the best in every case. The geostatistical characteristics of granulometric fractions content, soil bulk density and moisture content in the 0-10 cm layer of soil from the Trzebieszów and Urszulin communes are summarised in Table 1.

Spatial distributions of individual granulometric fractions contents, moisture and density showed spatial dependences in both the Urszulin and Trzebieszów communes. The shape of all investigated dependences was spherical. The parameters of semivariograms indicated that for many variables the nugget effect is present. This shown that in examined features there was a variability occurring at distances shorter than the minimum distance between the collected soil samples in field. In the case where the value of the nugget was a large part of the sill, and the range of spatial dependence was small, in the next measurement campaigns the step of sampling could be reduced to recognise more precisely the nature of the changes or to verify that the variable had no spatial dependence on the examined object. This was the case for clay content and soil bulk density in Trzebieszów and clay content in Urszulin. Semivariance saturation values were comparable with the values of the variance determined in the conventional way; this means that there were no relevant deterministic components (trends) in the analysed distributions. The spatial ranges of correlations in particle size distribution, density and moisture content of soil in communes Urszulin and Trzebieszów were from 0.01 to 0.06°, which

corresponds to the spatial distances of about 1.1 to 6.6 km. In Trzebieszów commune, sand, silt and soil moisture achieve the longest range of spatial correlation length, and clay the smallest. In the case of Urszulin commune, the longest spatial relationship was noted for soil moisture and the shortest for all granulometric soil fractions contents. To improve the estimation for the Urszulin commune, cross-semivariograms between distributions of granulometric fractions were additionally determined. Between the content of sand and silt a negative correlation of cross-semivariance occurred, and between the content of clay and silt – a positive relationship. The range of spatial dependence for each of the test granulometric fractions was approximately 0.01° .

Table 1. Geostatistical characteristics of distributions of measured soil properties in the soil layer 0-10 cm (based on Usowicz *et al.* 2009)

Variable	Nugget	Sill	Range ($^\circ$)*	r^2
Sand content in Trzebieszów commune	34.6	99.2	0.05	0.993
Silt sand content in Trzebieszów commune	34.6	96.3	0.05	0.934
Clay sand content in Trzebieszów commune	0.012	0.150	0.01	0.619
Bulk density in Trzebieszów commune	0.009	0.017	0.02	0.108
Soil moisture (gravimetric) in Trzebieszów commune	0.001	0.006	0.04	0.721
Soil moisture (TDR) in Trzebieszów commune	0.002	0.004	0.05	0.429
Sand content in Urszulin commune	5.6	72.5	0.01	0.099
Silt sand content in Urszulin commune	0.1	62.2	0.01	0.040
Clay sand content in Urszulin commune	0.010	0.160	0.01	0.444
Bulk density in Urszulin commune	0.650	1.070	0.04	0.562
Soil moisture (gravimetric) in Urszulin commune	0.520	1.050	0.06	0.480
Soil moisture (TDR) in Urszulin commune	0.520	1.060	0.05	0.633

*At latitudes of Poland, 1° corresponds to a linear distance of approximately 110 km.

Spatial distributions for the individual parameters of the soil in the communes Trzebieszów and Urszulin were obtained using kriging and co-kriging methods, based on previously calculated geostatistical parameters, semivariograms and

cross-semivariogram models. Kriging was used for estimating all examined soil characteristics in the commune Trzebieszów and soil moisture and bulk density of the soil in commune Urszulin. The distribution of grain size composition of the soil in commune Urszulin was estimated using the co-kriging method, because this method gave a much better compatibility with the measured data than using the kriging method. In the next step, maps of spatial distributions of examined features within the considered objects were plotted (Fig. 5 up to Fig. 8) and the values of the errors made during the estimation were determined. Estimation errors for all tested soil characteristics were not greater than 10-15% of the analysed features. In the vicinity of the measuring points errors were much smaller, in the range of 2-4%. The largest errors occurred on the edges of the measuring grids.

According to the methodology, content of sand, silt and clay in the soil should add up to 100%. However, in estimated maps of granulometric fractions distributions (Fig. 5 and Fig. 7) there are places where the sum of the fractions is not equal to 100%. This is a result of estimation (approximation) and error of method used. Despite the imperfections of the spatial distributions of examined properties they provide valuable information about the range of occurrence of certain values and orientation of their changes. Distributions of the content of sand, silt (Fig. 5a, b) and soil bulk density (Fig. 6a) in commune Trzebieszów are latitudinal. More sand is present in the middle; there is also a greater bulk density of soil. In this area there is less of silt fraction. In Trzebieszów commune clay content distribution is irregular, island-like (Fig. 5c). The distribution of soil moisture in Trzebieszów commune, obtained from gravimetric measurements (Fig. 6b), shows much greater diversity and greater value than the value of soil moisture measurements obtained from the TDR probe (Fig. 6c). These results indicate a lower sensitivity of TDR, compared to the gravimetric method. However, by reason of the fact that the TDR method is much faster and non-destructive, it is acceptable in field measurements, but requires correction for bulk density and particle size distribution of the examined soil.

Distributions of the sand and silt contents for Urszulin commune (Fig. 7a,b) have a similar pattern; of course where there is more sand, silt must be less. Distributions are island-like with a slight north-western orientation. In the case of clay, "islands" with higher content of this fraction are clearly visible (Fig.7c).

The largest such "island", which is also the area with the highest clay content, is located on the south-west of the study area. The soil bulk density distribution (Fig. 8a) is also directed towards the north-west, but less clearly than sand and silt. The estimated distribution of soil moisture in community Urszulin has a distinct "island" of high moisture content in the west and a quite dry area in the east (Fig. 8b, c). As in the case of Trzebieszów commune, the gravimetric method was more sensitive than the TDR method. Spatial distributions of soil moisture obtained from both methods were similar, but smaller variation was visible on the soil moisture map obtained from the TDR measurements.

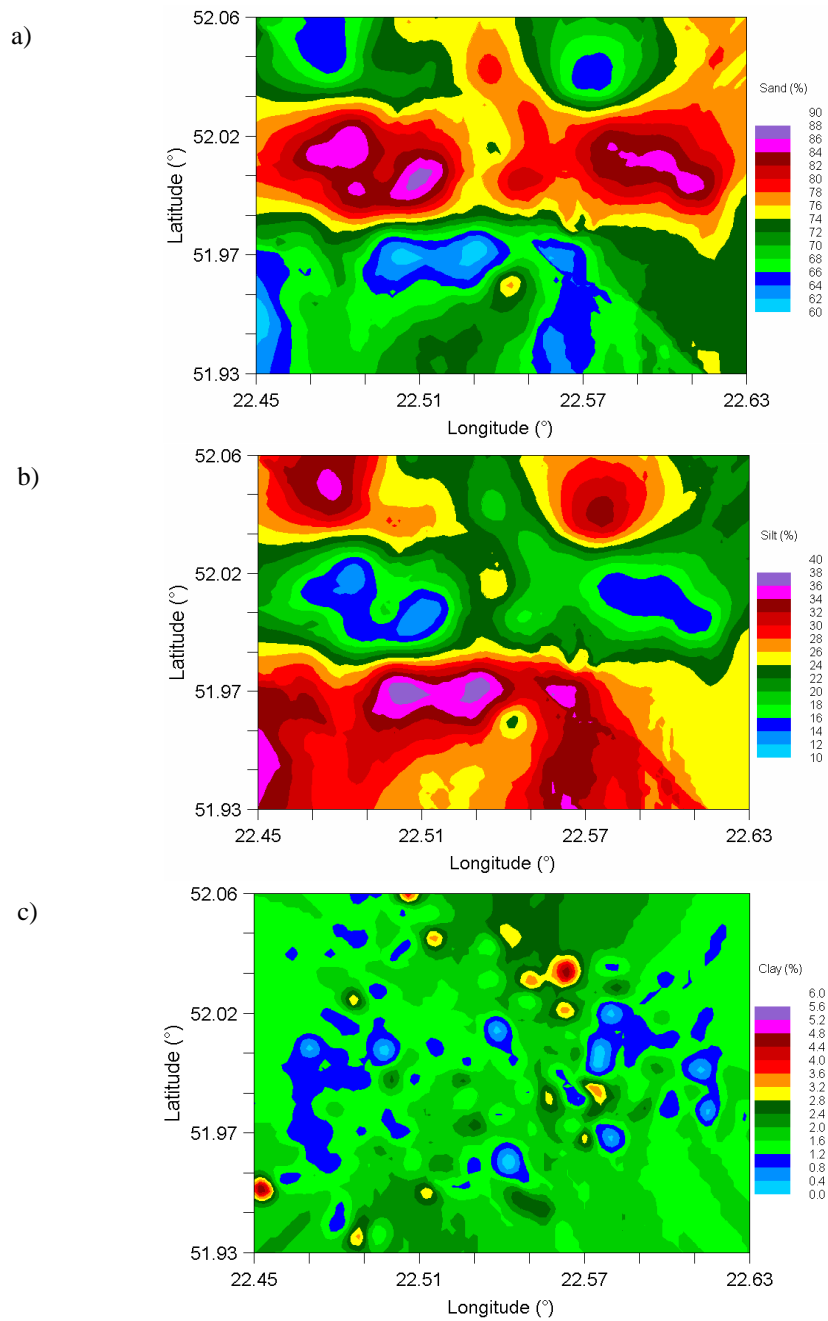


Fig. 5. Spatial distributions of sand (a), silt (b) and clay content (c) in the 0-10 cm soil layer in the area of Trzebieszów commune (Usoiwicz *et al.* 2009)

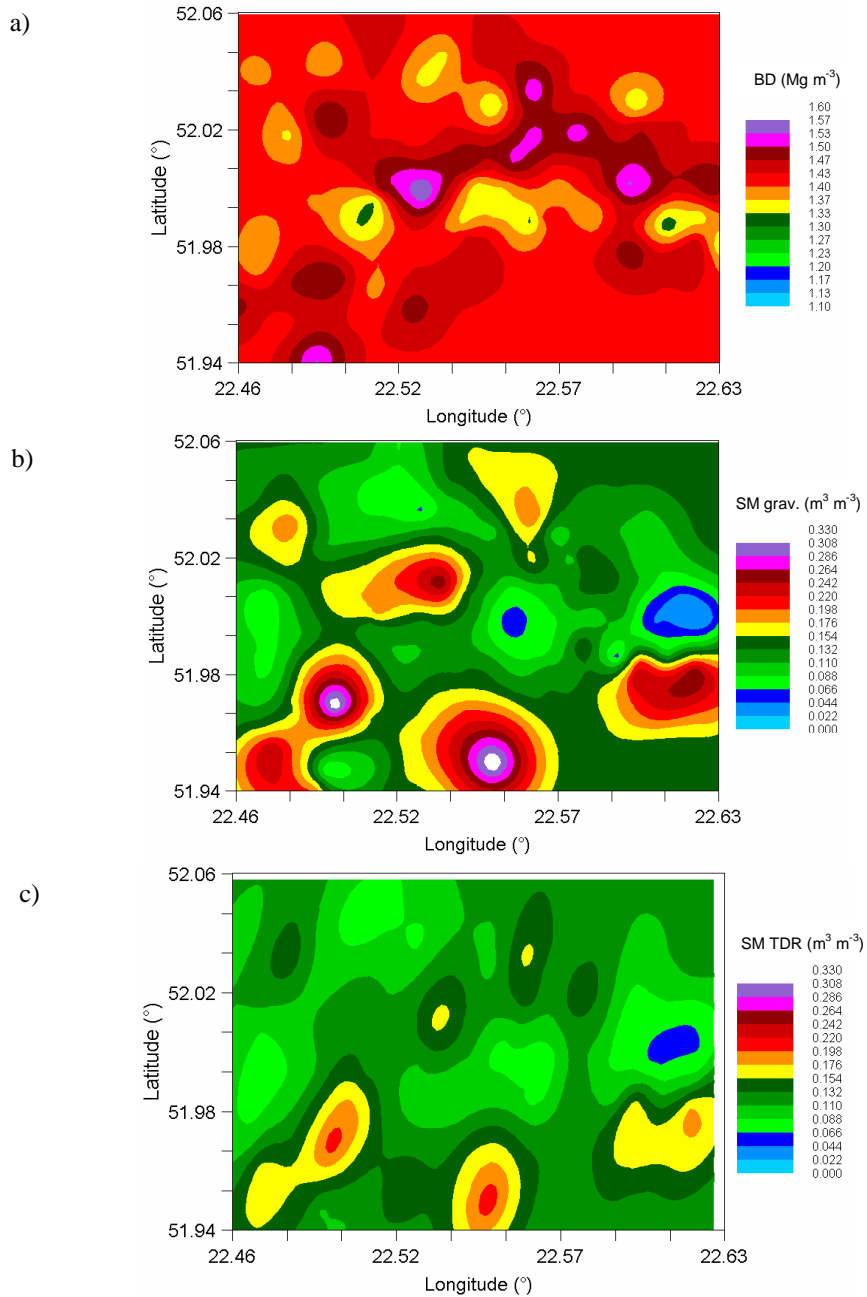


Fig. 6. Spatial distributions of soil bulk density (a) and soil moisture (measured by gravimetric (b) and TDR (c) methods) in the 0-10 cm soil layer in the area of Trzebieszów commune (Usovicz *et al.* 2009)

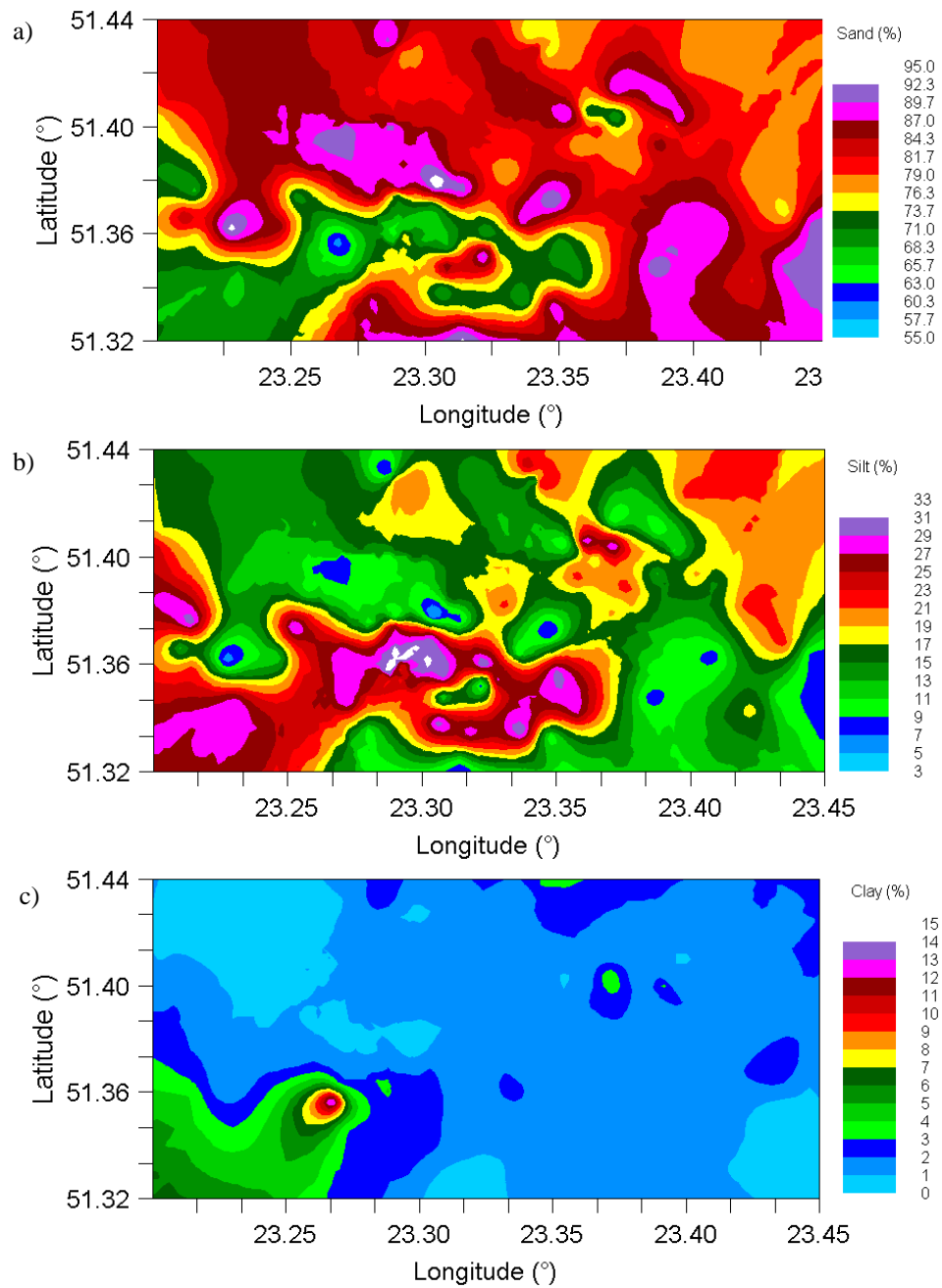


Fig. 7. Spatial distributions of sand (a), silt (b) and clay content (c) in the 0-10 cm soil layer in the area of Urszulin commune (Usovicz *et al.* 2009)

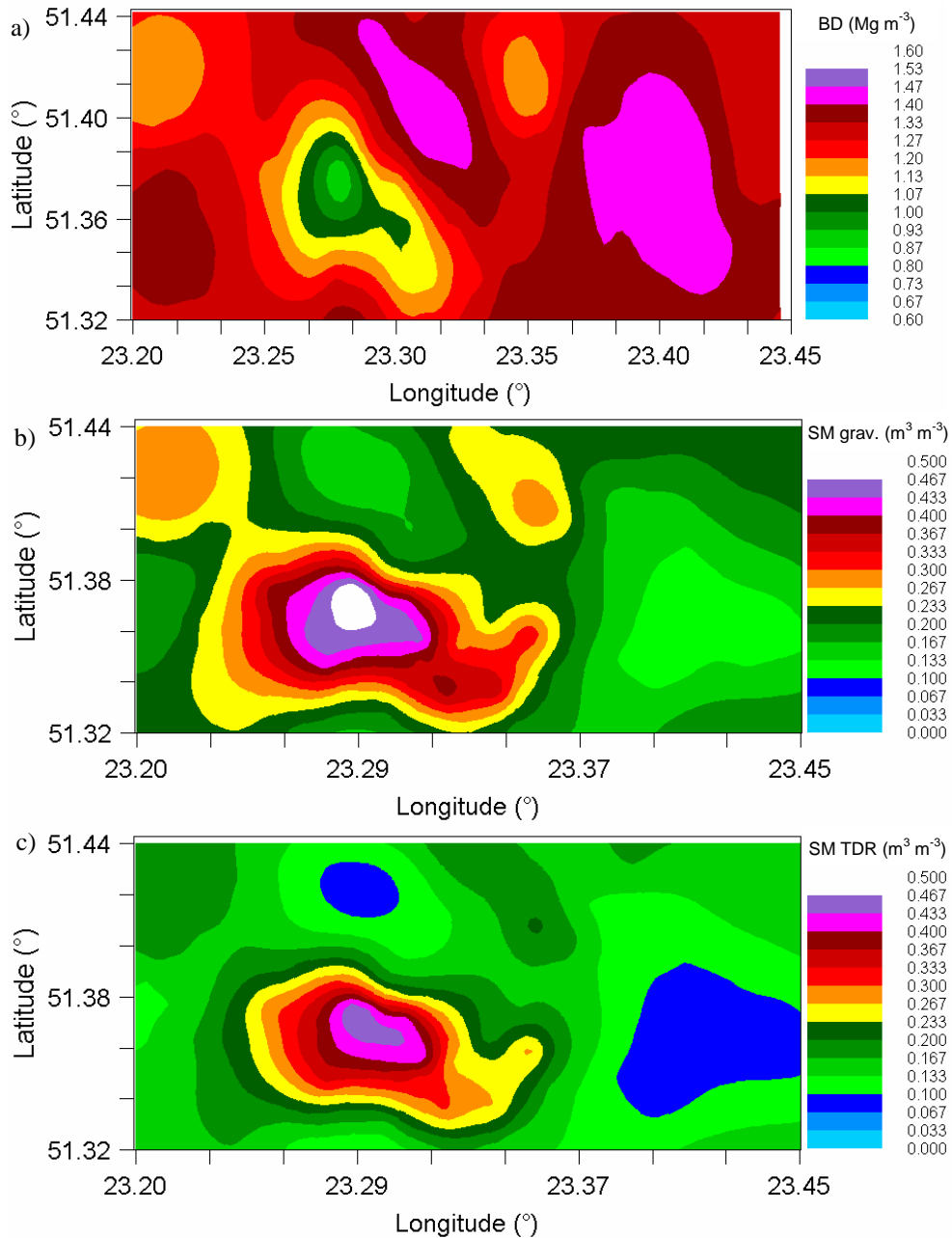


Fig. 8. Spatial distributions of soil bulk density (a) and soil moisture (measured by gravimetric (b) and TDR (c) methods) in the 0-10 cm soil layer in the area of Urszulin commune (Usovicz *et al.* 2009)

3.3. Evaluation of the impact of topography on soil moisture

On 01/10/2008 measurements of the surface soil moisture using a TDR probe (Easy Test) were carried out. In order to assess the impact of altitude on the moisture in the surface layer of soil, the slope was selected on which the 55 measurements of soil moisture were made (Fig. 9). The study area was located within the Poleski National Park, between the villages of Karczunek (Chełm district, Wierzbica commune) and Wojciechów (Włodawa district, Hańsk commune). Studied slope begins near an observation tower and ends in the Bagno Staw, which is a low carbonate moor. The entire area was planted with a similar type of meadow vegetation, only the lower part of the slope by bog vegetation (WIOSL 2010). In the upper parts, at a height of approx. 182 m above sea level, the area was quite dry (soil moisture approximately $0.10 \text{ m}^3 \text{ m}^{-3}$), while in the lower part, on the border of Bagno Staw, at the height of the order of 169 m above sea level – evidently wet, with exposed areas of surface water and therefore difficult to access. The distribution of altitude estimated by inverse distance weighting method is shown in Figure 10.

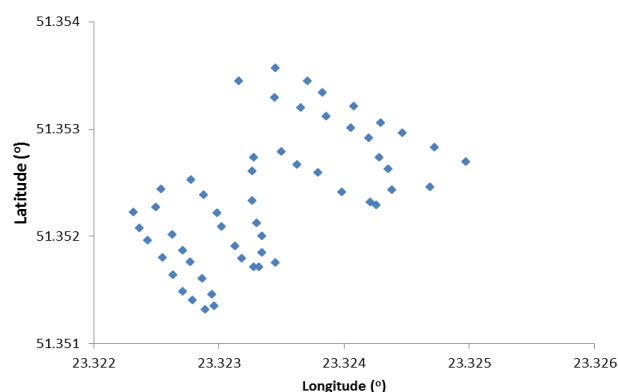


Fig. 9. Spatial distribution of soil moisture measuring points on 01/10/2008 in Poleski National Park

Coordinates and altitudes of measuring points were determined using a GPS device in the WGS-84 datum. The collected data were the subject of statistical and geostatistical analysis. The minimum value of soil moisture for the study area was $0.055 \text{ m}^3 \text{ m}^{-3}$ while the maximum was $0.638 \text{ m}^3 \text{ m}^{-3}$. Average moisture of the study area was $0.183 \text{ m}^3 \text{ m}^{-3}$ and standard deviation equal to 0.132. Skewness of the soil moisture data distribution was 2.33 and kurtosis 4.57. This distribution was right-skewed and leptokurtic because points with high humidity occurred significantly less often than those with low and medium soil moisture. Altitude ranged from 169.4 to 185.6 m above sea level. The measurement points were

selected so that the statistical distribution of altitude had a slight skew (0.11) and kurtosis (0.49) and was similar to the normal distribution in order to meet the assumptions of statistical analysis. The influence of the terrain altitude on surface soil moisture content was examined using Statistica program. Linear regression coefficients were calculated and their statistical significance was tested (Fig. 11).

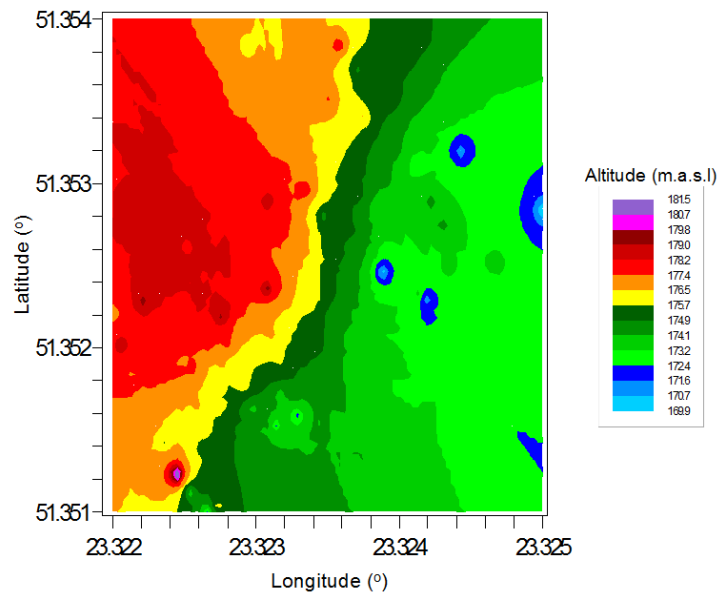


Fig. 10. Altitude of examined slope estimated by inverse distance weighting method for study area in Poleski National Park

Linear regression coefficient turned out to be negative and statistically significant at high significance level ($p < 0.01$), despite the low coefficient of determination (0.19), indicating poor fit of the linear model to the measured values. Therefore, it can be concluded that in the examined area with an increase in terrain altitude the surface soil moisture decreases. The probability of this thesis being untrue is approximately zero ($p < 0.0008$). As shown by other studies (Charpentier and Groffman 1992, Ladson and Moore 1992, Niemann and Edgell 1993), the claim that local soil moisture decreases with the height of terrain is not always true. Mostly, however, areas located higher are drier than the lower-lying, due to the gravitational runoff and other factors (Famiglietti *et al.* 1998). Then, the data on land altitude and soil moisture were subjected to a logarithmic transform, in order to bring them closer to a normal distribution. After transformation, the linear relationship between them somewhat weakened and the fit of linear model also slightly decreased ($r^2 = 0.17$), but computed linear regression coefficient was still statistically significant at high signifi-

cance level ($p < 0.01$). Thanks to the transform, skewness of moisture distribution was decreased twice (to 1.19) and kurtosis three times (to 1.41), which approximates the data distribution to the assumptions of geostatistical analysis conducted later. Semivariance surface analysis was performed to detect anisotropy in the soil moisture and altitude spatial distributions. For both of these variables, the lowest anisotropy occurs in the direction of 35° (Fig. 12).

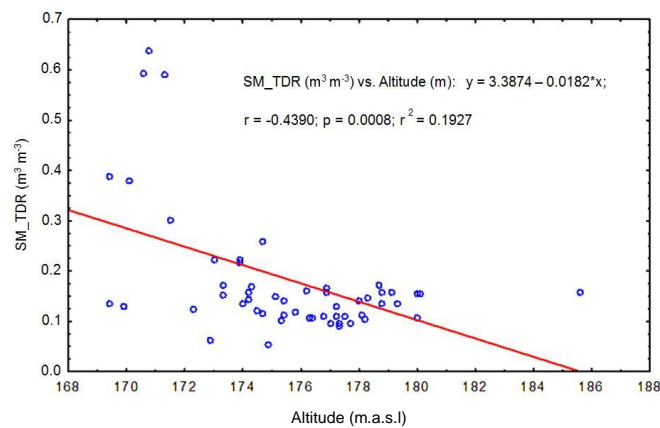


Fig. 11. Dependence of soil moisture (SM_TDR) on terrain altitude (r – Pearson correlation coefficient, p – probability of statistical insignificance of regression coefficient, r^2 – coefficient of determination)

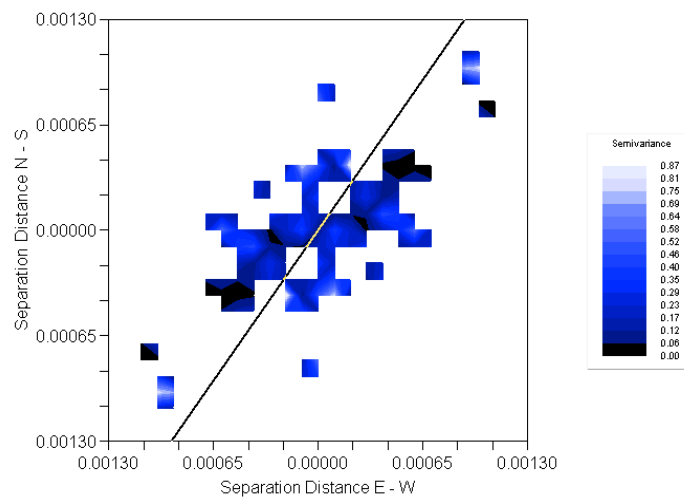


Fig. 12. Surface soil moisture semivariogram with the line of smallest anisotropy

The detected trend was removed using linear approximation in Surfer program. Then it could be assumed that the analysed soil moisture distribution fulfils the requirements of ergodicity and quasi-stationarity, obligatory for geostatistical analysis (Gotway and Hergert 1997). In the next step, the theoretical semivariogram was fitted to isotropic empirical semivariogram. It was a linear model, and after the removal of trend (most likely resulting from the change in terrain altitude) investigated soil moisture no longer showed spatial dependence. From the presence of a large nugget effect it can be concluded that the distance between the measuring points was too small or the measurement method used to determine the soil moisture generated an additional variability.

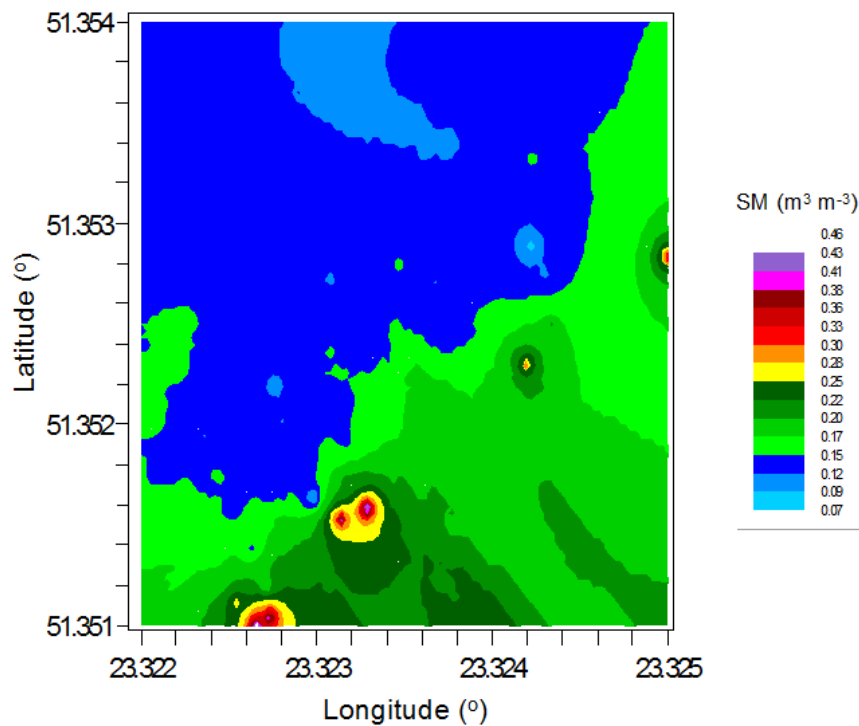


Fig. 13. Spatial distribution of soil moisture (SM) measured by TDR probe on 01/10/2008 in Poleski National Park

Then, based on the previously found relationship between altitude and moisture, by the co-kriging method, using a linear model, the continuous distribution of the surface soil moisture was estimated (Fig. 13). From the figure it can be seen that the south-eastern part of the study area, with lower height (compare with Fig. 10), the closest to the area of Bagno Staw, had moisture content greater than the north-

western part, placed higher. The line of azimuth 35° is clearly visible, along which the moisture content that did not change much. This line overlapped with the direction of the smallest anisotropy determined previously. Next, the accuracy of the estimation was assessed. The quality of interpolation was found to be satisfactory ($r^2 = 0.33$), but could be improved if more accurate trend analysis was performed, removing not only the linear component, but perhaps higher orders. Like in most studies of this type, to improve the quality of co-kriging estimates, more measurements and their more regular grid would be preferred.

3.4. Temporal analysis of soil moisture from satellite and ground-based measurements

To determine the dynamics of surface soil moisture for the eastern part of Poland in the years 2010 and 2011, data from a network of agro-meteorological stations (Fig. 2), belonging to the Institute of Agrophysics in Lublin were used. The study used data from the shallowest soil moisture sensors i.e. placed at a depth of 10 cm for the stations Białowieża, Biebrza, Trzebieszów and Wigry and at depth of 5 cm for the other stations. From the depth of 0-10 cm, in the nearest neighbourhood the stations' soil moisture sensors, soil samples were taken and soil particle size distribution was determined by the sedimentation method, according to recommended standards. In places already examined, soil was not collected because literature data was used (Usowicz *et al.* 2009). The names of the stations, their location and code (used in some Figures) and the particle size distribution of the soil around soil moisture sensors are presented in Table 2. Rainfall data collected by rain gauges installed in the majority of the stations were also used.

The data that was applied for analysis does not always cover the entire period of the years 2010 and 2011, because some of the stations were equipped with soil moisture sensors in the spring or summer of 2010. In addition, sometimes because of long-term low temperature, soil frost occurred, that occasionally generated erroneous readings and station failures. For these reasons, data from 2010 and 2011 are separated by a "winter break" and they were analysed separately. For each year, the mean and standard deviation were calculated. Also the minimum and maximum values were determined, and approximate days when the appearance of these values was specified. This information is presented in Table 3. The smallest annual average soil moisture for both years was observed at stations Biebrza and Wigry, i.e. those whose sensors are placed in soil containing the greatest levels of sand fraction among all the stations. Soil around the Urszulin station also contains a lot of sand, but it is located on a swamp, so in both years the annual averages and maximums of soil moisture were the largest observed.

Table 2. Information about the stations that provided data for soil moisture study

Name	Geographical location		Code	Particle size distribution of the soil in 0-10 cm layer (%)		
	longitude (°)	latitude (°)		sand (0.05-2.0 mm)	silt (0.002-0.05 mm)	clay (<0.002 mm)
Białowieża	23.7498	52.6695	06IA	68	28	4
Biebrza	22.6613	53.4666	08IA	97	1	2
Urszulin	23.2968	51.3856	03IA	83*	15*	2*
Cicibór	23.0992	52.0676	05IA	58	37	5
Felin	22.6247	51.2202	01IA	26*	68*	6*
Janów	22.4189	50.6914	10IA	86	9	5
Majdanek	23.4704	50.4782	11IA	22	73	5
Trzebieszów	22.5650	51.9885	04IA	72*	26*	2*
Wigry	23.0025	54.0240	09IA	87	11	2

*literature data (Usowicz *et al.* 2009).

The year 2010 was characterised by greater than 2011 average soil moisture. For most of the stations, the 2010 mean soil moisture was higher on average by $0.06 \text{ m}^3 \text{ m}^{-3}$, except for Biebrza, for which 2011 was more moist by $0.02 \text{ m}^3 \text{ m}^{-3}$. In examining the standard deviations it can be noted that 2011 was more variable in terms of soil moisture, but perhaps this is due to the longer measurement series than a year earlier. In 2010, for most of the stations, the days with the lowest soil moisture occurred in July. In 2011, for most stations, the driest day of the year occurred on the 7th or 9th of June. In 2010, the group of neighbouring stations: Trzebieszów, Białowieża, Biebrza and Wigry, reached the maximum soil moisture in a similar period of 5-8th of November. In 2011, at stations located on soils with sand content greater than 80% (Biebrza, Urszulin, Janów, Wigry), the maximum soil moisture was recorded in the summer, between 22/07/2011 and 01/08/2011. At other stations, the day with maximal soil moisture appeared in winter thaws or in the spring (February, March, April).

Table 3. Statistical parameters of soil moisture measured at automatic stations

Station name	Year	Mean value ($\text{m}^3 \text{m}^{-3}$)	Standard deviation ($\text{m}^3 \text{m}^{-3}$)	Minimum ($\text{m}^3 \text{m}^{-3}$)	Day of minimum	Maximum ($\text{m}^3 \text{m}^{-3}$)	Day of maximum
Białowieża	2010	0.29	0.058	0.12	24/05/2010	0.35	05/11/2010
	2011	0.22	0.078	0.02	29/06/2011	0.36	13/04/2011
Biebrza	2010	0.13	0.019	0.05	12/07/2010	0.17	08/11/2010
	2011	0.15	0.033	0.09	09/06/2011	0.23	22/07/2011
Urszulin	2010	0.33	0.059	0.15	03/07/2010	0.43	02/09/2010
	2011	0.29	0.119	0.12	07/06/2011	0.51	01/08/2011
Cicibór	2010	0.18	0.063	0.05	23/08/2010	0.38	21/03/2010
	2011	0.12	0.043	0.06	07/06/2011	0.31	16/03/2011
Felin	2010	0.31	0.074	0.08	16/07/2010	0.43	02/03/2010
	2011	0.19	0.063	0.07	07/06/2011	0.35	06/02/2011
Janów	2010	0.21	0.057	0.08	19/07/2010	0.31	19/05/2010
	2011	0.14	0.068	0.06	09/06/2011	0.31	31/07/2011
Majdanek	2010	0.33	0.034	0.22	23/07/2010	0.40	21/03/2010
	2011	0.25	0.072	0.08	09/06/2011	0.39	18/03/2011
Trzebieszów	2010	0.16	0.029	0.06	17/07/2010	0.21	06/11/2010
	2011	0.15	0.042	0.07	28/05/2011	0.24	15/03/2011
Wigry	2010	0.13	0.026	0.06	12/07/2010	0.17	06/11/2010
	2011	0.13	0.033	0.06	07/06/2011	0.18	27/07/2011

In further studies, a series of 450 satellite images of the surface soil moisture observed by the SMOS were used. These data were from 2010-2011, and like the ground data they were divided by a “winter break” because SMOS conversion algorithm is not able to determine soil moisture if the surface is frozen and/or covered by snow (Mahmoodi 2011). Measurements are obtained from ascending orbits and were made between 3 and 6 in the morning. For each examined image, nine areas of interest were selected. Their centres lie close to the automatic agrometeorological stations where soil moisture data series were collected. For each

image individually, satellite data describing the areas around the stations were spatially averaged in order to obtain approximate SMOS resolution given in the literature (Mahmoodi 2011), reaching sizes of about 50×50 km. The location of areas of interest on the exemplary SMOS image, along with added points in which soil moisture stations are placed, is shown in Figure 14.

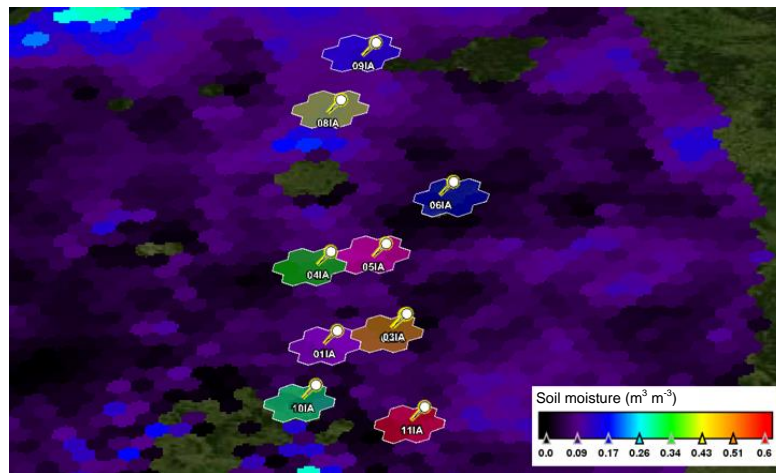


Fig. 14. Location of areas of interest on the exemplary SMOS image, along with soil moisture stations (the codes are explained in Table 2.)

For each area of interest, separately for 2010 and 2011, statistical analysis of SMOS data was performed. The annual mean, standard deviations, minimums and maximums of soil moisture were calculated (Tab. 4). In contrast to the ground data, it was not possible to determine the exact day of the extreme values of soil moisture because SMOS satellite passes over the Polish territory approximately every 3 days, and the satellite data used in this study were averaged over time in a 7-day-wide moving rectangular window. The average annual soil moisture measured by SMOS in 2010 was higher than the moisture in 2011. The difference is visible for each of the areas and equals an average of approximately $0.04 \text{ m}^3 \text{ m}^{-3}$. After dividing the standard deviation by the average, according to SMOS measurements, 2011 also appears to be more variable than 2010. SMOS satellite recorded the lowest average annual soil moisture in the area around the station Białowieża in 2011. On average, the driest in the year 2010 was the area around Janów. SMOS satellite observed the highest average annual soil moistures around the Biebrza station. This is understandable, since this area is covered by one of

the largest wetlands in Europe. In the studied years, the highest examined values recorded by the SMOS satellite soil moistures were also observed there.

Table 4. Statistical parameters of soil moisture measured by SMOS in the areas around the stations

Station name	Year	Mean value ($\text{m}^3 \text{m}^{-3}$)	Standard deviation ($\text{m}^3 \text{m}^{-3}$)	Minimum ($\text{m}^3 \text{m}^{-3}$)	Maximum ($\text{m}^3 \text{m}^{-3}$)
Białowieża	2010	0.09	0.044	0.01	0.19
	2011	0.04	0.036	0.01	0.21
Biebrza	2010	0.21	0.062	0.10	0.37
	2011	0.14	0.053	0.03	0.35
Urszulin	2010	0.10	0.044	0.00	0.20
	2011	0.08	0.047	0.01	0.35
Cicibór	2010	0.11	0.045	0.03	0.22
	2011	0.08	0.041	0.03	0.22
Felin	2010	0.13	0.051	0.02	0.28
	2011	0.10	0.052	0.00	0.33
Janów	2010	0.08	0.034	0.02	0.18
	2011	0.06	0.040	0.01	0.28
Majdanek	2010	0.15	0.046	0.02	0.27
	2011	0.12	0.053	0.01	0.26
Trzebieszów	2010	0.13	0.055	0.01	0.26
	2011	0.09	0.055	0.02	0.37
Wigry	2010	0.14	0.030	0.07	0.23
	2011	0.12	0.043	0.02	0.22

In order to compare surface soil moisture obtained from ground-based measurements and SMOS satellite, data obtained from the stations were prepared in the same manner as the previously used SMOS data: Arithmetic averaging was done using a moving rectangular window with one day step. This window averaged the data from 7 days and assigned obtained mean value to the central day, and then

moved forward by one day, averaged 7 days, assigned value to middle one, moved forward etc. Then the data from the ground stations and from the SMOS satellite were plotted on a common graph with the addition of daily rainfall “background” measurements (Figs. 15-23). The exception was the station Felin, where rainfall data was not available.

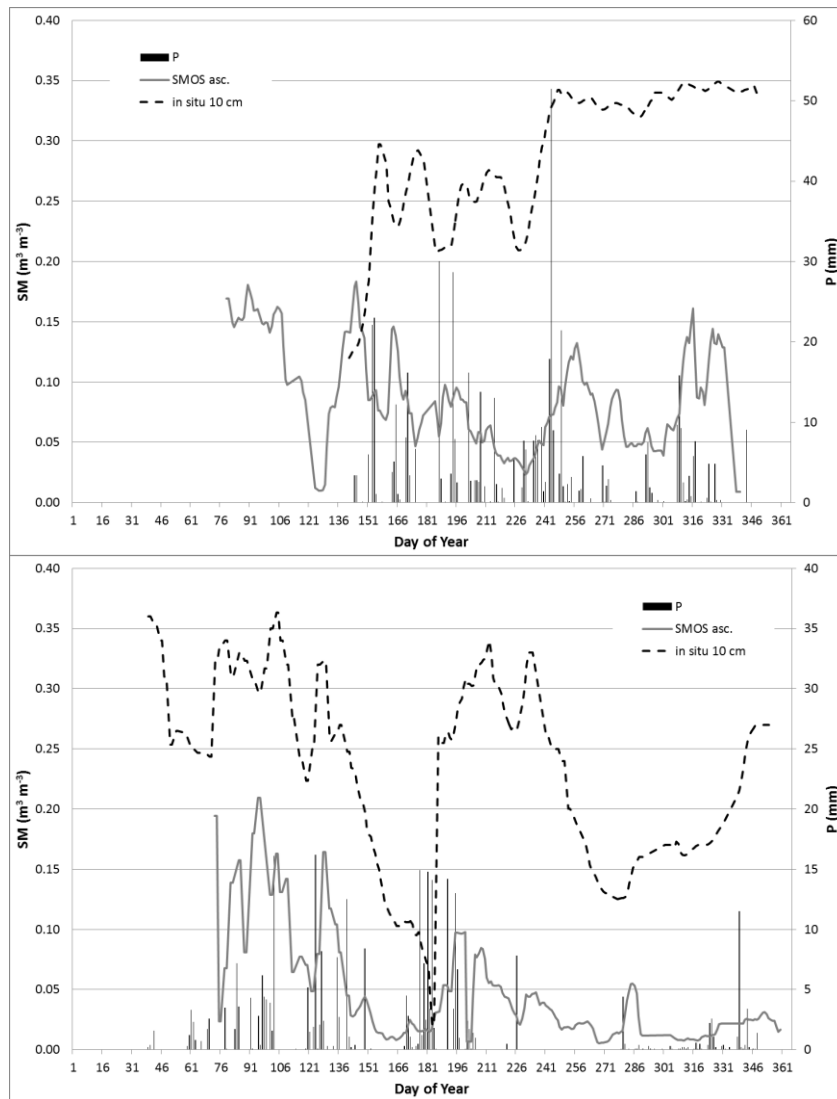


Fig. 15. Soil moisture (SM) and daily rainfall (P) for the area of Białowieża station, 2010 (top figure) and 2011 (bottom figure)

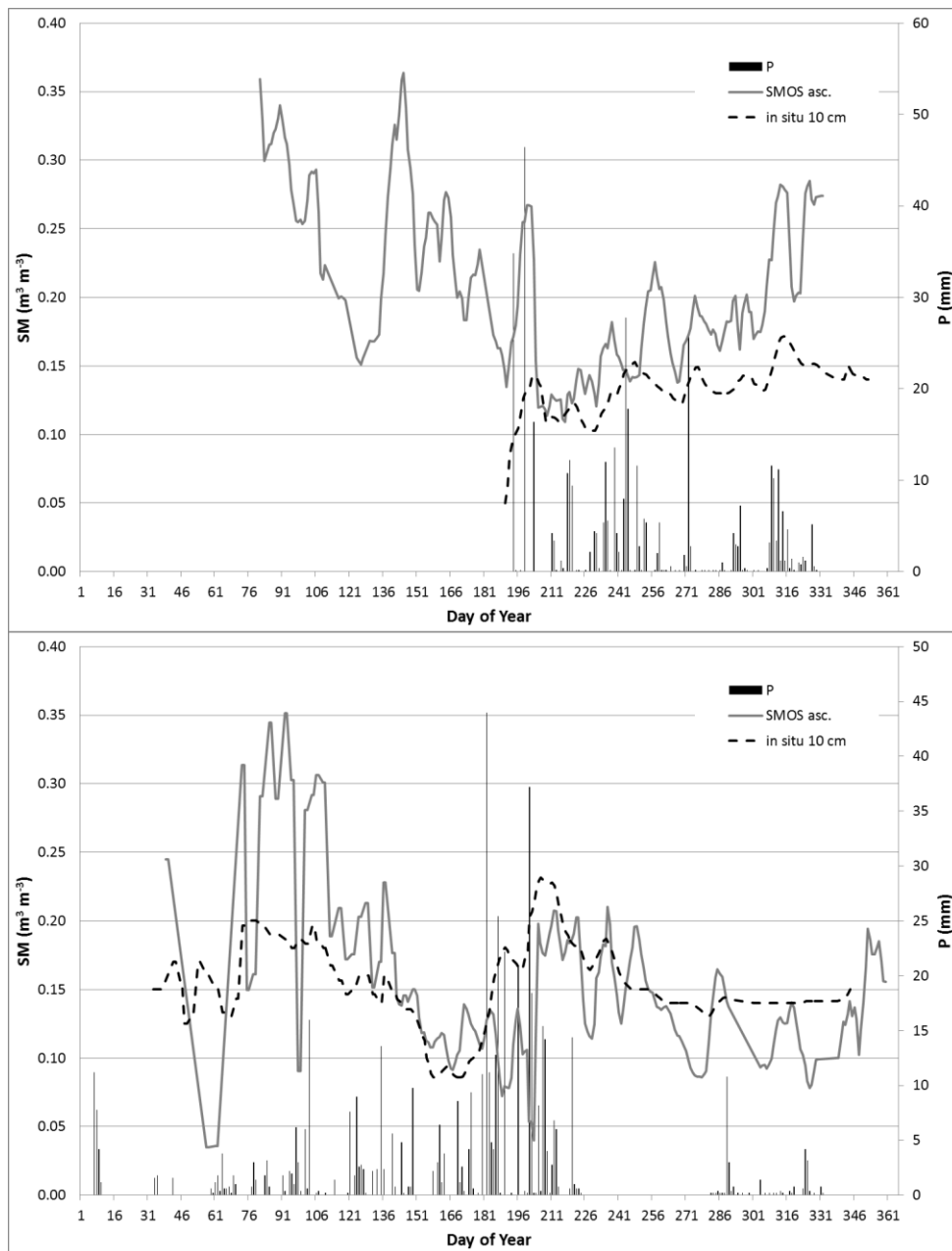


Fig. 16. Soil moisture (SM) and daily rainfall (P) for the area of Biebrza station, 2010 (top figure) and 2011 (bottom figure)

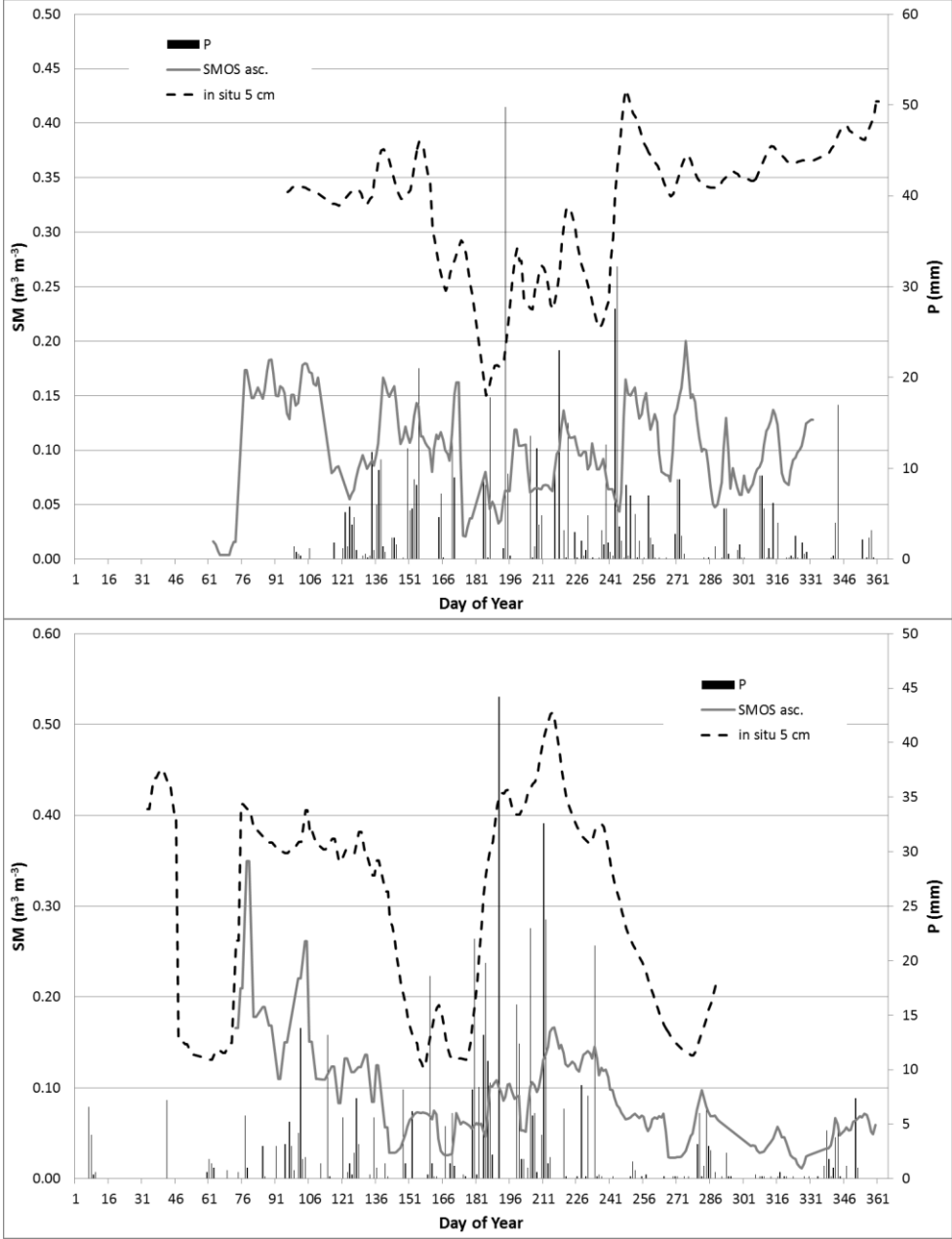


Fig. 17. Soil moisture (SM) and daily rainfall (P) for the area of Urszulin station, 2010 (top figure) and 2011 (bottom figure)

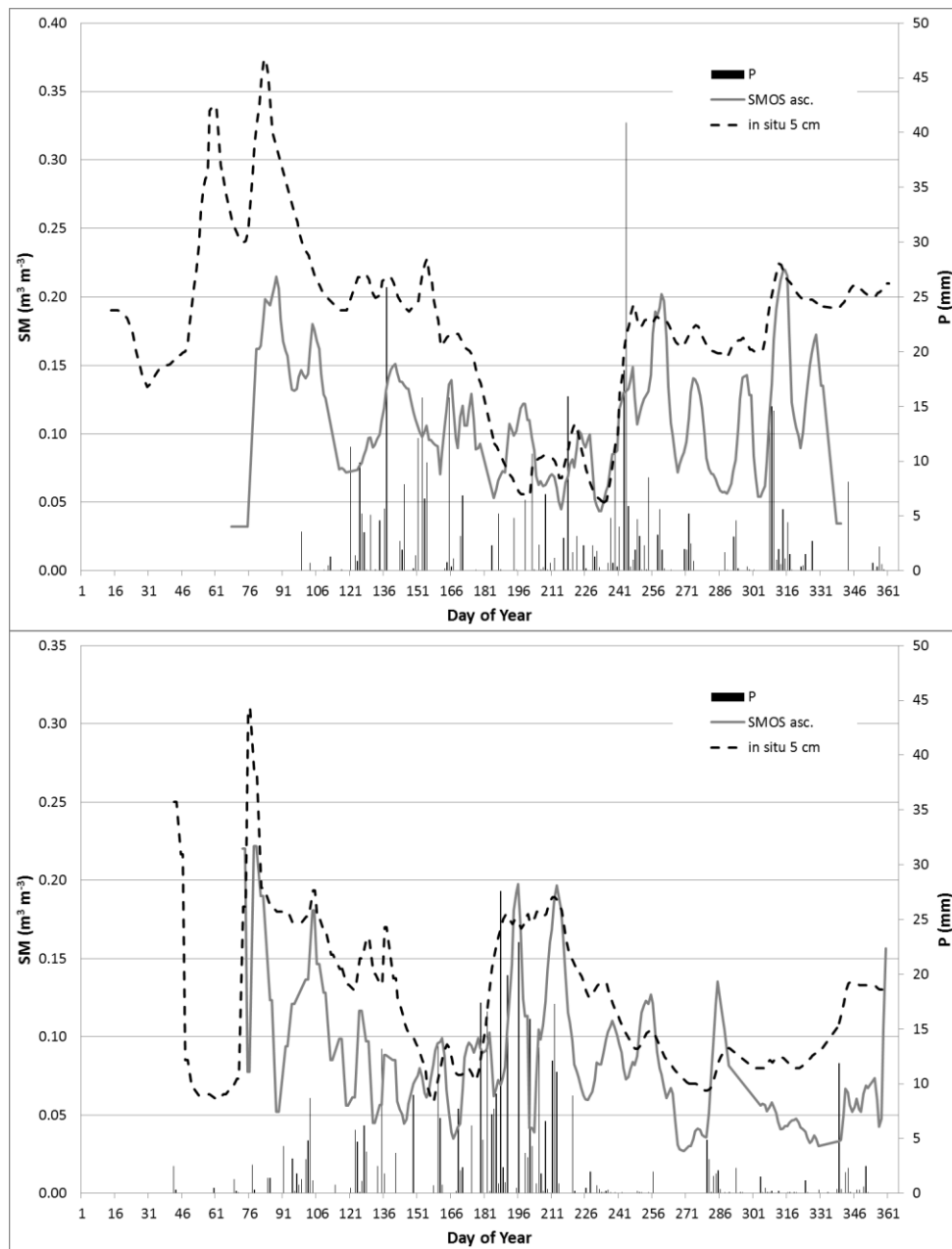


Fig. 18. Soil moisture (SM) and daily rainfall (P) for the area of Cicibór station, 2010 (top figure) and 2011 (bottom figure)

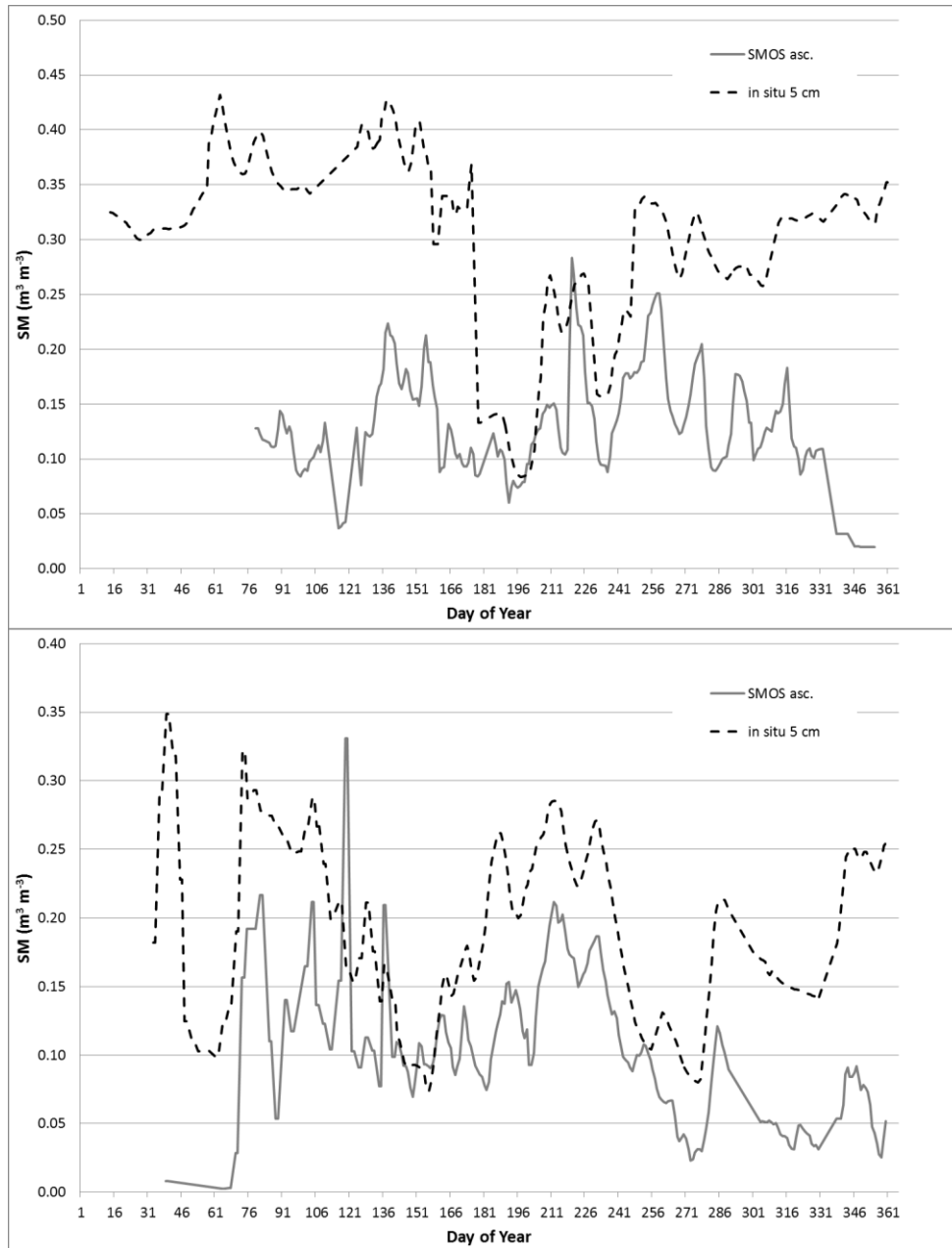


Fig. 19. Soil moisture (SM) for the area of Felin station, 2010 (top figure) and 2011 (bottom figure)

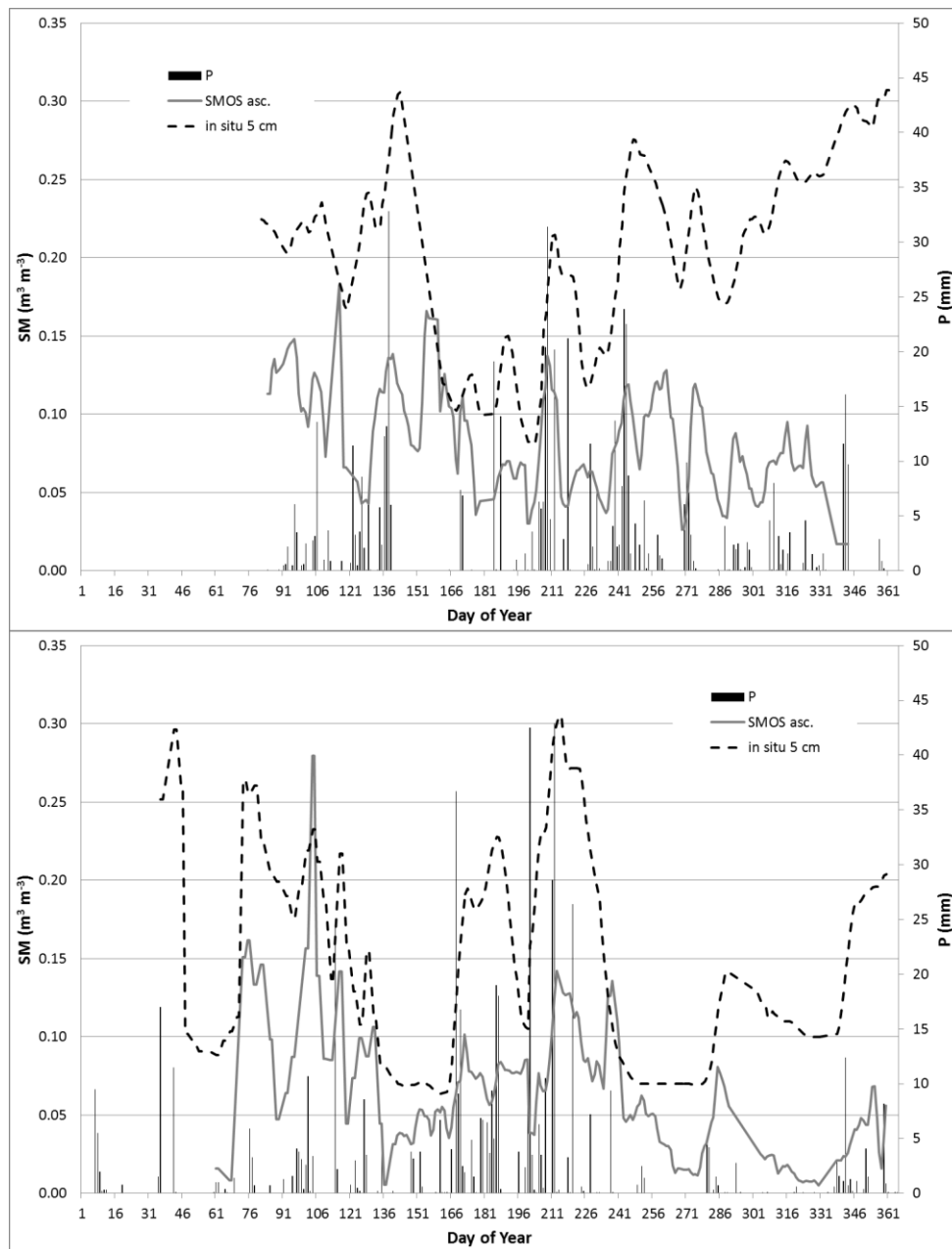


Fig. 20. Soil moisture (SM) and daily rainfall (P) for the area of Janów station, 2010 (top figure) and 2011 (bottom figure)

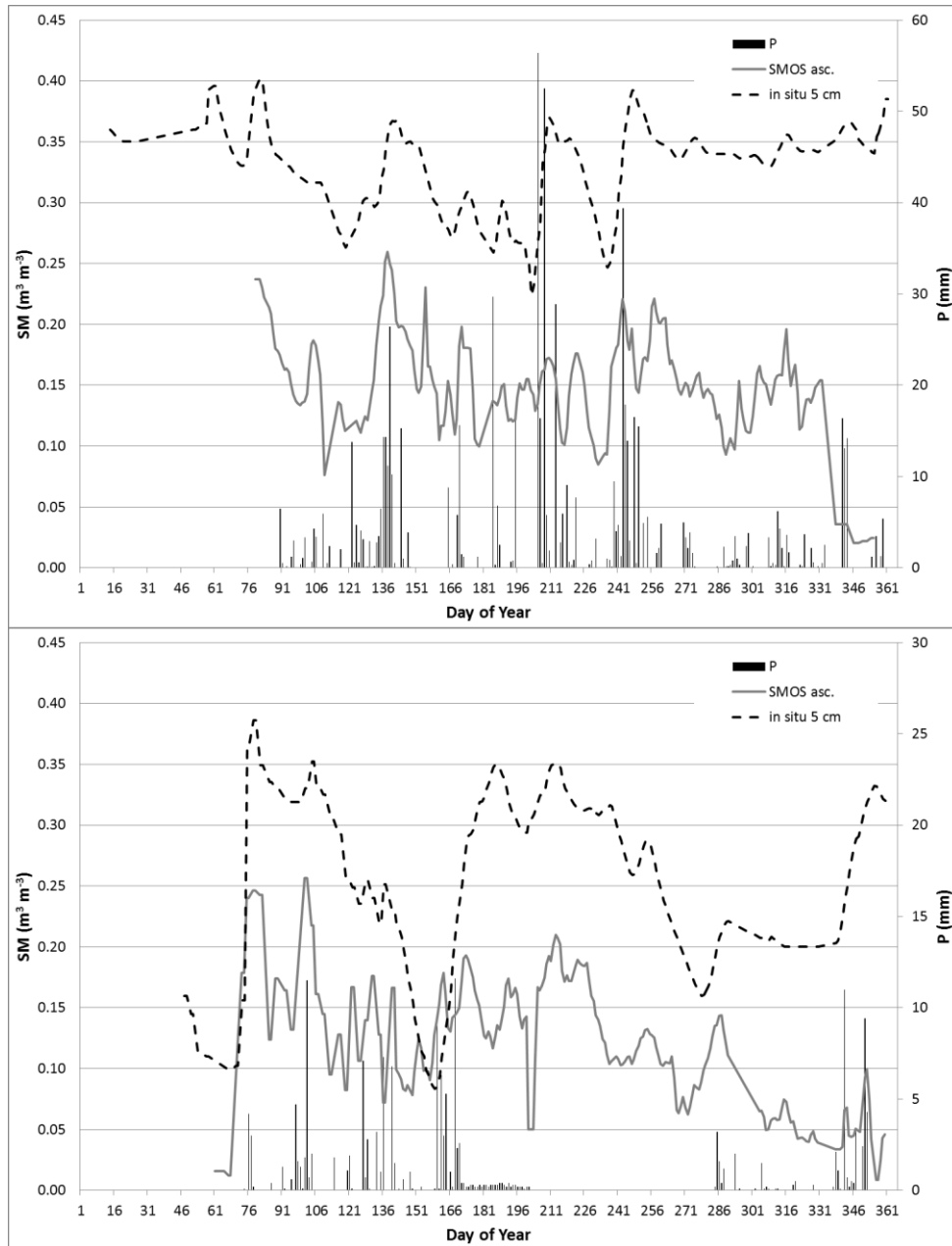


Fig. 21. Soil moisture (SM) and daily rainfall (P) for the area of Majdanek station, 2010 (top figure) and 2011 (bottom figure)

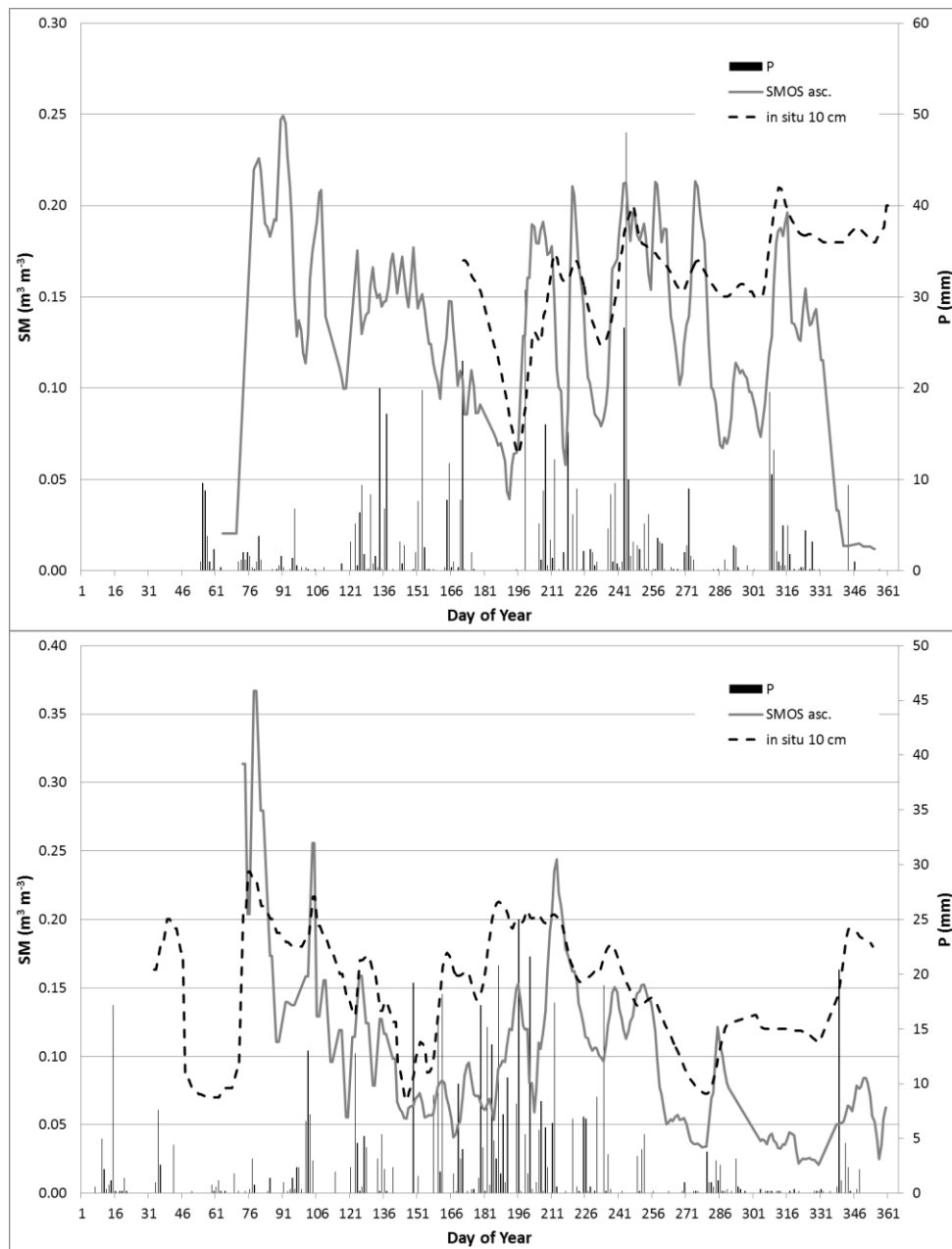


Fig. 22. Soil moisture (SM) and daily rainfall (P) for the area of Trzebieszów station, 2010 (top figure) and 2011 (bottom figure)

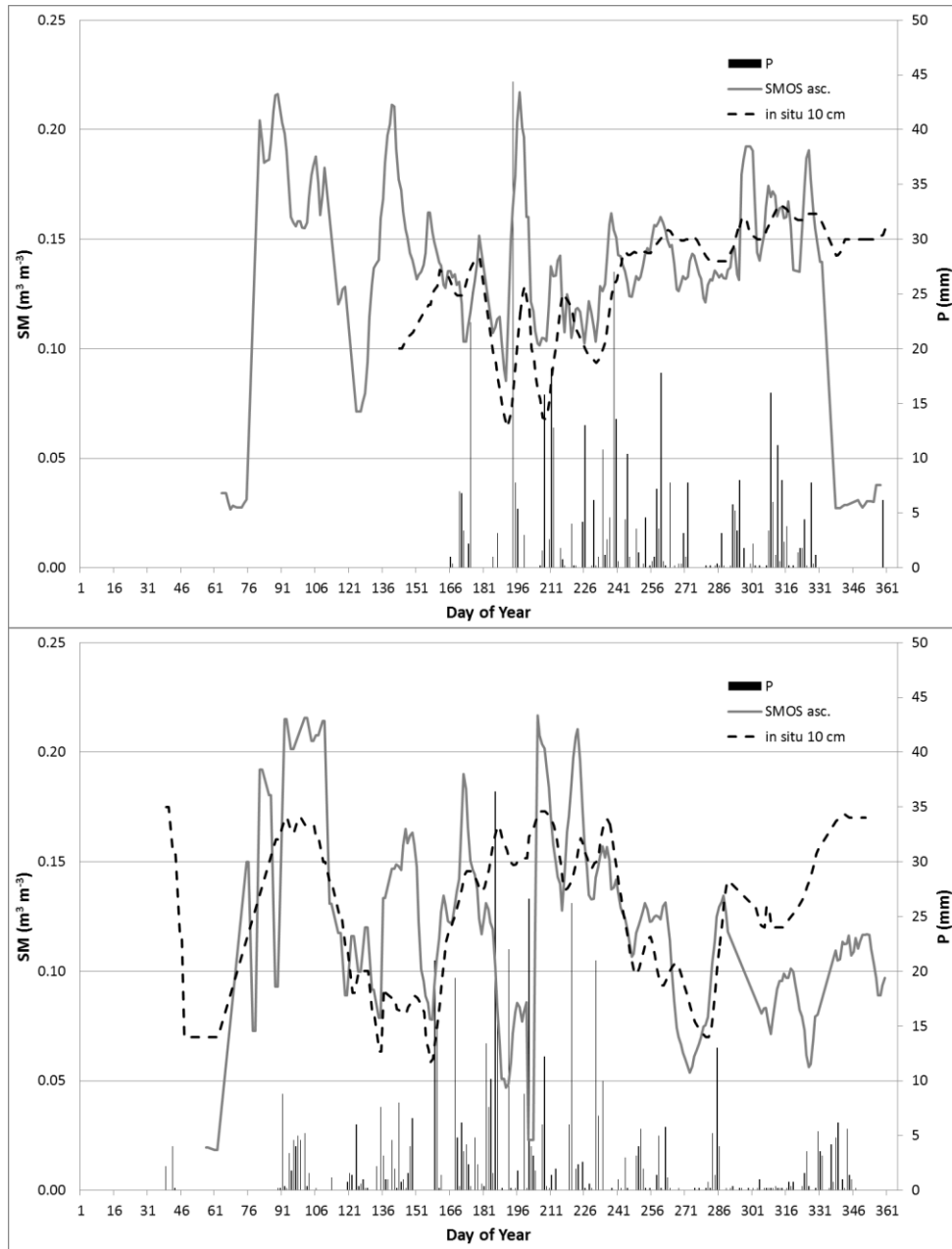


Fig. 23. Soil moisture (SM) and daily rainfall (P) for the area of Wigry station, 2010 (top figure) and 2011 (bottom figure)

From the above comparison of the time series of soil moisture measured by SMOS and rainfall and soil moisture measured *in situ* it can be concluded that there is good compatibility of trends observed from satellites and by the stations. Soil moisture measured at the stations does not always increase with small rainfall; as in the case of high temperature and/or wind, water from rain can quickly evaporate from the surface before it reaches the sensor located at a depth of 5 or 10 cm. Increase in soil moisture, associated with such minor precipitation, can be detected by SMOS which is sensitive to water accumulated even in a very thin surface layer of soil or dew. Because SMOS measures the moisture content of a more dynamic soil surface than buried a little deeper *in situ* sensors, satellite data for both studied years, for all areas, are characterised by higher coefficients of variation than ground-based data. On the other hand, SMOS does not detect rain if it took place after the satellite pass and evaporated before the next measurement. Thus, in the figures of time series there appear places where SMOS supposedly does not respond to rainfall. Trends of SMOS and ground-based soil moistures are sometimes shifted in time because the sensors placed in the soil have a kind of “inertia”: It takes some time before the water from the deeper layers of the soil evaporates into the atmosphere or water from precipitation reaches the sensor. Another factor was also applied averaging, which resulted in smoothing of lines and sometimes in small shifts. The comparison of annual averages revealed that for both examined years soil moisture observed by SMOS was lower than that measured by the ground stations. Most likely this was due to the fact that the satellite observed the surface layer of soil which (if not raining) is usually drier than the deeper layer where the sensors of measuring stations are placed. An example can be the annual averages of soil moisture measured by the station Urszulin which show that soils there are the wettest of all examined soils. However, in the SMOS measurements, the area around this station appeared to have soil moisture below the average. The exception were the areas around stations Biebrza and Wigry, where the average soil moisture measured by SMOS was comparable or larger than the values obtained from the ground stations. This is due to the specific location of those stations. Both lie on small hills, on sandy soil, probably with low water retention (Table 2), in immediate neighbourhood of marshes, swamps or lakes. Because of big pixel size, SMOS satellite covers the wet areas and water bodies around the stations, while the sensors detect small amounts of water stored in the sandy soil in which they are embedded. Good compatibility of trends observed by SMOS and ground-based measurements, and underestimation of soil moisture by SMOS, were observed also during measurements in Australia (Rudiger *et al.* 2011), Germany (Dall’Amico *et al.* 2011), the United States (Al Bitar *et al.* 2011, Jackson *et al.* 2012) and Denmark (Bircher *et al.* 2011). Overes-

timation of soil moisture by SMOS was observed only during the measurement campaign in Africa (Gruhier *et al.* 2012).

For further examination of the relationship between the SMOS satellite measurements and ground-based measurements of soil moisture (made by the stations) scatter plots of these quantities were drawn (Figs. 24-32). For each area of interest, separately for each year, the coefficients of linear regression were calculated and their statistical significances were tested. After that, determination coefficients of the linear model fit were determined.

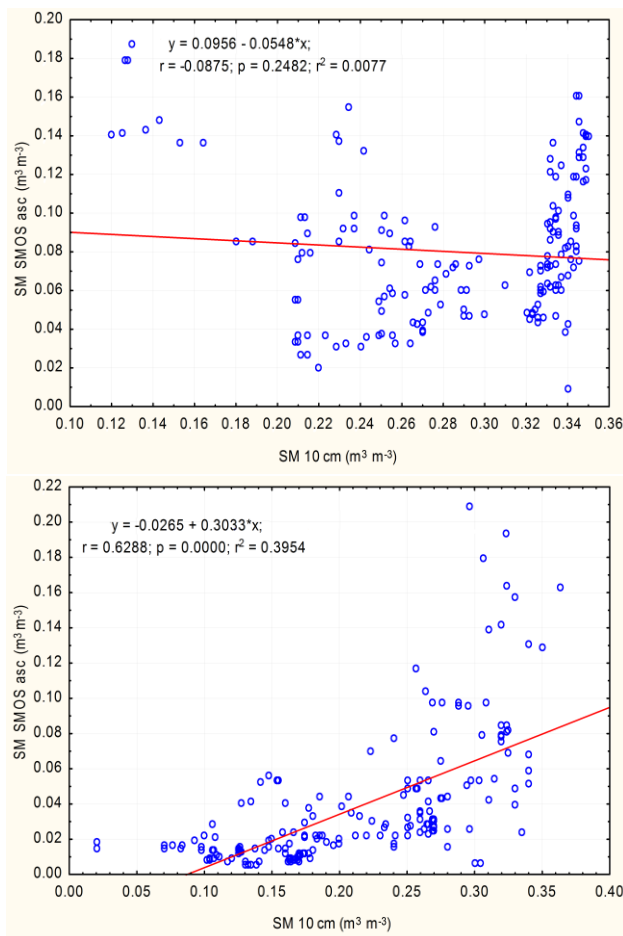


Fig. 24. Scatter plot of soil moisture measured by SMOS (SM SMOS asc) vs. measured 10 cm below ground (SM 10 cm) at station Białowieża in 2010 (top figure) and 2011 (bottom figure) (r – Pearson correlation coefficient, p – probability of regression coefficient statistical insignificance, r^2 – determination coefficient)

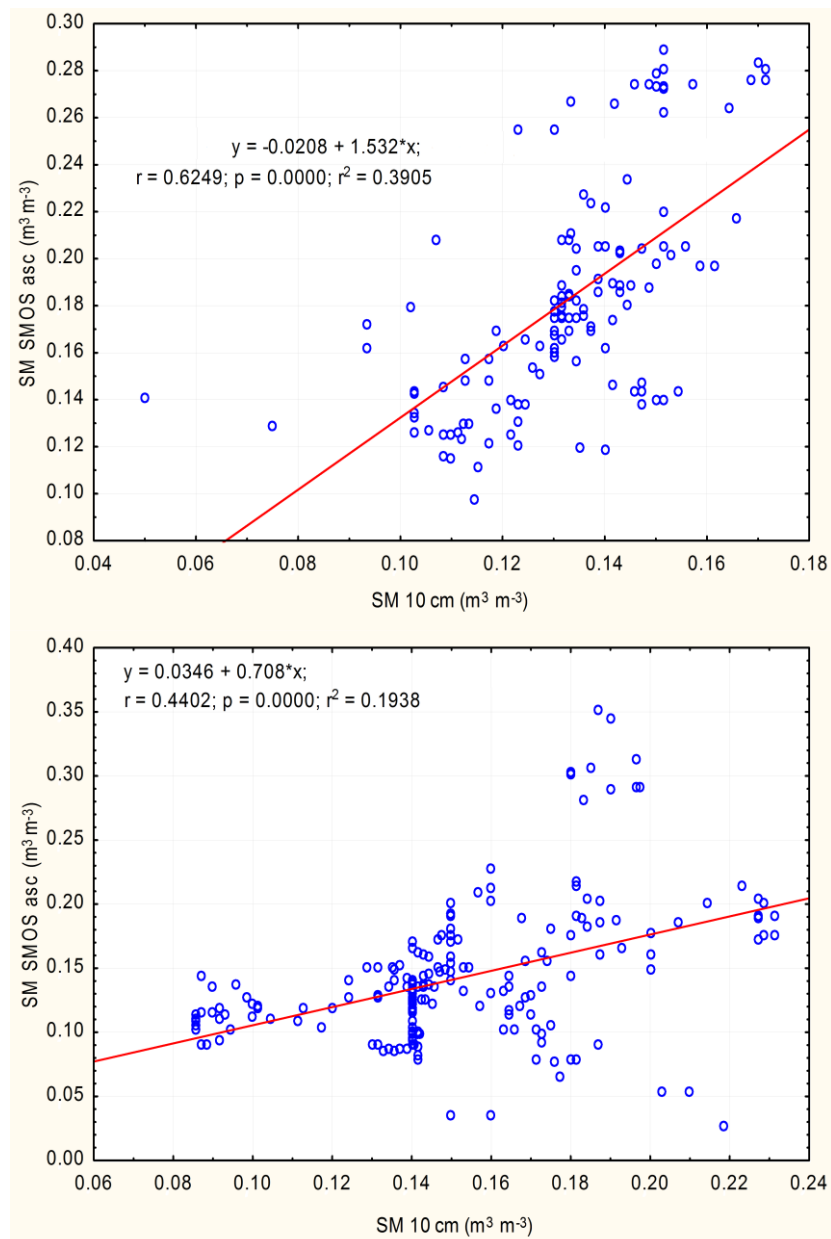


Fig. 25. Scatter plot of soil moisture measured by SMOS (SM SMOS asc) vs. measured 10 cm below ground (SM 10 cm) at station Biebrza in 2010 (top figure) and 2011 (bottom figure) (r – Pearson correlation coefficient, p – probability of regression coefficient statistical insignificance, r^2 – determination coefficient)

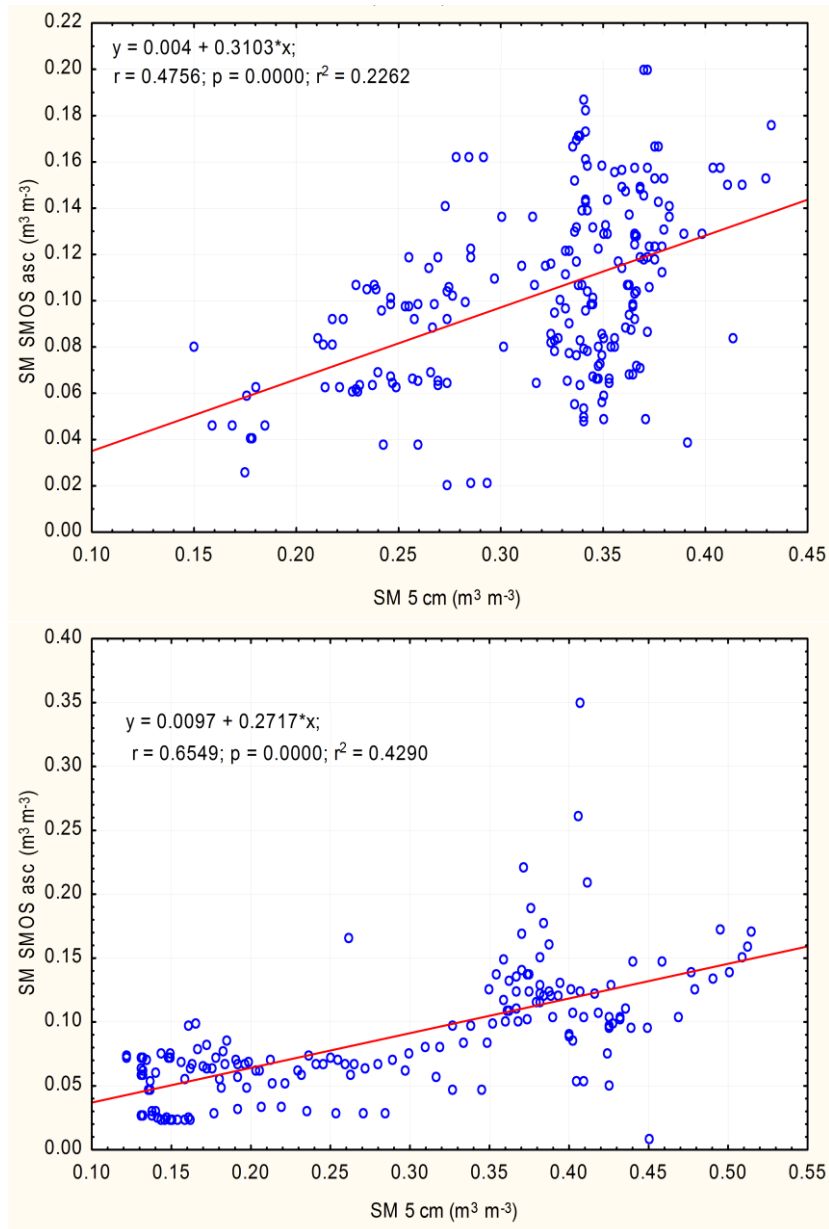


Fig. 26. Scatter plot of soil moisture measured by SMOS (SM SMOS asc) vs. measured 5 cm below ground (SM 5 cm) at station Urszulin in 2010 (top figure) and 2011 (bottom figure) (r – Pearson correlation coefficient, p – probability of regression coefficient statistical insignificance, r^2 – determination coefficient)

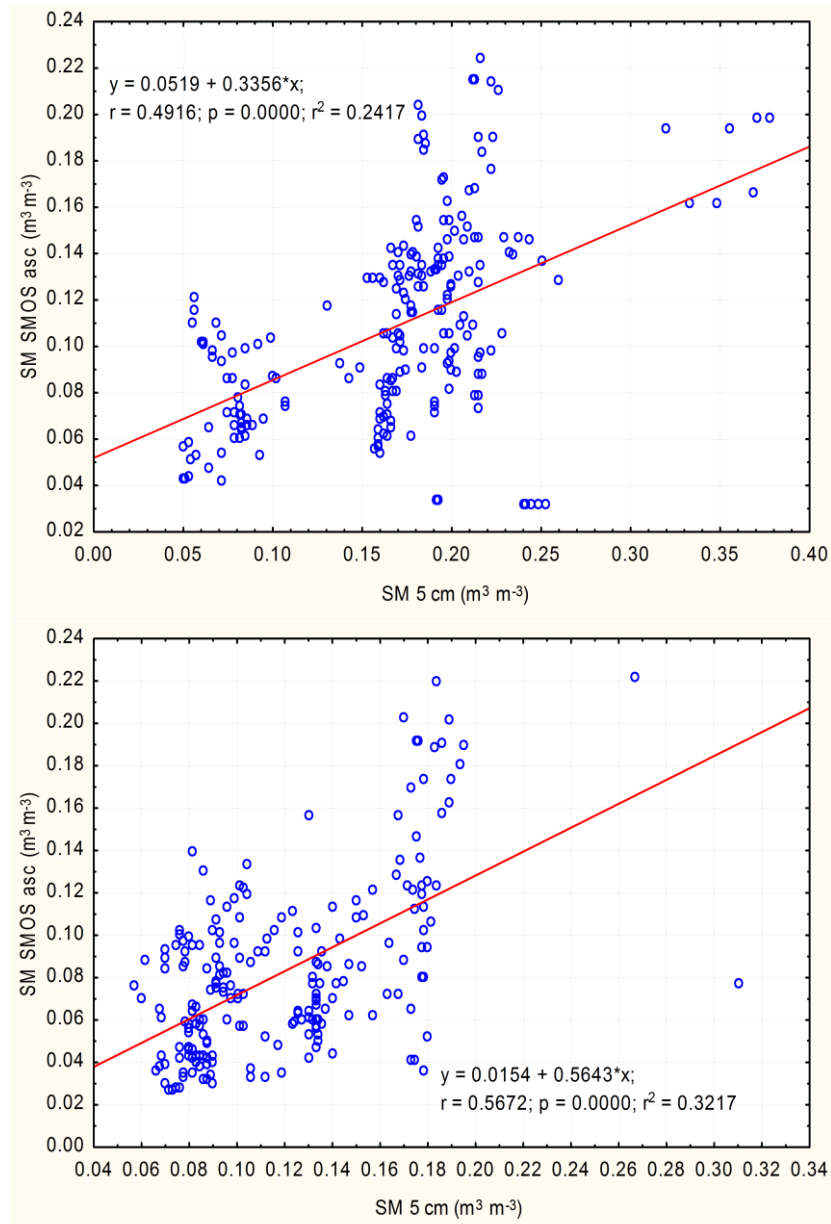


Fig. 27. Scatter plot of soil moisture measured by SMOS (SM SMOS asc) vs. measured 5 cm below ground (SM 5 cm) at station Cicibór in 2010 (top figure) and 2011 (bottom figure) (r – Pearson correlation coefficient, p – probability of regression coefficient statistical insignificance, r^2 – determination coefficient)

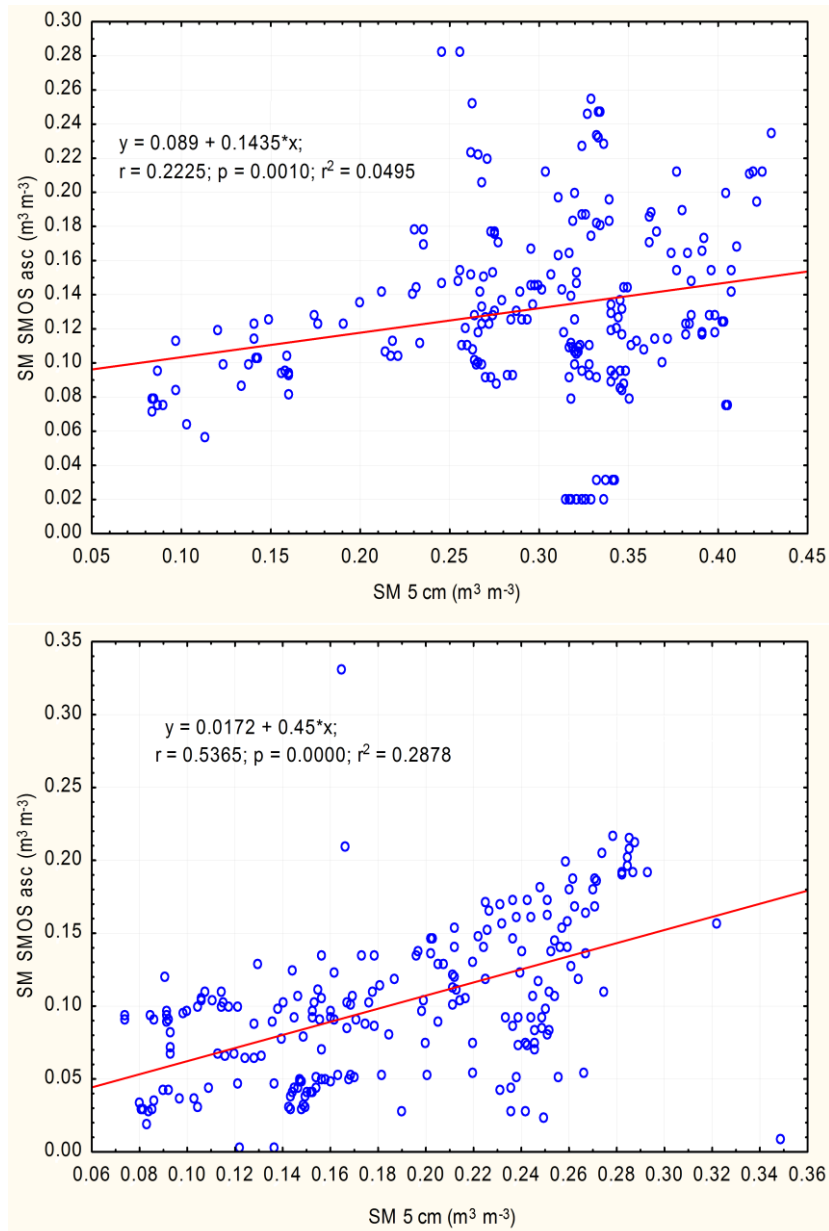


Fig. 28. Scatter plot of soil moisture measured by SMOS (SM SMOS asc) vs. measured 5 cm below ground (SM 5 cm) at station Felin in 2010 (top figure) and 2011 (bottom figure) (r – Pearson correlation coefficient, p – probability of regression coefficient statistical insignificance, r^2 – determination coefficient)

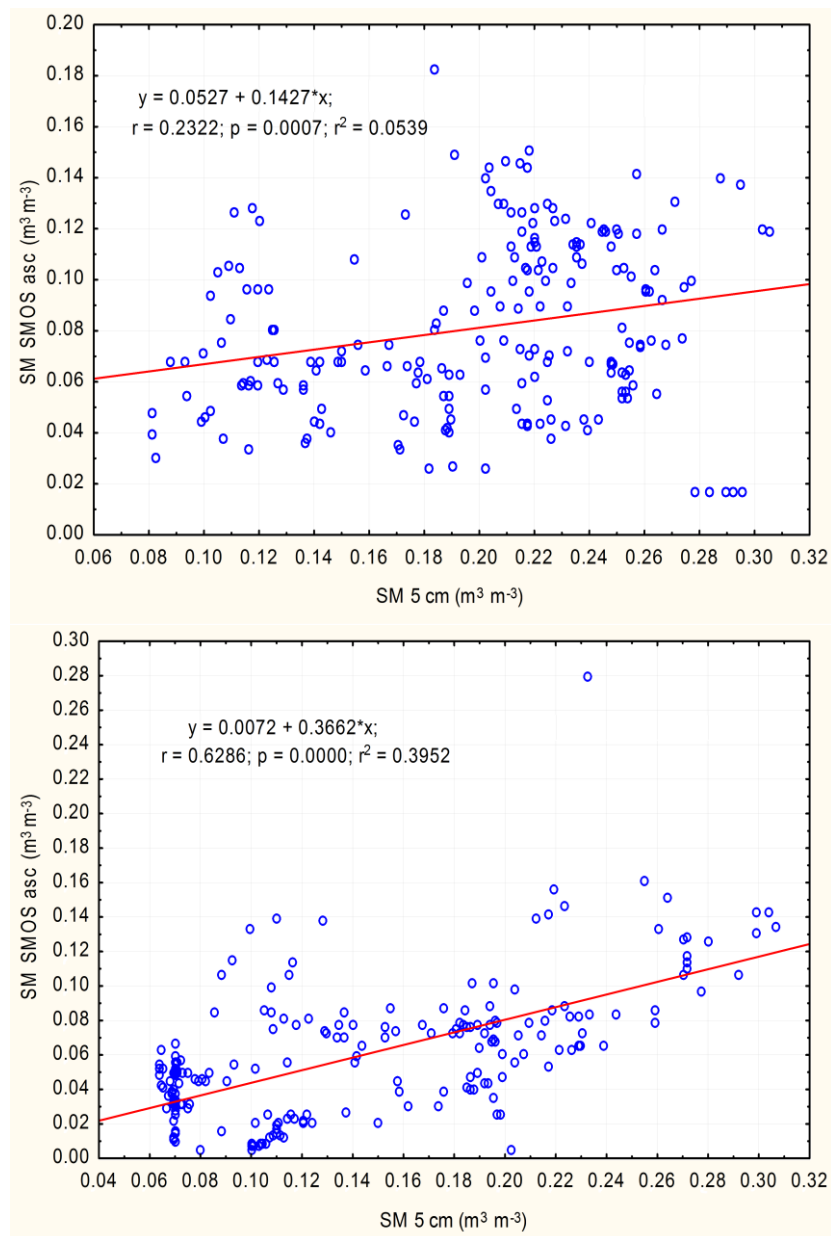


Fig. 29. Scatter plot of soil moisture measured by SMOS (SM SMOS asc) vs. measured 5 cm below ground (SM 5 cm) at station Janów in 2010 (top figure) and 2011 (bottom figure) (r – Pearson correlation coefficient, p – probability of regression coefficient statistical insignificance, r^2 – determination coefficient)

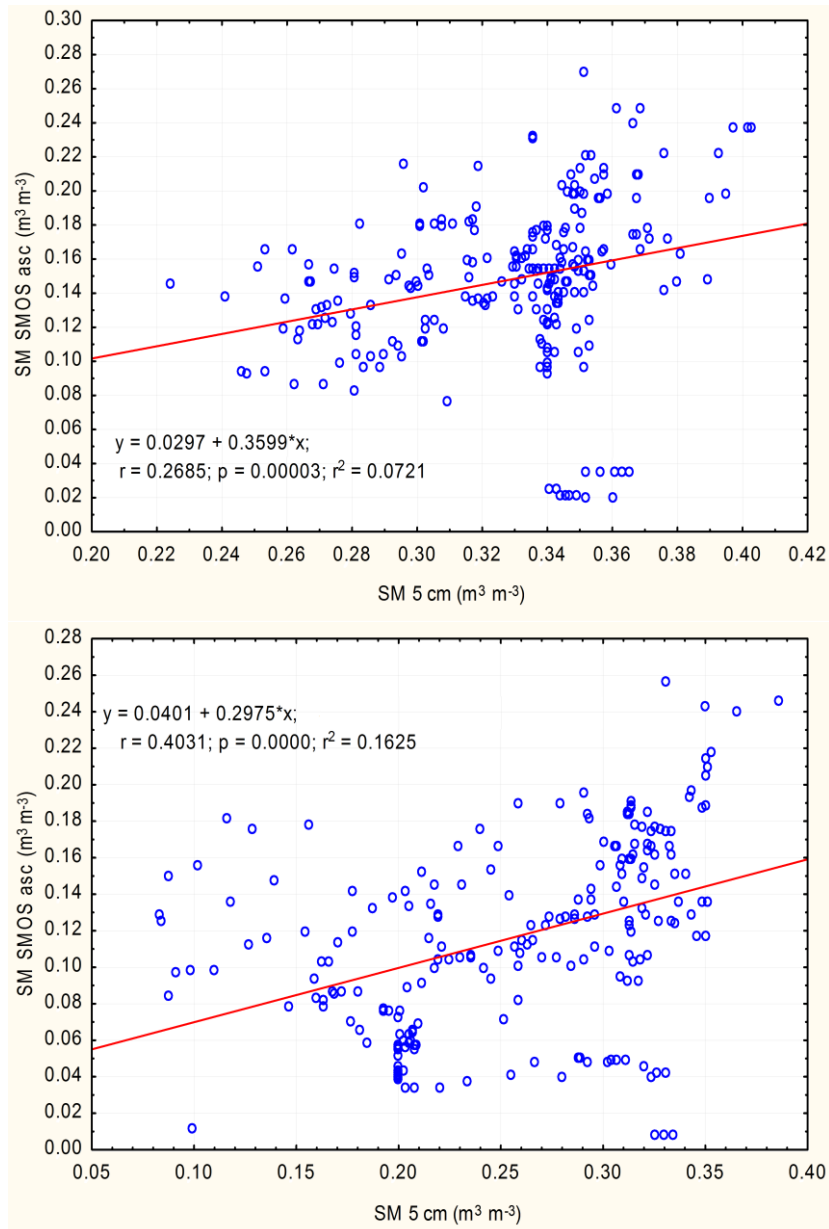


Fig. 30. Scatter plot of soil moisture measured by SMOS (SM SMOS asc) vs. measured 5 cm below ground (SM 5 cm) at station Majdanek in 2010 (top figure) and 2011 (bottom figure) (r – Pearson correlation coefficient, p – probability of regression coefficient statistical insignificance, r^2 – determination coefficient)

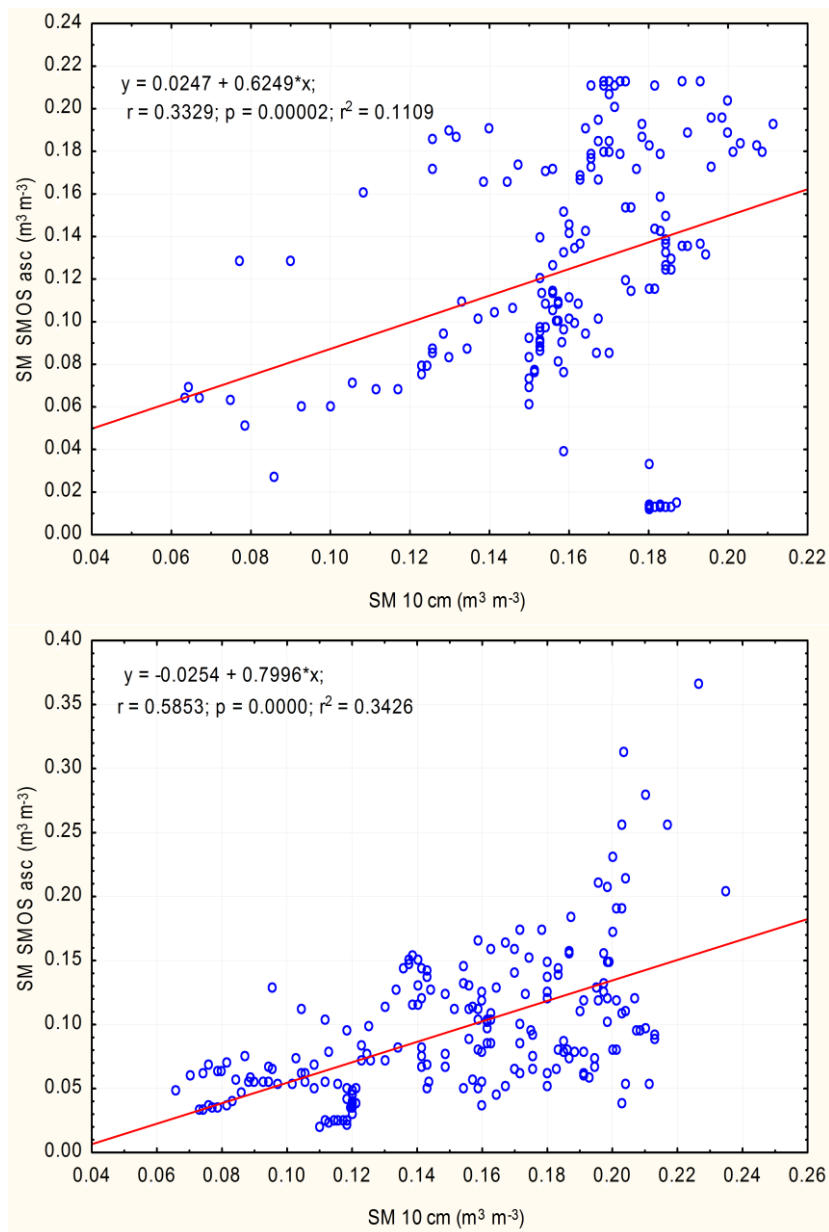


Fig. 31. Scatter plot of soil moisture measured by SMOS (SM SMOS asc) vs. measured 10 cm below ground (SM 10 cm) at station Trzebieszów in 2010 (top figure) and 2011 (bottom figure) (r – Pearson correlation coefficient, p – probability of regression coefficient statistical insignificance, r^2 – determination coefficient)

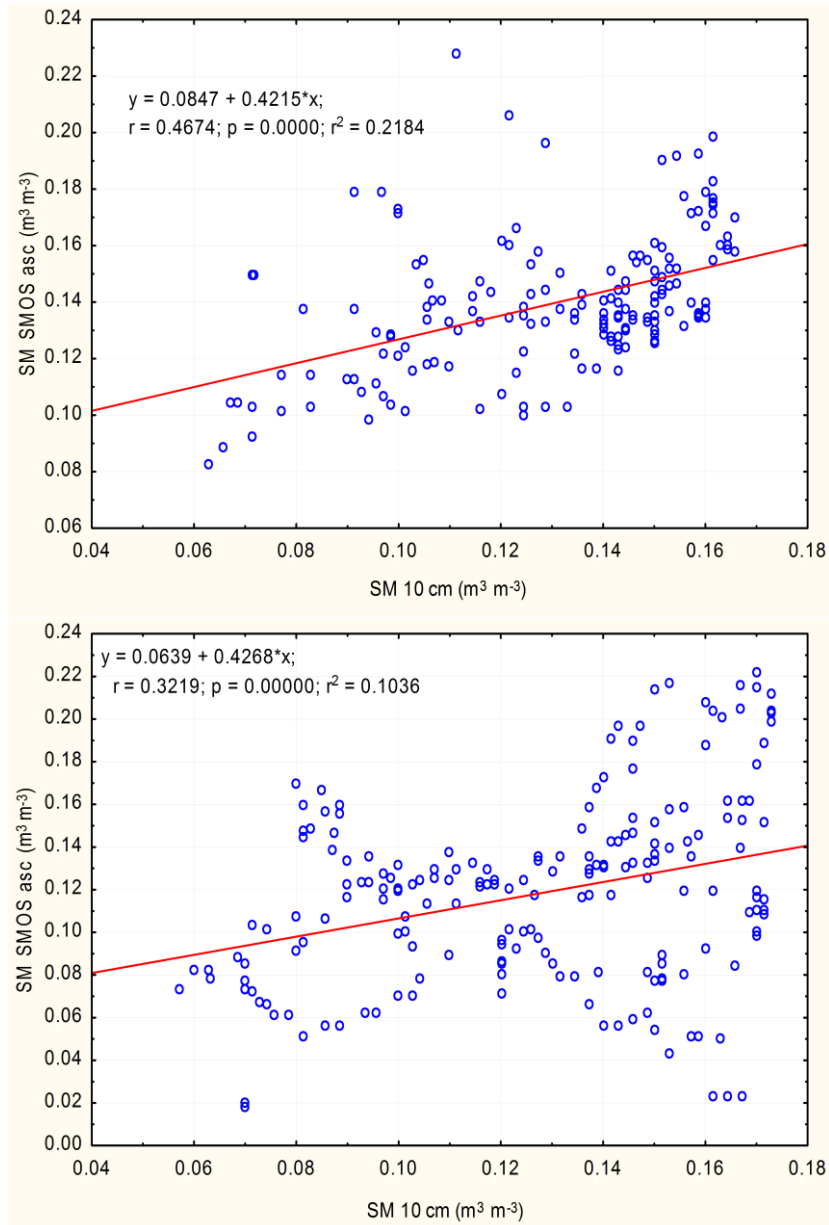


Fig. 32. Scatter plot of soil moisture measured by SMOS (SM SMOS asc) vs. measured 10 cm below ground (SM 10 cm) at station Wigry in 2010 (top figure) and 2011 (bottom figure) (r – Pearson correlation coefficient, p – probability of regression coefficient statistical insignificance, r^2 – determination coefficient)

The obtained linear regression coefficients were positive and statistically significant at a high level of significance ($p < 0.01$). This means that with an increase in soil moisture measured by ground-based measurement methods soil moisture observed by SMOS also increases, and this claim is reliable for most of the stations. The exception was the Białowieża station in 2010, where the linear regression coefficient was negative and statistically insignificant. This was most likely due to the location of the station in the Białowieża National Park. There are dense forests with old and tall trees. In such areas, the SMOS algorithm in 2010 did not work well (Mahmoodi 2011), however, in 2011 it was improved, as evidenced by the better compatibility of the results obtained from the same area a year later. The improved algorithm meant that for most of the investigated areas the determination coefficients were higher in 2011. For the areas of Białowieża, Biebrza, Urszulin, Cicibór, Janów and Trzebieszów, the values of determination coefficients reached the range of 0.32-0.42. This means a weak correlation of ground and satellite measurements, but these values are comparable with those obtained in other experiments of this type (Al Bitar *et al.* 2011, Bircher *et al.* 2011, Dall'Amico *et al.* 2011, Gruhier *et al.* 2012, Jackson *et al.* 2012), in which the obtained coefficients of determination were in the range of 0.40-0.62, but using shorter series of measurement to which it is usually easier to fit a regression model.

Discrepancies between the ground and SMOS measurements arise from many reasons. The first, and probably most important, is the effect of scale. SMOS measurements include areas with approximate minimal dimensions of 45×45 km. Each such a large area of land, especially in Europe, is very heterogeneous in terms of land cover, soil type and often topography. This has an impact on the high variability of soil moisture within such an area. For this reason, a single measuring station, even at high measurement accuracy, can hardly be representative of the SMOS pixel, at least at such a large variation which occurs in Europe. Another reason for the discrepancy is different depths of measurement. SMOS measures the moisture content of the surface, a very dynamic layer of soil. Satellite measurement includes a depth which varies with the moisture, soil type and other factors. It reaches a layer maximum 5 cm in depth (Escorihuela *et al.* 2010), while the shallowest sensors of measuring stations are placed at a depth of 5 or 10 cm. Deeper dynamics is smaller, which was discussed earlier. Discrepancies also arise with different methods of measurement: SMOS is a passive interferometer (radiometer), located at the level of the Earth's orbit, and thus sensitive to interferences. SMOS algorithm uses multiple external data which may also be affected by errors or insufficient accuracy, for example the surface temperature needed for the calculations of soil moisture is not measured physically, but modelled (ECMWF 2007, ECOCLIMAP 2010, Mahmoodi 2011). The data coming from ground-based, *in situ* measurements of soil moisture are collected by active sen-

sors, sensitive to physical and chemical parameters of the soil. Hence, errors can be caused by imperfections in the calibration, poor installation or sensor failures. Reasons for the differences are certainly much more and require further research.

SMOS satellite measures large areas, but so far it was not examined at on what depth and not confirmed practically with what accuracy. Ground stations measure soil moisture accurately, which is easy to verify, but within a small area.

3.5. Surface soil moisture assessment using ASAR

The study used a radar image of the eastern part of Poland made by the ASAR instrument on 30/08/2007, with a resolution of 30 m. It was an APP (Alternated Partial Polarisation) scene, i.e. with two switchable polarisations.

For analyses, the area of the image covering a part of the Polesie region was selected. The data had very inaccurately assigned spatial coordinates, so the first step required undergoing a process of geolocation, i.e. setting the correct geographic coordinates: The data were visualised in the BEAM software. Then, twenty clearly visible characteristic elements of the radar image were selected, such as bends of the coastline of lakes and forests border folds. After finding the same places in the Google Maps optical images (Google Maps 2012), it was possible to assign them to the correct geographic coordinates. Knowing the location of these points, using the BEAM, on the remaining pixels in the ASAR image a projection on the grid coordinates in WGS-84 datum was carried out. The approximation of the positions was made using a third degree polynomial function. Correctness of geolocation was checked by selecting the next twenty characteristic points occurring on both the ASAR image and the optical image from Google Maps and comparing the coordinates. The resulting accuracy was found satisfactory, since discrepancies usually do not exceed 30 meters. The biggest errors of geolocation (several tens of meters) appeared at the edges of the considered part of ASAR image, which anyway were cut to obtain a rectangular shape. After that operation, the remaining scene covered an area of latitudes from 51°20' N to 51°29' N and longitudes of 23°09' E to 23°21' E. This area has been of interest for the Institute Agrophysics for many years. A significant number of ground measurements have been carried out there, and the agrometeorological station Urszulin is located.

The next step in the preparation of ASAR image to obtain data on soil moisture was the conversion (using BEAM program) of each pixel digital value to the backscattering coefficients σ_{HH}^0 and σ_{VV}^0 , in accordance with the procedures contained in ASAR images user manual (ASAR 2007), followed by their expression in decibels.

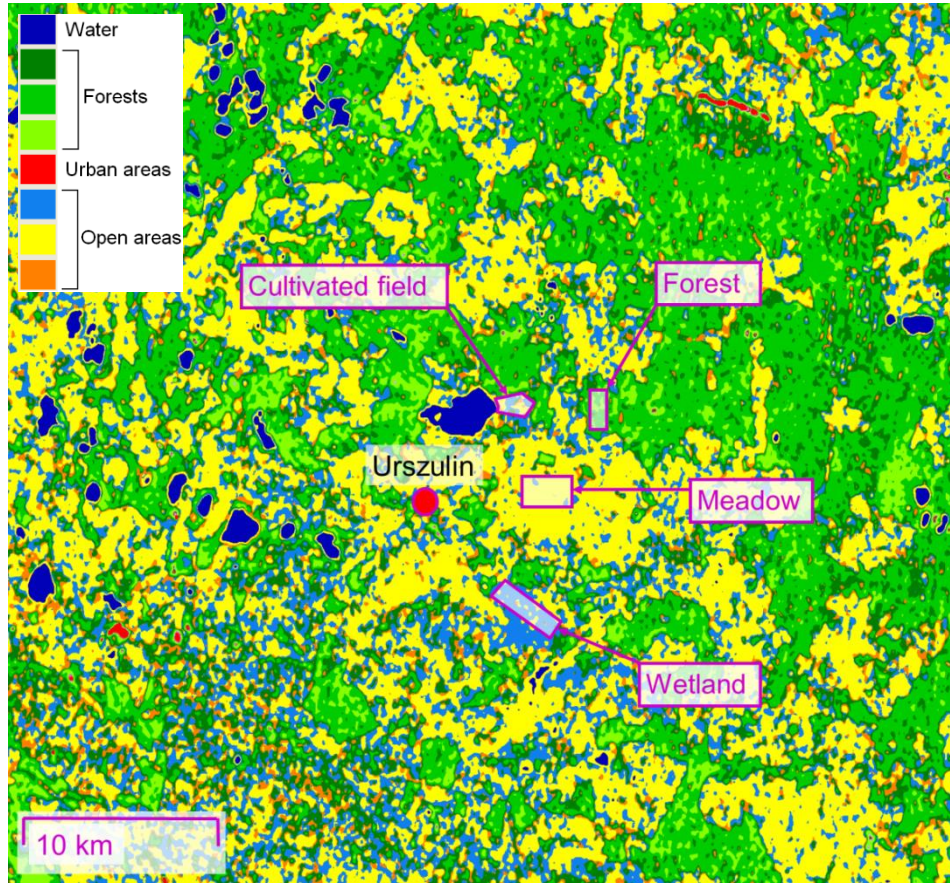


Fig. 33. Satellite map of the West Polesie (Wishart classification (Usovicz *et al.* 2009)) with selected areas for analysis of soil moisture derived from ASAR. Red circle indicates agrometeorological station Urszulin

The dielectric constant of the soil was obtained using the Dubois empirical model (Dubois *et al.* 1995). This model joins the radar backscattering coefficients σ^{θ} for polarizations HH and VV, the incidence angle α of the radar beam, the real part of the dielectric constant of the soil ε , length of the applied electromagnetic wave λ and surface roughness ks , using two equations:

$$\sigma_{vv}^{\theta} = 10^{-2.37 \frac{\cos^3 \alpha}{\sin^3 \alpha}} 10^{0.046 \varepsilon \tan \alpha} (ks \cdot \sin^3 \alpha)^{-1.1} \lambda^{0.7}, \quad (51)$$

$$\sigma_{HH}^0 = 10^{-2.75 \frac{\cos^{1.5} \alpha}{\sin^5 \alpha}} 10^{0.028 \varepsilon \tan \alpha} (ks \cdot \sin^{1.4} \alpha) \lambda^{0.7}. \quad (52)$$

Using BEAM, applying simple mathematical operations (López-Martínez *et al.* 2005), dielectric constant of the soil corresponding to each ASAR pixel was calculated, despite not knowing the surface roughness ks . The Dubois model can be used only for areas satisfying the condition

$$\frac{\sigma_{HH}^0}{\sigma_{VV}^0} < 1. \quad (53)$$

Pixels that did not meet the above condition were not taken into account in further considerations. The Dubois model cannot also be applied for areas covered with a very dense or thick layer of vegetation, or with a large surface roughness. This limitation provides the criterion

$$\frac{\sigma_{HV}^0}{\sigma_{VV}^0} < -11. \quad (54)$$

Unfortunately, the last condition could not be used because examined radar image did not have data required to calculate the σ_{HV}^0 . According to the literature (Dubois *et al.* 1995, López-Martínez *et al.* 2005) the Dubois model works well in areas with low and not very dense layer of vegetation, for which the vegetation index $NDVI < 0.4$. From the resultant dielectric constant (ε), soil moisture (SM) was calculated. This was done by finding the roots of the third degree polynomial which is the Topps formula (Topp *et al.* 1980)

$$\varepsilon = 3.03 + 9.3SM + 146SM^2 - 76.7SM^3. \quad (55)$$

This formula was used because it combines the soil moisture with its dielectric constant in a simple manner. It does not require the information about the amount of bound water, the soil density or porosity, which would be very difficult to obtain, especially for such large and variable regions as those contained in the ASAR radar image used. Of course, the ease of application of the above formula is reflected in its moderate accuracy.

For further studies four significantly different areas of the radar image were selected, known from the direct inspection of the area: swamp Bagno Bubnów, meadow Krowie Bagno, forest in the vicinity of the village Dominiczyn and a set of cultivated fields in the surroundings of Wytyczno village (Fig. 33). The resulting distributions of soil moisture (using IDW estimation) are shown in Figures 34

to 37. All obtained spatial distributions are similar to noise; there are no specific structures or bigger areas with high or low soil moisture. This is most likely the effect of the impact of the vegetation layer growing on the soil, but also of the variability of land, soil type and the amount of water contained therein. The calculated moisture of soil surface layer of each of these areas was subjected to statistical analysis, the results of which are presented in Table 5.

Table 5. Selected descriptive statistics calculated on the basis of ASAR soil moisture data for the studied areas

Statistical measure	Studied area			
	cultivated fields	forest	meadow	swamp
Mean ($\text{m}^3 \text{m}^{-3}$)	0.085	0.083	0.088	0.093
Number of pixels	3103	1259	1928	2295
Coefficient of variation CV (%)	35	45	30	32
Minimum ($\text{m}^3 \text{m}^{-3}$)	0.003	0.003	0.027	0.016
Maximum ($\text{m}^3 \text{m}^{-3}$)	0.211	0.214	0.187	0.236
Skewness before/after transformation	0.53/0.07	0.41/-0.02	0.58/-0.16	0.44/0.04
Kurtosis before/after transformation	0.30/-0.02	-0.36/-0.55	0.04/-0.17	-0.03/0.40

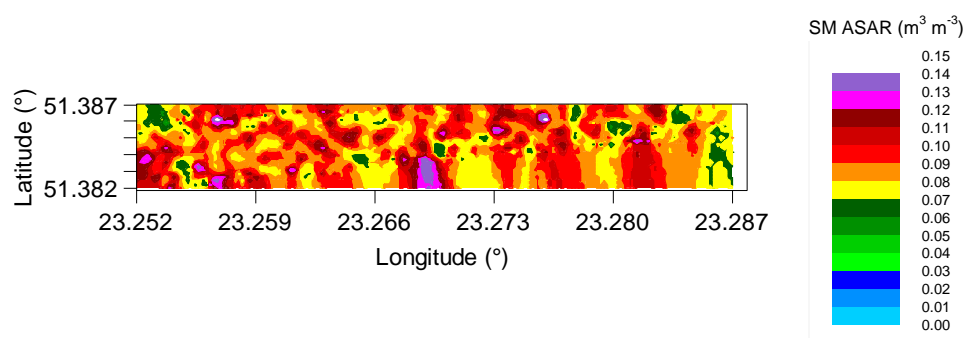


Fig. 34. Spatial distribution of soil moisture calculated from ASAR data (SM ASAR) on 30/08/2007 in Bagno Bublów swamp

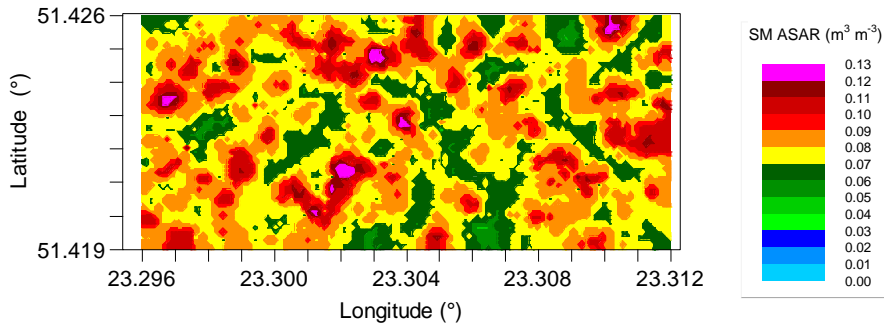


Fig. 35. Spatial distribution of soil moisture calculated from ASAR data (SM ASAR) on 30/08/2007 in Krowie Bagno meadow

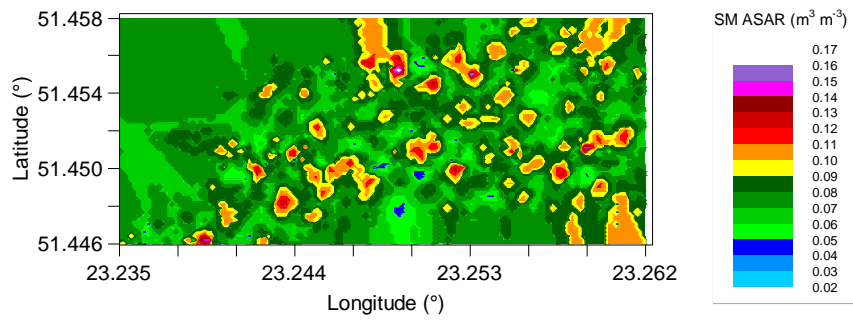


Fig. 36. Spatial distribution of soil moisture calculated from ASAR data (SM ASAR) on 30/08/2007 in the area of cultivated fields near Wytyczno village

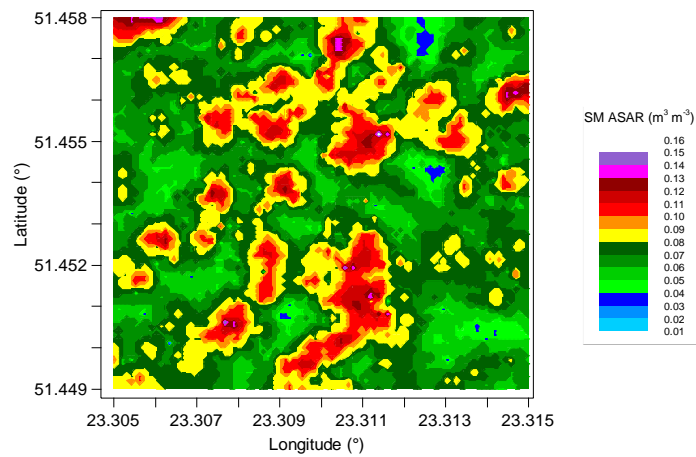


Fig. 37. Spatial distribution of soil moisture calculated from ASAR data (SM ASAR) on 30/08/2007 in the area of forest near Dominiczyn village

The swamp test area was characterised by the largest maximum and the highest average soil moisture. Other areas have similar, lower than swamp, soil moisture. In the area of tested forest, the largest coefficient of variation (CV) was observed. This can be interpreted as a large variation in soil moisture, but most likely it is the result of not applying the criterion of low vegetation (inequality 54). The forest is a thick layer of plants with very variable surface, and if it had been possible to check the condition (54), probably that area would have been rejected as a place where the Dubois model should not be used. The smallest CV was observed on the meadow, which indicates that this area was the most isotropic among all the examined areas. This is probably because the meadow is very flat and entirely covered with a similar type of vegetation, so it could be expected that there will be uniform distribution of soil moisture. All the tested areas showed a positive skewness of soil moisture statistical distributions, so they were right-skewed. Statistical distributions for the cultivated fields and meadow were leptokurtic (positive kurtosis), while for the forest and swamp – platykurtic (negative kurtosis). Because of the asymmetry and non-zero kurtosis, soil moisture data were subjected to appropriate transformation in order to bring them closer to Gaussian distributions, to fulfil the basic assumptions of geostatistical analysis. When choosing the type of transform, particular attention was paid to minimising the skewness (even at the expense of increasing kurtosis), because the lack of symmetry of distribution of the tested dataset has a strong destructive impact on the correctness of the subsequent geostatistical concluding. Data on soil moisture from the areas of the examined fields, forest and meadow were treated by a logarithmic transform, while the swamp – by square root transformation. Spatial distributions of soil moisture were tested for the detection of trends. The analysis was performed for each area separately and did not reveal significant trends. For each of the studied areas, it could be assumed that the soil moisture distributions satisfy the condition of ergodicity and quasi-stationarity required for geostatistical analysis (Gotway and Hergert 1997). Spatial variation was examined using semivariograms. Semivariance analysis was performed to detect the surface anisotropy of the distribution of soil moisture. In all four studied areas, the directions of the smallest anisotropies, then values of nuggets (C_0), sills ($C+C_0$) and apparent ranges (A) were determined. These values are shown in Table 6. In the next step, theoretical models were fitted to the calculated soil moisture semivariograms and their matching parameters were determined: coefficients of determination (R^2) and residual sums of squares (RSS) (Tab. 6).

Table 6. Selected geostatistical parameters calculated from ASAR soil moisture data for the studied areas

Semivariogram parameter	Examined area			
	Cultivated fields	Forest	Meadow	Swamp
Theoretical model name	pure nugget	Gaussian	spherical	exponential
R ²	0.535	0.224	0.138	0.039
RSS	2.392×10 ⁻⁴	9.642×10 ⁻⁵	2.164×10 ⁻⁶	2.288×10 ⁻⁶
Apparent range (°)*	0.0280	0.0003	0.0005	0.0012
Nugget	0.0242	0.0075	0.0083	0.0006
Sill	0.0242	0.0421	0.0896	0.0027

*At latitudes of Poland, 1° corresponds to a linear distance of approximately 110 km.

The semivariograms for the area of forest and meadow were characterised by very fast saturation, at distances of 0.0003° and 0.0005° respectively, which at Polish latitudes corresponds to a distance of approximately 40 and 60 m. This is a distance equal to approximately the size of one or two ASAR pixels. With such a resolution of tested image (30 m), it can be assumed that using it, it is not possible to study more detailed spatial distributions of soil moisture for the examined forest and meadow. The very short spatial dependence in the forest was caused most likely by a strong impact of vegetation layer growing on the ground. As mentioned before, to obtain information on soil moisture in a forest the Dubois model is not appropriate. The ASAR radar data used, taken on 30/08/2007, does not provide the opportunity of use another model because of the lack of some polarisations. Soil moisture obtained for the forest area probably did not coincide with the reality and was falsified by high trees growing on the ground. For the the studied area of cultivated fields, for which semivariogram is described by a pure nugget model, there was no spatial dependence in the distribution of soil moisture. Clearest spatial dependence was present in the area of the tested swamp. Its length was 0.0012°, which corresponds to approx. 130 m. This relationship was also quite short, of the order of four ASAR pixels. Swamp has the longest range of autocorrelation, probably because it is the area with the hydrological processes the least disturbed by human activity; it is in fact a part of the swamp Bagno Bębnow reservoir, protected under the Poleski National Park (WIOSL 2010).

So short (or lack of) soil moisture spatial dependence for all four areas indicates a high variability of studied regions, as well as a strong influence of vegetation layer. The latter effect is indeed minimised by using the appropriate radar

frequency, but unfortunately still large. Short spatial relationships between soil moisture values in each point of the radar image make descriptive statistics sufficient to describe examined areas: mean, coefficient of variation (CV), minimum and maximum are presented in Table 5.

3.6. Soil moisture assessment using ground measurements and ASAR

On the same day on which the examined ASAR radar image was made, ground-based measurements of surface soil moisture were conducted. 72 measurements of soil moisture (Fig. 38), using TDR probes, covering part of the West Polesie, including areas of previously studied swamp and meadow (Fig. 33), were made. Coordinates were determined using a GPS device in the WGS-84 datum. The collected data were subjected to statistical and geostatistical analysis. Average soil moisture content for the whole area was $0.117 \text{ m}^3 \text{ m}^{-3}$, minimal $0.040 \text{ m}^3 \text{ m}^{-3}$ and maximal $0.547 \text{ m}^3 \text{ m}^{-3}$. With such a large range, the coefficient of variation (CV) was 83%. The statistical distribution of the data was right-skewed (skewness equal to 2.54) and strongly leptokurtic (kurtosis equal to 6.66), so in order to bring it closer to normal distribution a logarithmic transform was applied. After that the skewness and kurtosis reduced to 1.16 and 0.80, respectively. After the analysis of surface semivariance, it was found that there was no significant trend and the smallest anisotropy direction was selected. Then, to the empirical semivariogram, a theoretical model was fitted. The soil moisture distribution semivariogram from that day can be described by a linear model with a sill of 0.371 and a very strong nugget effect ($C_0 = 0.318$). No spatial dependencies made the description of the study area simple: it does not need better statistical descriptors than the average and standard deviation. Using the obtained geostatistical information, by the IDW method, spatial distribution of soil moisture was estimated (Fig. 39). This distribution was island-like; areas with very high soil moisture were separated from each other by dry areas. North-eastern part of the study area was clearly wetter.

In a further part of the investigations, the results of all TDR measurements of soil moisture were compared with the results calculated previously from the ASAR satellite image using the Dubois model and Topps model. Soil moisture data calculated from ASAR image were taken with a spatial accuracy equal to or better than the size of a pixel, i.e. it was assumed that it is reasonable to compare the soil moisture calculated from ASAR pixel with those ground-based measurements that were located within this given pixel. Both sets of points were compared by calculating the linear regression coefficient. This ratio turned out to be negative and close to 0. This would lead to the wrong conclusion that the higher soil moisture calculated from ASAR data, the lower the soil moisture measured *in situ*. Howev-

er, the regression coefficient analysis revealed that it was not statistically significant at the significance level $p = 0.05$, thus taking into account the whole of the study area there can be no correlation of ground-based measurements of soil moisture with ASAR satellite measurements. In a further step of research, the fact was used so that for particular areas the correlations in spatial distributions of soil moisture were short or did not appear at all, for both for the ASAR image and TDR ground-based measurements. To describe the spatial distributions of soil moisture calculated from ASAR image for cultivated fields, meadow, forest and swamp, the mean value and standard deviation were sufficient, the same for ground-based measurements. So the mean values of the ground-based and satellite measurements were calculated and summarised in Table 7. The comparison did not take into account the forest, because of the expected large effect of the vegetation layer, and the area of cultivated fields due to very small amount of ground-based measurements taken there, which would not be representative of such heterogeneous area.

The separation of areas with the same type of land cover gives a slightly better performance than the analysis of the whole area. As one would expect, the swamp turned out to be moister than the meadow, both in the satellite and ground-based measurements, as can be seen from Table 7. Unfortunately, the obtained results were still far from compatibility because soil moisture derived from ASAR data was significantly underestimated compared to that detected in ground-based measurements. This underestimation was probably due to the fact that the reflection or scattering of the radar beam sent by ASAR is sensitive not only to the water present in the soil, but also to the water contained in the plants growing on the tested areas. Vegetation layer can be considered as a mixture of air and plants. Even if the plants contained a lot of water and would have a high dielectric constant, the mixture of air and plants has low density. As a consequence, dielectric constant of such a mixture recorded by radar is small and significantly underestimates dielectric constant of the underlying soil, and consequently the resulting moisture content. Furthermore, the differences between TDR and ASAR measurements may result from the fact that the satellite is measuring the surface, usually drier, soil layer with a thickness of at most 5 cm (ASAR 2007), while the TDR probe used reaches a depth of approximately 10 cm.

Table 7. Mean soil moisture ($\text{m}^3 \text{m}^{-3}$) obtained from ground-based and satellite measurements on 30/08/2007

Technique	Examined area	
	meadow	swamp
ASAR (satellite)	0.088	0.093
TDR (ground-based)	0.137	0.194

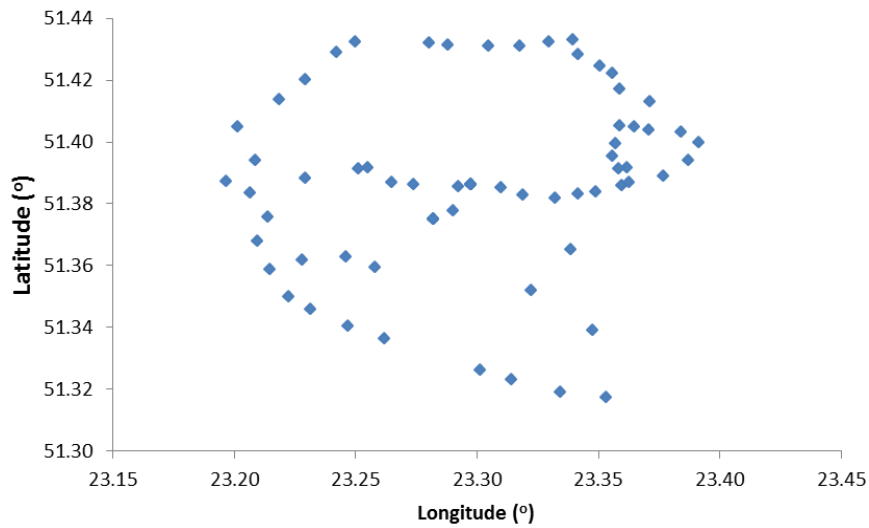


Fig. 38. Distribution of ground-based points on the area of Western Polesie, on the day of ENVISAT satellite passes (30/08/2007)

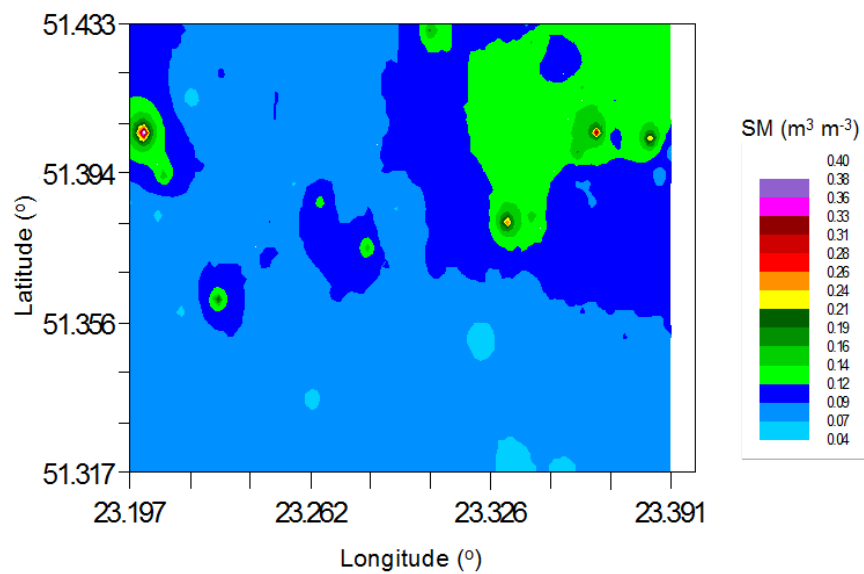


Fig. 39. Soil moisture (SM) distribution on the area of Western Polesie, on the day of ENVISAT satellite pass (30/08/2007). SM was measured by TDR probe

The presumed effect of the vegetation layer on the results may have been large, but insufficient data contained in the examined ASAR image did not allow for the elimination of areas with too thick vegetation layer through the use of condition (54). In order to characterise the vegetation layer, a satellite image made by the MERIS instrument was used. It was of the type MER_FR (Meris Full Resolution) data, i.e. with spatial resolution of 300 m. Out of all the available MERIS photos which include the tested area in West Polesie, the image made on 16/07/2007 was chosen. Although ASAR and MERIS instruments are mounted on the same satellite ENVISAT, MERIS images were closer in time to the ASAR, and ground-based measurements of soil moisture, not covered by clouds that prevent analysis of the vegetation layer parameters, were not available. It was therefore assumed that the vegetation layer of the study area did not change from 16/07/2007 to 30/08/2007. The first step was to check the accuracy of geolocation of selected MERIS image. It was therefore visualised using BEAM, and then the coordinates of the characteristic points in MERIS image and from Google Maps were compared. The examined image has coarse resolution, so coordinates comparison was based mainly on large and highly visible landscape elements (e.g. lakes). With a resolution of 300 m it is difficult to estimate the geolocation error, but from visual comparison it seemed to be correct. Then the MERIS image underwent the necessary adjustments, was checked for the presence of clouds and then the Normalised Difference Vegetation Index (NDVI) was calculated, in accordance with the procedures contained in the BEAM software (BEAM 2007). According to the literature (Dubois *et al.* 1995, López-Martínez *et al.* 2005), the Dubois model, used to determine the dielectric constant of the soil, can be used in areas where $NDVI < 0.4$. Among the 72 measurement points obtained on 30/08/2007, rejected were those located in the area of ASAR pixels which did not meet the condition (53) and MERIS pixels that did not meet the condition of $NDVI < 0.4$. After this operation, data on soil moisture derived from ASAR were compared with data obtained using TDR ground probe, via Statistica software (Fig. 40). Linear regression coefficient was calculated and its statistical significance was tested.

The application of Dubois and then Topps models to the ASAR data overestimated the received soil moisture in relation to the values measured *in situ*, which is consistent with research of other authors (Álvarez-Mozos *et al.* 2007, Hajnsek 2001, Koyama 2012, Leconte *et al.* 2004, McNairn *et al.* 2010). Linear regression coefficient is not statistically significant at the $p = 0.05$ significance level, which is caused, among others, by the small amount of data. This was caused by the application of the radical constraint $NDVI < 0.4$, because of which many of the 72 ground-based measurement points had to be rejected from the analysis. Planning of places where soil moisture was measured during the measurement campaign of 30/08/2007, fulfilling all the requirements of the models at the same time, could

not be done better because the MERIS image was made available by the European Space Agency after the ground measurements conducted in August 2007.

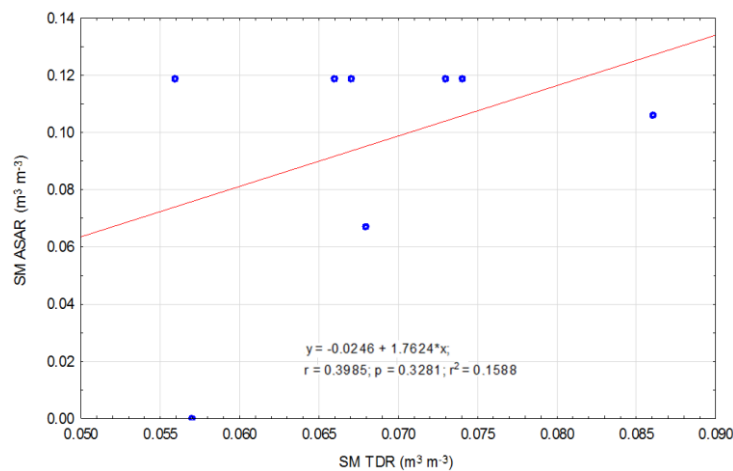


Fig. 40. Comparison of soil moisture measured on Earth (SM TDR) with the modelled soil moisture from satellite data (SM ASAR) (r – Pearson correlation coefficient, p – probability of regression coefficient insignificance, r^2 – coefficient of determination)

The coefficient of determination describing the fit of the linear model to the relationship between soil moisture measured on the ground and from the satellite level is low ($r^2 = 0.16$), however, due to the large number of factors that impact the process, it is the result obtained also by other authors, for example Koyama received $r^2 = 0.18$ (Koyama 2012).

As can be seen from the above considerations, obtaining the correct soil moisture from ASAR image is a non-trivial task. Compatibility of obtained soil moisture with ground-based measurements depends on the type and size of the area selected for analysis. Vegetation has a very large impact on the correctness of the resulting soil moisture.

3.7. The distributions of soil moisture for selected days

In order to investigate the distributions of surface soil moisture for Poland, 11 SMOS satellite images were selected. They were prepared using BEAM software (BEAM 2007), and presented on the Google Earth (Google Earth 2012) background (Fig. 41. up to Fig. 51). Measurements were made by the satellite always between the 3 and 6 am. Particular dates of SMOS measurements were chosen in order to examine the distributions of surface soil moisture during frost, thaw, after

rain, in times of drought and large RFI (Radio Frequency Interferences) (Table 8). Information about those events was obtained by visualising SMOS data and examining time series of soil temperature and moisture and precipitation derived from the network of IA PAS agrometeorological stations. SMOS data selected for analysis were collected in year 2011, since those of 2010 contained a lot of RFI, which is visible in the images as a lack of data. This makes spatial analyses and correct geostatistical inference difficult. Data from 2011 are complete and continuous in space, thanks to the improved conversion algorithm as well as the intervention of the European Space Agency in the offices of the individual countries, responsible for reduction of illegal radio emissions (Oliva *et al.* 2011). In Poland such an entity is the Office of Electronic Communication. SMOS soil moisture data were filtered from RFI by their provider, the Brockmann Consult Company. The most “contaminated” pixels were empty and in those places dark green Google Earth background (Google Earth 2012) is visible. Areas with smaller, but present RFI showed significantly overestimated soil moisture. This can be seen in the image from 22/07/2011 (Fig. 47), when nearly the whole Poland was covered with large RFI and in the north of Berlin there appeared very large, probably falsified soil moisture values. Another reason for the “holes” in the data may be frost or snow lying on the surface of soil. After freezing, water significantly reduces its dielectric constant (Behari 2005), and therefore is invisible to the SMOS soil moisture sensors, sometimes so much that the conversion algorithm returns the value NaN (Not a Number – empty pixel). It is very well seen in the image dated 05/02/2011 (Fig. 41), where only a narrow strip to the north and south of Warsaw and the north-western part of Poland were sufficiently thawed, so that SMOS could depict value of soil moisture there. Picture dated 08/03/2011 (Fig. 42) is characterised by an island-like structure caused by local frosts. The lack of data in the north-eastern and the southern, hilly part of Poland, shows that day frost on these (considered to be cooler) areas, having a wider reach. The next image (Fig. 43) shows as if almost the entire Poland thawed, resulting in increasing amount of data and increase in soil moisture values. Then one could observe the soil drying out after thawing (Fig. 44) and one of the driest days during the growing season (Fig. 45). Later, one can observe quite moist soil after rains in July (Fig. 46) and its gradual drying (Fig. 48, Fig. 49) which eventually led to drought in early November (Fig. 50). On the distribution from 17/12/2011 (Fig. 51.) wetter soil is visible, which was a consequence of rainfall that occurred earlier in the northern and southern parts of Poland, recorded by IA PAS network of agrometeorological stations.

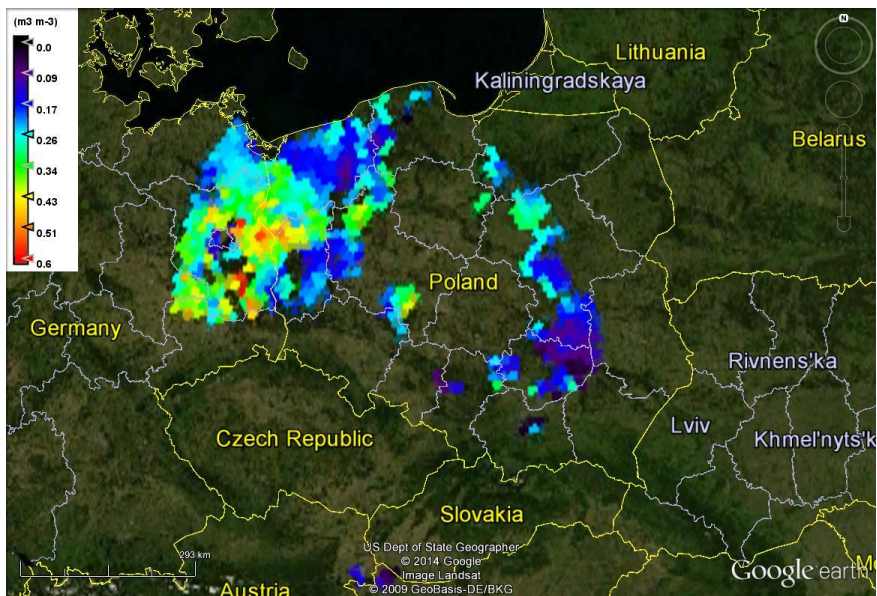


Fig. 41. Distribution of soil moisture at the time of a partial thawing (05/02/2011) on the Google Earth background (Google Earth 2012)

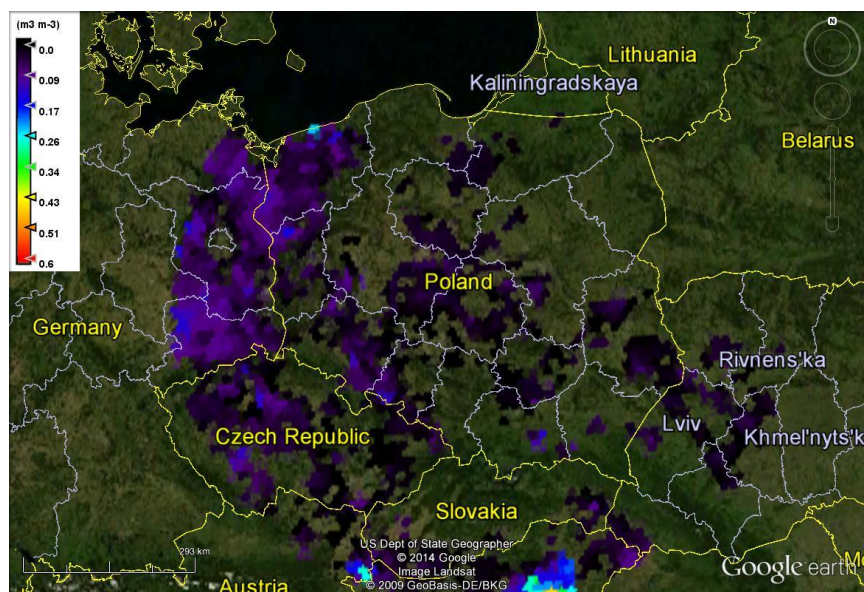


Fig. 42. Distribution of soil moisture during frost (08/03/2011) on the Google Earth background (Google Earth 2012)

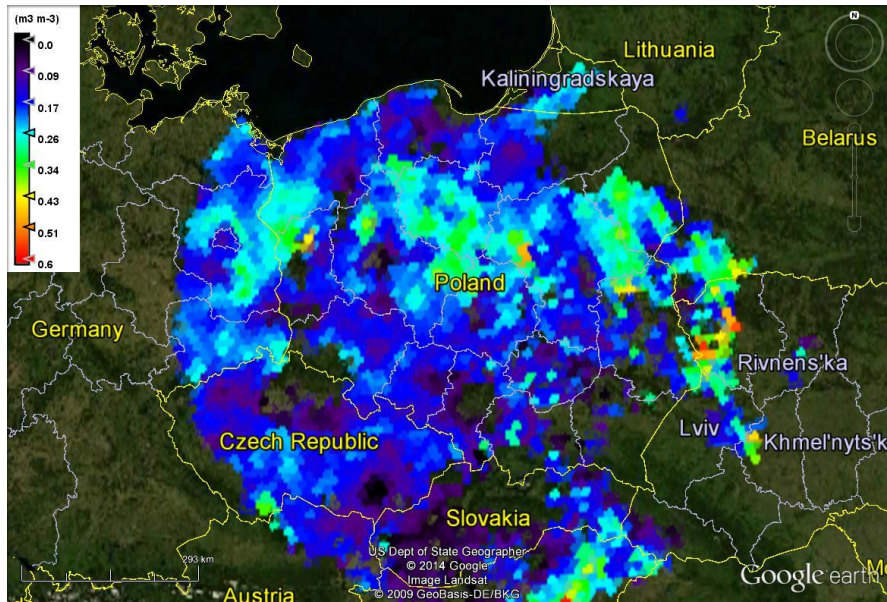


Fig. 43. Distribution of soil moisture during thawing (14/03/2011) on the Google Earth background (Google Earth 2012)

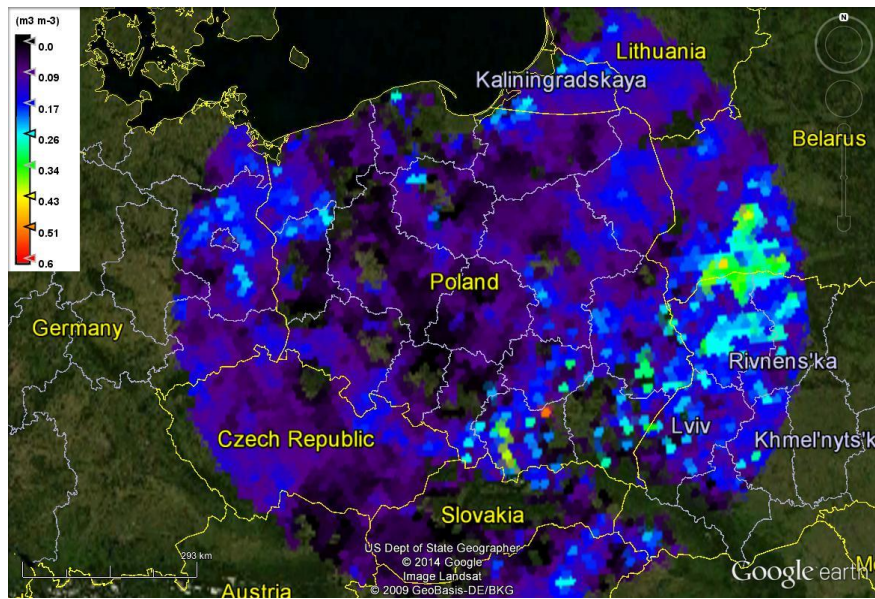


Fig. 44. Distribution of soil moisture during drying after thawing and rainfall (11/05/2011) on the Google Earth background (Google Earth 2012)

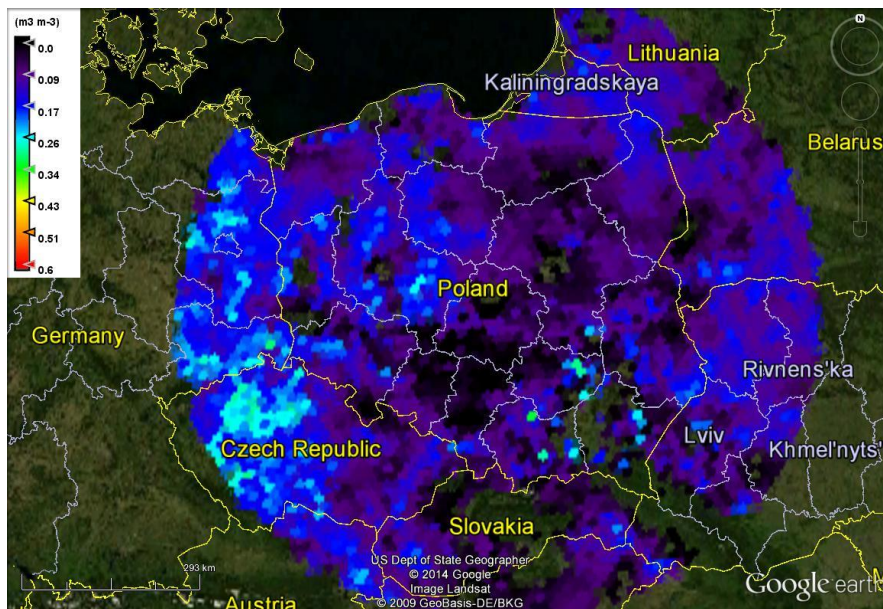


Fig. 45. Distribution of soil moisture during drought (19/06/2011) on the Google Earth background (Google Earth 2012)

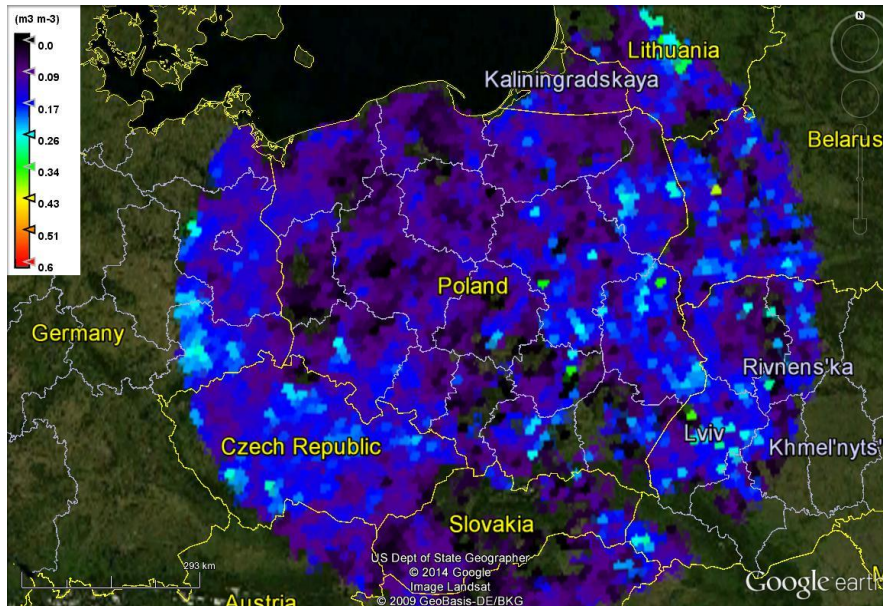


Fig. 46. Distribution of soil moisture after rain (14/07/2011) on the Google Earth background (Google Earth 2012)

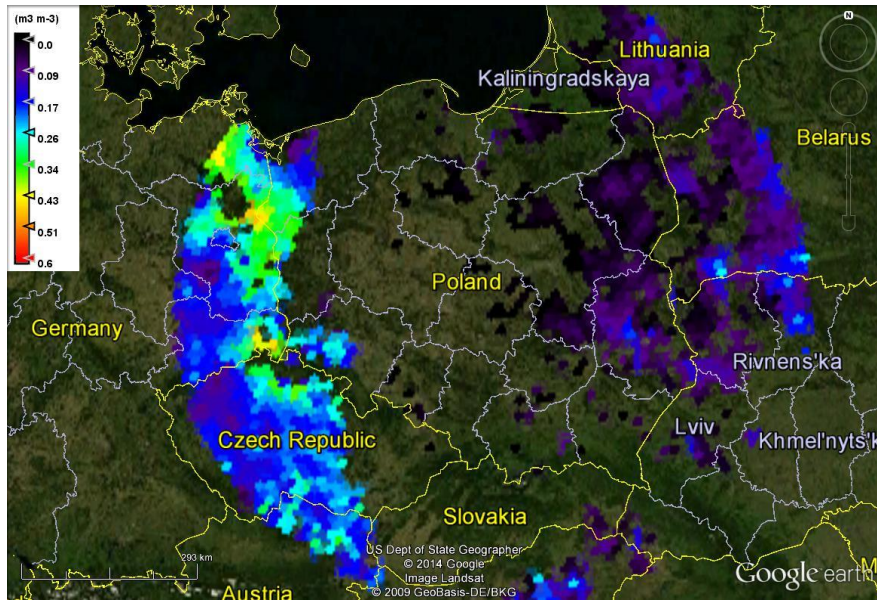


Fig. 47. Distribution of soil moisture disturbed by RFI (22/07/2011) on the Google Earth background (Google Earth 2012)

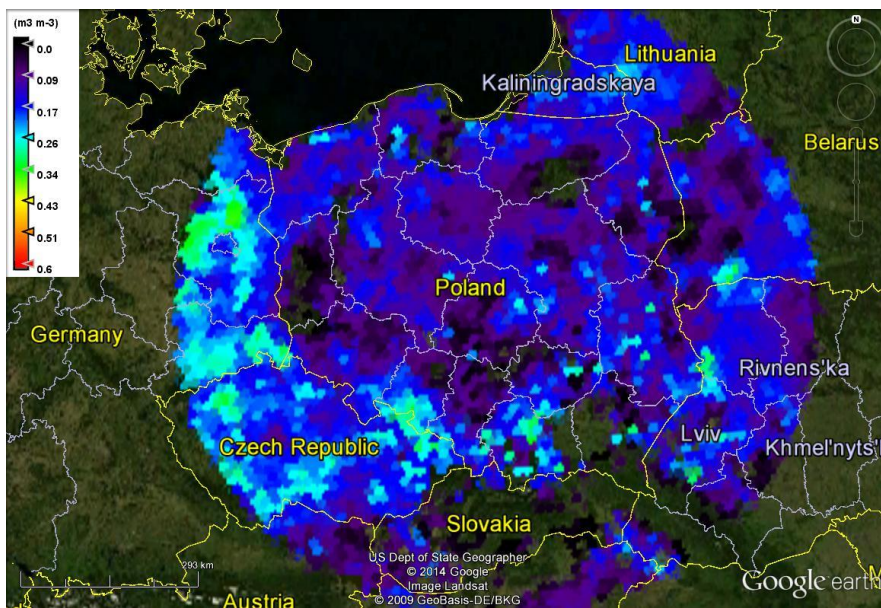


Fig. 48. Distribution of soil moisture during drying after rainfalls (15/08/2011) on the Google Earth background (Google Earth 2012)

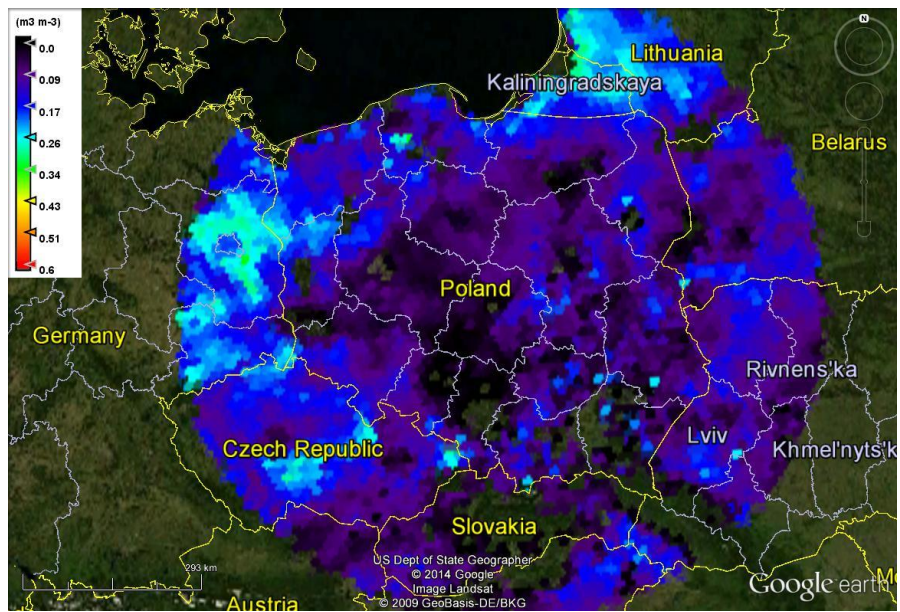


Fig. 49. Distribution of soil moisture, continued drying (16/09/2011), on the Google Earth background (Google Earth 2012)

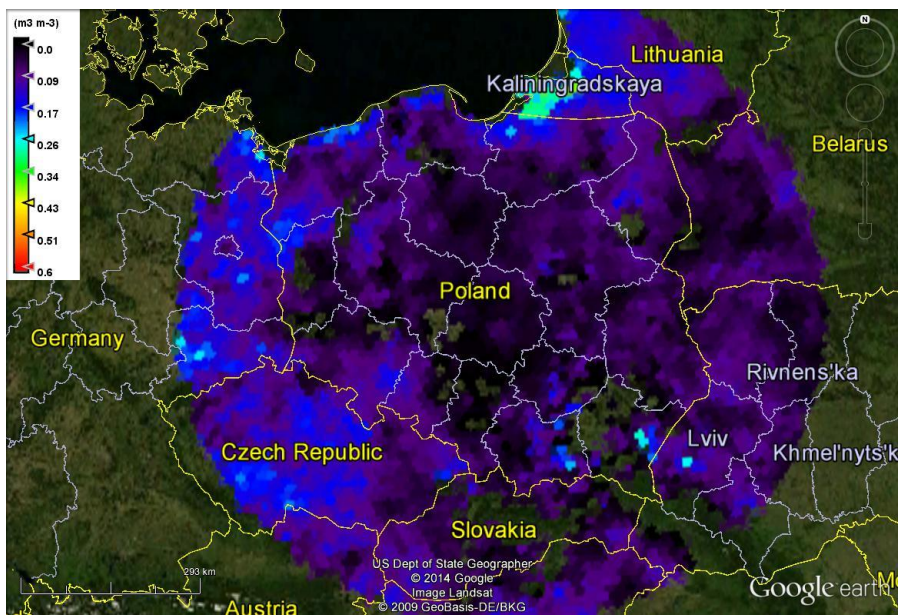


Fig. 50. Distribution of soil moisture during the driest day of the year (01/11/2011) on the Google Earth background (Google Earth 2012)

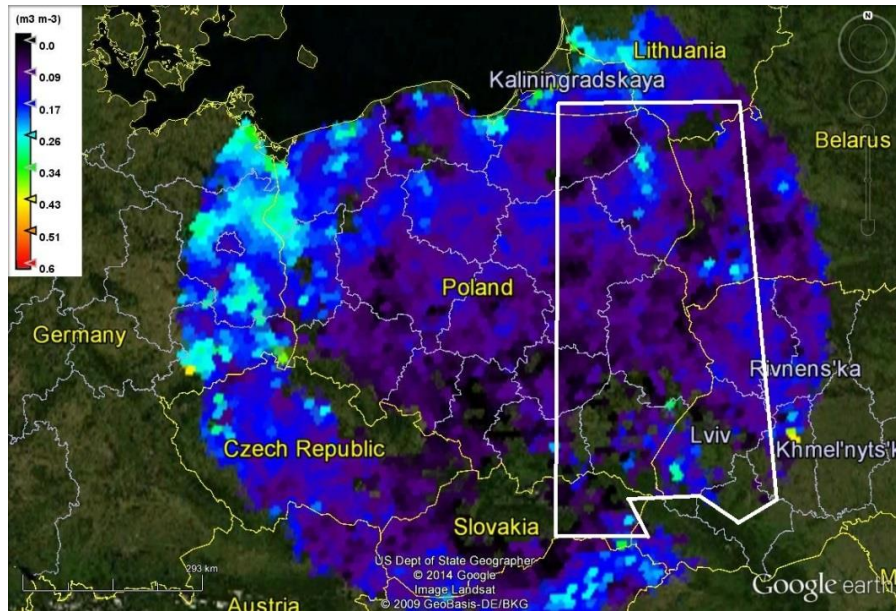


Fig. 51. Distribution of soil moisture after rainfalls in some parts of Poland (17/12/2011) on the Google Earth background (Google Earth 2012), together with marked area selected for statistical and geostatistical analysis (thick white solid line)

In order to find any correlations between the soil moisture distributions and soil granulometric composition, maps of sand and clay content (Fig. 52) for the Polish territory (Marczewski *et al.* 2010) were used. They have been estimated, using the kriging method, from approximately 1200 soil samples. Samples were collected inside the Polish territory, so the distributions outside the borders are probably only an inaccurate extension (Marczewski *et al.* 2010). No map of the silt fraction distribution is available, but it is approximately complementary to the content of sand and clay, to 100%. From the plotted maps of sand and clay content (Fig. 52) one can see that the soil with the highest content of sand fraction (over 70%) is placed in the latitudinal belt located in central and northern Poland. The area of Żuławy Wiślane is an exception because there the content of sand does not exceed 58%. Quite similar is the distribution of clay content, however in the locations where the largest fraction of the sand is observed, clay is the least. From the latitudinal outline, again the derogation is Żuławy Wiślane area. In areas with a high sand content, melt-down of snow usually proceeded more quickly, as evidenced by the distribution of soil moisture on 05/02/2011 (Fig. 41).

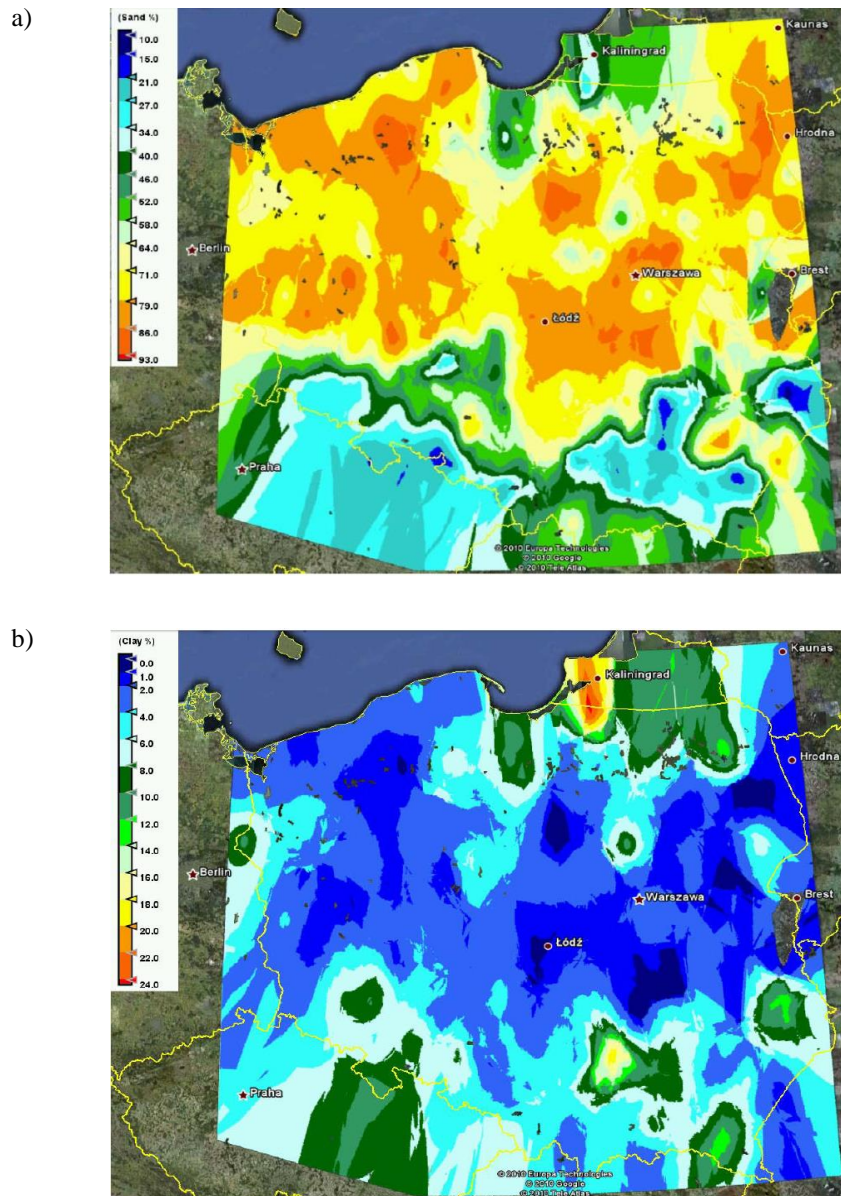


Fig. 52. Spatial distribution of sand (a) and clay (b) content in the 0-20 cm soil layer in the area of Poland (Marczewski *et al.* 2010)

It can be noticed that sandy soils are sometimes named “the warm soils”. These soils are less susceptible to freezing, as evidenced by the occurrence of places where SMOS algorithm showed soil moisture (and so the soils were unfrozen) on 08/03/2011 (Fig. 42). On the remaining selected dates, the correlation between soil moisture and particle size distribution is not clearly visible. Because SMOS measures only the surface layer of soil, it is possible that in such a large scale the surface soil moisture depends most strongly on temperature and rainfall.

In order to characterise the statistical and geostatistical properties of visualised distributions of surface soil moisture, in further analyses the area was limited (due to the large amount of data) to the eastern part of Poland and the adjacent areas outside its borders. The selected area is shown only in Figure 51, however, the analysis was performed also for all 11 images selected previously. The southern part of the study area has an irregular shape, because mountainous regions covered with thick vegetation were excluded from the analysis. So far SMOS conversion algorithm is not able to provide data on soil moisture for such areas (Mahmoodi 2011). In each tested SMOS image 1150 points were taken, each representing a DGG pixel in the ISEA4H9 system (Kotarba 2010). Points from which the data were sampled were therefore distributed in a regular grid and spaced about 15 km. Data from the selected area were subjected to statistical analysis, the results of which are shown in Table 8. Data from 05/02/2011 are among the first derived from SMOS that year. Earlier images were empty, because, as already mentioned, the algorithm does not provide SMOS soil moisture in frozen or snow covered areas. This can be seen also in the low number of data from 05/02/2011, where from 1150 collected, only for 91 points soil moisture was obtained. Maximum soil moisture content that day was $0.32 \text{ m}^3 \text{ m}^{-3}$, which may indicate places with water accumulated from snowmelt. After that time there was a frost, which determined missing data from 08/03/2011 and the sharp decline in soil moisture. A few days later a meltdown began, that data from 14/03/2011 show as an increase in average soil moisture. The maximum soil moisture observed that day was $0.57 \text{ m}^3 \text{ m}^{-3}$. Later (11/05/2011), the drying after the winter and spring rainfall can be observed. 19/06/2011 was one of the driest days during the vegetation period, when the average moisture content of the surface soil layer for the study area was $0.08 \text{ m}^3 \text{ m}^{-3}$. Later there were rains, which is visible in data from 14/07/2011 as an increase in average soil moisture. The image dated 22/07/2011 stands out with plenty of RFI that falsified soil moisture readings and significantly increased the amount of “empty” DGG pixels. This was followed by rain, followed by drying of the soil, which is illustrated by data from 15/08/2011 and 16/09/2011. On 11/10/2011, some IA PAS agrometeorological stations rec-

orded precipitation and the next 20 days were dry and quite warm. This led to a state that can be described as drought, because the average soil moisture on 01/11/2011 in the selected area was only $0.06 \text{ m}^3 \text{ m}^{-3}$, as evidenced by SMOS data. After significant rainfall, but not covering entire Poland, the average surface soil moisture calculated for the study area from SMOS data on 17/12/2011 increased to $0.09 \text{ m}^3 \text{ m}^{-3}$. All examined distributions of soil moisture generated by the SMOS satellite had a positive skewness, and so were right-skewed. This is due to the fact that the satellite observes only the surface layer of the soil, where the probability of occurrence of a low moisture content or freezing is higher than the probability of occurrence of a large amount of water. Almost all tested distributions were leptokurtic (they had positive kurtosis). Before the geostatistical analysis, to bring the distributions to as close to the normal distribution as possible, they were treated by the square root transform. Then, empirical semivariograms were tested. Analysis of spatial distribution of SMOS soil moisture, carried out for each data set, in most cases did not show significant trends. It was therefore assumed that each of the examined distributions of soil moisture in the adopted scale satisfies ergodicity and quasi-stationarity required for geostatistical analysis (Gotway and Hergert 1997). The exception was the day of 05/02/2011, when a trend was observed, most likely due to the occurrence of zones of frozen soil. The second from the selected days, on which there was a trend in soil moisture distribution, was on 22/07/2011. That day, the trend was quite small and probably caused by zoned RFI. In a further step, an analysis of the surface semivariance was done in order to minimise anisotropy in soil moisture distribution. Next, the values of nuggets, sills and ranges of spatial autocorrelation (apparent ranges) were calculated (Tab. 9). Then, to the calculated values of soil moisture semivariograms, theoretical models were adjusted and their fit was identified by calculating the coefficients of determination (r^2) (Tab. 9). Exemplary histograms, surface semivariogram and empirical semivariogram with fitted theoretical model are shown in Figure 53. Spatial dependences occurring in the surface soil moisture distributions for the selected area were in the range of 1° - 3° . The exception was the driest of the studied days, 01/11/2011, when the spatial correlations of soil moisture were not disturbed for a long time by any rainfall. Spatial correlation length on that day was 4.32° , which is about 470 km. This result is comparable to other studies, for example in Russia (Vinnikov *et al.* 1996). Adjustment of theoretical models to the empirical semivariograms was good or very good, worse only for data collected in March, on days of ground frost and thaw, when the highest maximum soil moisture was observed.

Table 8. Statistical parameters of SMOS soil moisture for the chosen area on selected days in 2011

Date	Mean ($\text{m}^3 \text{m}^{-3}$)	Standard deviation	Minimum ($\text{m}^3 \text{m}^{-3}$)	Maximum ($\text{m}^3 \text{m}^{-3}$)	Skewness	Kurtosis	Number of pixels	Comments
05/02/2011	0.158	0.076	0.03	0.32	0.25	-0.83	91	partial thaw
08/03/2011	0.026	0.023	0.00	0.13	1.89	4.72	179	ground frost
14/03/2011	0.208	0.091	0.01	0.57	0.66	0.96	516	thaw
11/05/2011	0.121	0.065	0.00	0.53	1.32	3.19	999	drying after thaw and precipitation
19/06/2011	0.084	0.049	0.00	0.30	0.65	0.44	1021	one of the drier days during the vegetation period
14/07/2011	0.119	0.058	0.00	0.40	0.68	0.96	1010	after rainfall
22/07/2011	0.048	0.039	0.00	0.26	1.38	2.82	468	a lot of RFI
15/08/2011	0.117	0.061	0.00	0.40	0.55	0.58	961	drying after rain
16/09/2011	0.092	0.049	0.00	0.25	0.51	-0.08	1042	drying, continued
01/11/2011	0.059	0.035	0.00	0.28	1.49	4.73	1025	drought, lack of rainfall for 20 days
17/12/2011	0.090	0.048	0.00	0.31	0.79	1.30	939	after significant rainfall in some parts of Poland

Table 9. Geostatistical parameters and semivariogram models of SMOS soil moisture distribution for the chosen area on selected days of the year

Date	Semivariogram model	Nugget	Sill	Apparent range (°)*	Model fit (r ²)
05/02/2011	Gaussian	0.0035	0.0236	2.9687	0.883
08/03/2011	exponential	0.0014	0.0060	0.9300	0.315
14/03/2011	exponential	0.0017	0.0113	2.6400	0.538
11/05/2011	exponential	0.0014	0.0089	2.0400	0.721
19/06/2011	exponential	0.0010	0.0088	1.0800	0.945
14/07/2011	exponential	0.0041	0.0082	2.2200	0.883
22/07/2011	exponential	0.0022	0.0097	3.1950	0.908
15/08/2011	exponential	0.0006	0.0044	1.2300	0.965
16/09/2011	exponential	0.0027	0.0082	1.9500	0.944
01/11/2011	exponential	0.0028	0.0060	4.3200	0.846
17/12/2011	exponential	0.0010	0.0030	2.0610	0.925

*At latitudes of Poland, 1° corresponds to a linear distance of approximately 110 km.

For the images where the data loss was more than 15%, using the geostatistical parameters calculated previously, by a method of kriging, values of soil moisture on selected area were estimated to obtain continuum. Exemplary estimates for these two dates are shown in Figures 54a and 55a. The conducted validation (Fig. 54b and Fig. 55b) showed that even with a significant loss of data, the kriging method estimates well the spatial distribution of surface soil moisture (coefficients of determination equal to 0.52 and 0.66 for 05/02/2011 and 22/07/2011, respectively).

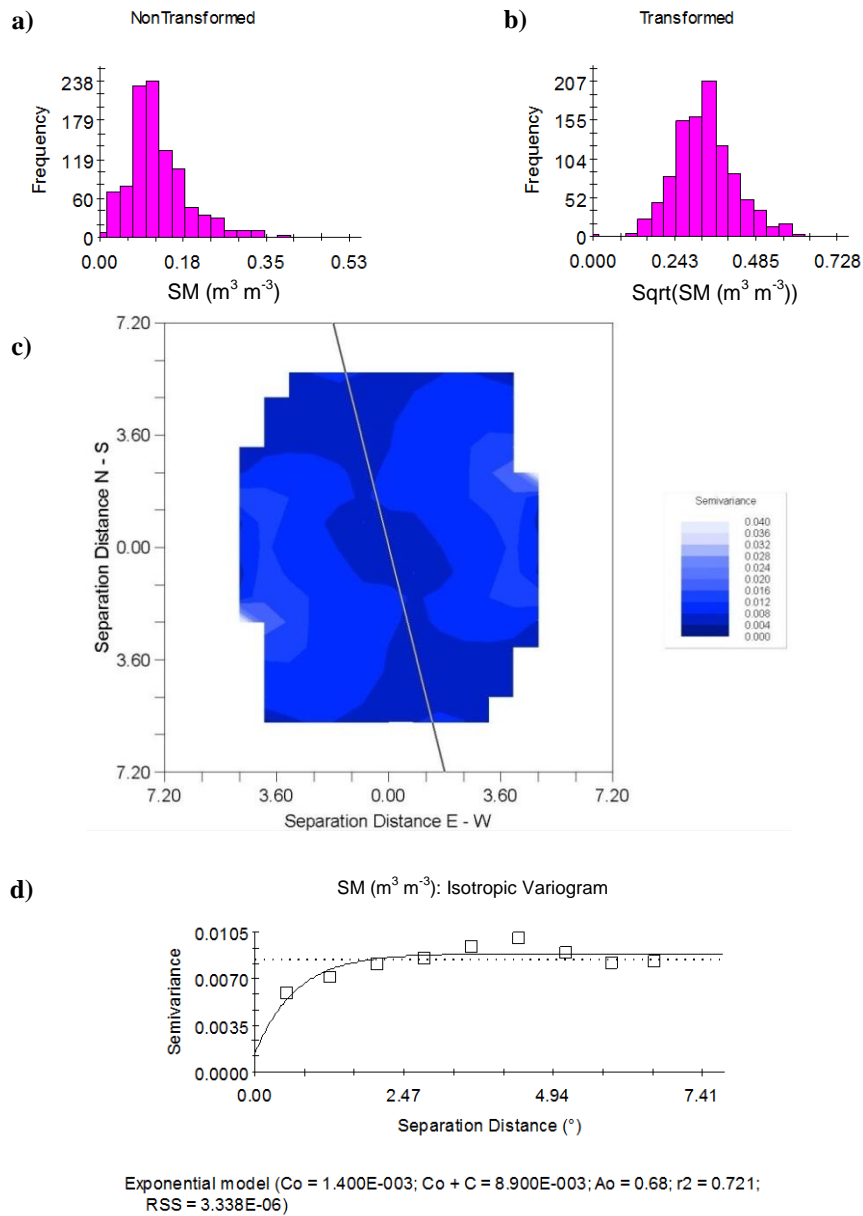


Fig. 53. Geostatistical characterisation of soil moisture (SM) measured by the SMOS satellite on 11/05/2011: a) histogram of original data, b) histogram of transformed data, c) surface semivariogram with line of smallest anisotropy, d) empirical semivariogram with fitted model and the parameters (C_0 – value of the nugget, $C_0 + C$ – sill, A_0 – range, r^2 – coefficient of determination, RSS – residual sum of squares)

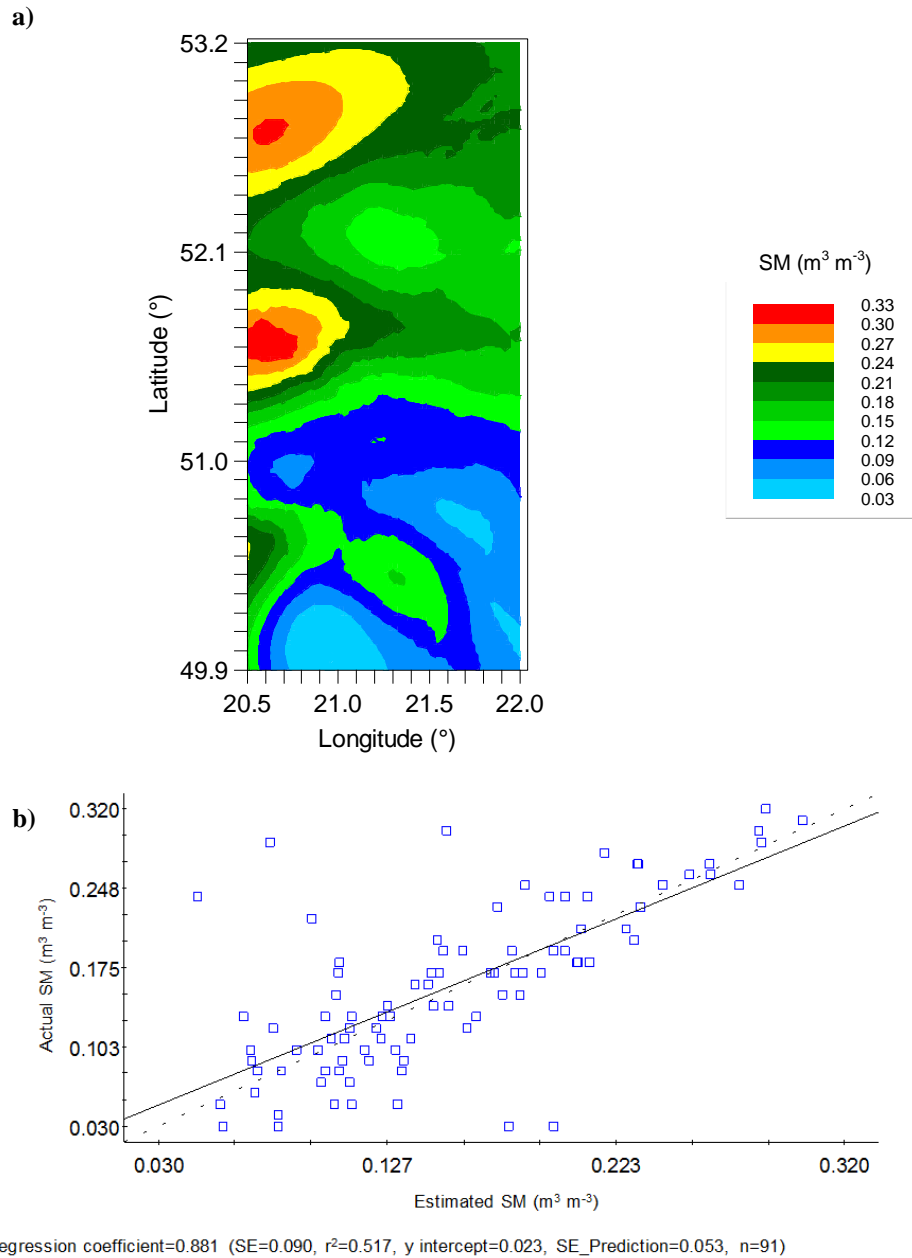


Fig. 54. Spatial distribution of soil moisture (SM) on 05/02/2011 estimated from 91 SMOS data via kriging method (a) and the validation of interpolation used (b)

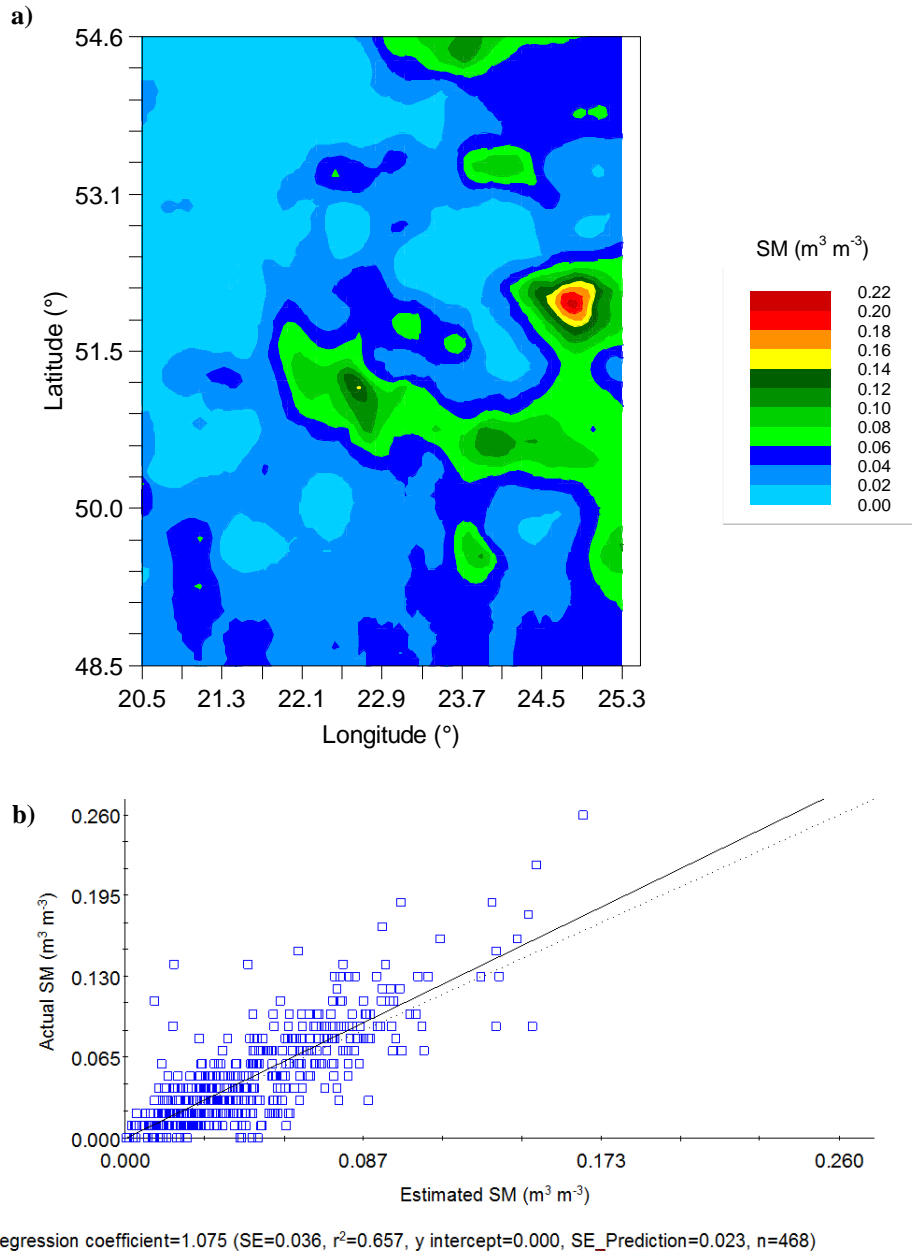


Fig. 55. Spatial distribution of soil moisture (SM) on 22/07/2011 estimated from 468 SMOS data via kriging method (a) and the validation of interpolation used (b)

3.8. Soil moisture assessment using ground-based and SMOS measurements

On 18/10/2010, ground-based measurements of the surface soil moisture were carried out using Easy Test TDR probe. 55 measurements were made, covering a part of West Polesie (Fig. 56). In the majority, measurement points were located in the immediate vicinity of the measurements from 2007 (see section 3.6).

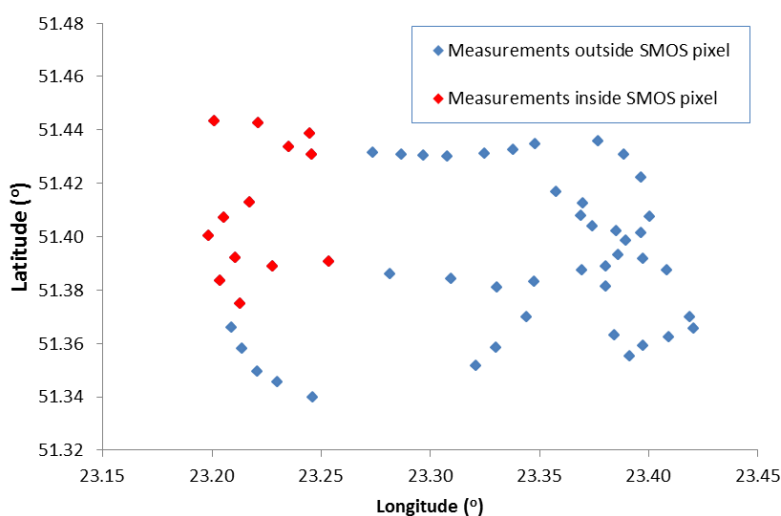


Fig. 56. Spatial distribution of ground-based measurement points in West Polesie on 18/10/2010

All the spatial coordinates were determined using the Global Positioning System (GPS) according to WGS-84 datum. The collected data were subjected to statistical and geostatistical analysis. Average surface soil moisture for the study area was $0.174 \text{ m}^3 \text{ m}^{-3}$, minimal $0.07 \text{ m}^3 \text{ m}^{-3}$ and maximal $0.72 \text{ m}^3 \text{ m}^{-3}$ (flooded area). The statistical distribution of the data was right-skewed (skewness equal to 2.57) and strongly leptokurtic (kurtosis equal to 9.31). After a logarithmic transformation, made in order to bring it closer to normal distribution, skewness and kurtosis decreased to 0.55 and 0.14, respectively. Then an analysis of surface semivariance was done and the smallest anisotropy direction was selected. The spatial distribution of soil moisture was tested for the detection of trends. For the study area it could be assumed that the measurement data satisfy the condition of ergodicity and quasi-stationarity required by the geostatistical analysis (Gotway and Hergert 1997). Then, to the empirical semivariogram, theoretical model was fitted and values of nugget, sill and range of spatial autocorrelation were specified. The semivariance of surface soil moisture distribution was described by a linear model with sill equal to 0.282 and a very strong nugget effect ($C_0 = 0.256$). This indicated no spatial rela-

tionships or their very complicated nature, thus a single model insufficiently describes the examined spatial autocorrelations. It was therefore assumed that for the description of the study area statistical descriptors such as the mean and standard deviation are sufficient. Using the obtained geostatistical information, spatial distribution of soil moisture was estimated using the inverse distance weighting method (IDW) (Fig. 57), because in the absence of spatial relationships kriging equations were unstable. The resulting distribution shows that the wettest areas were in the north-eastern and south-western parts of the study area. In the central part, the soil moisture was close to the average, with one small “island” of high soil moisture.

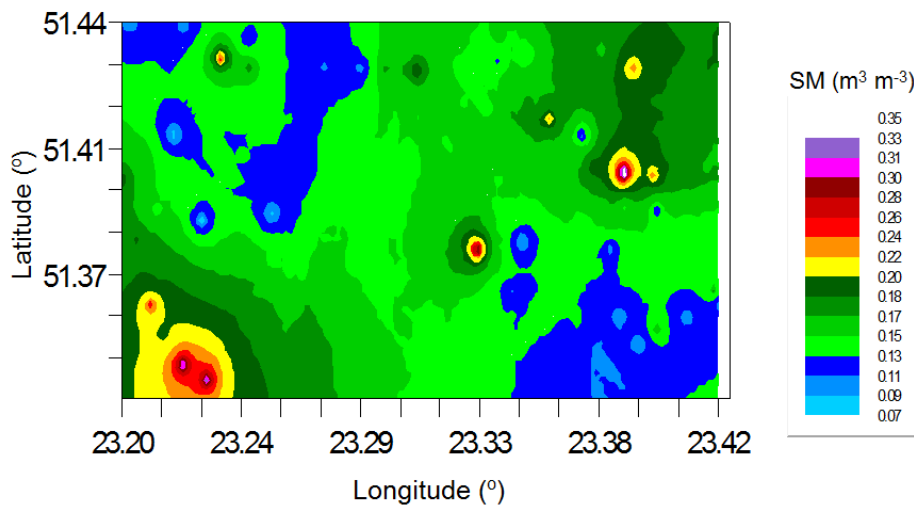


Fig. 57. Spatial distribution of soil moisture (SM) estimated using IDW method on the basis of TDR measurements in the West Polesie area on 18/10/2010

Later in the studies, a SMOS image was used, containing spatial distribution of surface soil moisture averaged for days 16-21/10/2010. Measurements were performed between 3 and 6 a.m. SMOS data were visualised on a DGG grid in ISEA4H9 geolocation system (Kotarba 2010) using Beam software. Unfortunately, due to interferences, these data did not cover the whole of the studied area, and only 13 of the 55 *in situ* measurements taken on 18/10/2010 were inside the SMOS DGG pixel area (Fig. 58). According to the literature (Mahmoodi 2011), in order to achieve adequate resolution, the data from SMOS pixel must be averaged over the neighbouring DGG areas. So to the arithmetic mean were included: the pixel within which ground-based measurements had been taken and three pixels around it, because the other three were empty (no data).

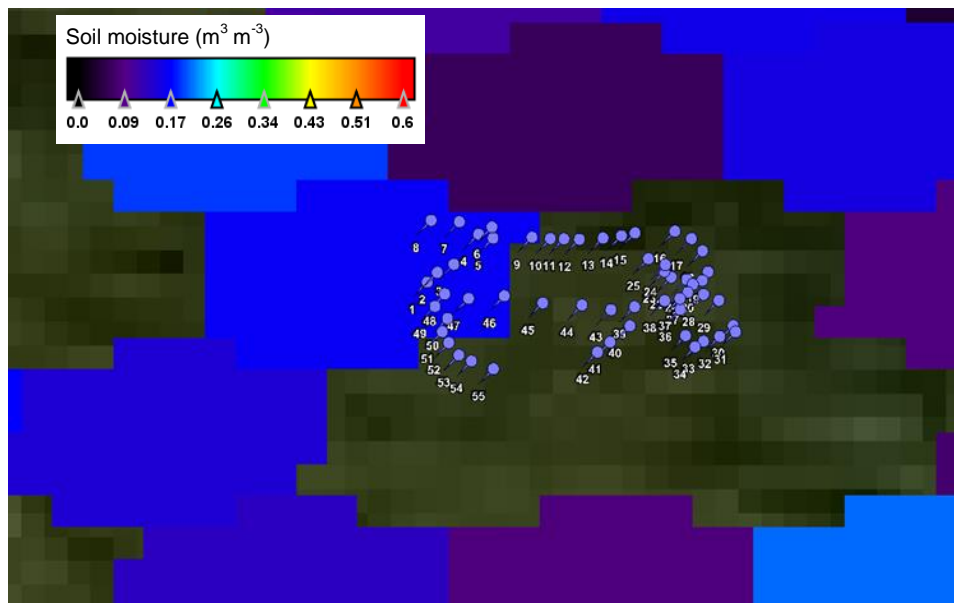


Fig. 58. Distribution of ground-based measurement points in West Polesie on 18/10/2010 on the background of distribution of soil moisture derived from SMOS satellite (dark green areas indicate no data)

So, 13 *in situ* measurements were compared with 4 satellite measurements. The arithmetic mean of the measurements from ground TDR soil moisture probe was $0.138 \text{ m}^3 \text{ m}^{-3}$, while the average surface soil moisture observed by SMOS was equal to $0.139 \text{ m}^3 \text{ m}^{-3}$, which is almost identical. The data from both, *in situ* and satellite measurements were insufficient, so it was impossible to determine whether their statistical distributions were similar to the normal distribution. Although this assumption was not verified, to compare the resulting averages Student's t-test for two samples with unequal variances, with a significance level of 0.05, was performed. The test showed that there was no reason to reject the zero hypothesis, stating that the average SMOS data were equal to the average of the ground-based measurements. Since the hypothesis was not rejected, and since the amount of input data was not sufficient and did not have a normal distribution, it was not possible to check what was the error of acceptance of hypothesis claiming equality of averages of ground and SMOS soil moistures. In such a case, according to the statistical rules, there is no basis to conclude that the investigated averages were different. It can therefore be assumed that in the analysed area, on the day of the measurements, averaged SMOS data reflected the surface soil moisture fairly well. However, by reason of the poor statistical representation caused by partial lack of data, for more general conclusions the repetition of field campaign is required.

4. CONCLUSIONS

The study investigated the spatial distributions and time series of surface soil moisture, soil bulk density and soil particle size distribution. The distributions of soil moisture measurements were obtained from ground-based measurements (TDR and gravimetric methods) and satellite images (SMOS and ASAR). The time series were obtained from the network of 9 automatic agrometeorological stations belonging to the Institute of Agrophysics PAS in Lublin and a series of SMOS satellite images. Data on physical parameters of soil and vegetation were obtained from own research (ground-based and satellite) and from the literature. It was confirmed that the TDR method well estimates the soil moisture. The effect of terrain altitude on surface soil moisture on a local scale was examined. For the years 2010-2011, time series of soil moisture measured on the ground and from satellites in Eastern Poland were analysed, taking into account the properties of the soil. Soil moisture distributions on commune scale were examined and, taking into account the vegetation of the area, satellite and ground measurements were confronted. Surface soil moisture distribution maps were obtained for the entire territory of Poland, and then their properties were tested for the area of eastern Poland, taking into account the spatial distribution of individual soil granulometric fractions. All analyses were performed using statistical and geostatistical methods.

The result of the work is completed to-date database of soil moisture time series, part of which is publicly available in International Soil Moisture Network (ISMN 2012) from Vienna University of Technology. The maps of the distributions of surface soil moisture and soil particle size distributions for the area of the two communities and the whole of Poland were obtained. The objectives of the study, posed at the beginning of the work, were therefore achieved.

The main conclusions of the work are:

1. The TDR method is fast and gives satisfactory results, so it can be used for routine measurements of soil moisture. It should be taken into account that the TDR method overestimates the values at lower soil moisture and underestimates the obtained soil moisture at higher moisture contents.
2. Locally, a negative correlation between soil moisture and altitude exists. The influence of topography on surface soil moisture is quite weak and can be affected by the variability of soil and vegetation.
3. SMOS satellite measurements reflect well the trends of soil moisture observed on the ground and can be used to detect wet areas and the phenomena of drought, snow and frost.
4. SMOS satellite indicates soil moisture content usually lower than the *in situ* measurements, although this depends on the soil properties and the environment around the ground reference.

5. Satellite measurements of soil moisture using ASAR instrument are affected by large error due to the presence of vegetation, which underestimates the resulting soil moisture. Compliance with ground-based measurements occurs only in areas of low or sparse vegetation.

6. Taking into account the soil moisture in Eastern Poland, year 2011 was drier and more variable than 2010.

7. In the event of interference of satellite measurements, resulting in some loss of the data, geostatistical methods allow for a good interpolation of missing measurements.

5. REFERENCES

- Al Bitar A., Leroux D., Kerr Y., Merlin O., Richaume P., Sahoo A., Wood E.F., 2011. Evaluation of SMOS soil moisture products over continental US using the SCAN/SNOTEL network. *IEEE T. Geosci. Remote Sens.*, vol. 50, No. 5, 1572-1586.
- Álvarez-Mozos J., González-Audicana M., Casalí J., 2007. Evaluation of empirical and semiempirical backscattering models for surface soil moisture estimation. *Canadian Journal of Remote Sensing*, vol. 33, No. 3, 176-188.
- ASAR Product Handbook, 2007. <http://envisat.esa.int/handbooks/asar/CNTR.htm>.
- Baup F., Mougin E., de Rosnay P., Timouk F., Chênere I., 2007. Surface soil moisture estimation over the AMMA Sahelian site in Mali using ENVISAT/ASAR data. *Rem. Sens. Environ.*, vol. 109, 473-481.
- BEAM 2007 software. <http://www.brockmann-consult.de/cms/web/beam>.
- Behari J., 2005. Microwave dielectric behavior of wet soils. Anamaya Publishers, Remote Sensing and Digital Image Processing, vol. 8, 1-164.
- Bircher S., Skou N., Jensen K. H., Walker J.P., Rasmussen L.A., 2011. Soil moisture and temperature network for SMOS validation in Western Denmark. *Hydrol. Earth Syst. Sci. Discuss.*, vol. 8, 9961-10006.
- Brus D., 1993. Incorporating models of spatial variation in sampling strategies for soil. PhD Thesis, Wageningen Agricultural University, The Netherlands, 1-211.
- Castelli F., Rodriguez-Iturbe I., 1995. Soil moisture-atmosphere interaction in a moist semigeostrophic model of baroclinic instability. *J. Atmos. Sci.*, vol. 52, 2152-2159.
- Chang J., Wetzel P.J., 1991. Effects of spatial variations of soil moisture and vegetation on the evolution of a prestorm environment: a numerical case study. *Mon. Wea. Rev.*, vol. 119, No. 6, 1368-1390.
- Charpentier M.A., Groffman P.M., 1992. Soil moisture variability within remote sensing pixels. *J. of Geophys. Res.*, vol. 97, 18987-18995.
- CMEM 2007 (Community Microwave Emission Model) software. <https://software.ecmwf.int/wiki/display/LDAS/CMEM>
- Connell L.D., Gilfedder M., Jayatilaka C., Bailey M., Vandervaere J.P., 1999. Optimal management of water movement in irrigation bays. *Environmental Modelling & Software*, vol. 14, 171-179.
- Dall'Amico J.T., Schlenz F., Loew A., Mauser W., 2011. First results of SMOS soil moisture validation in the Upper Danube Catchment. *IEEE T. Geosci. Remote Sens.*, vol. 50, No. 5, 1507-1516.
- Dastoor A., Krishnamurti T.N., 1991. The landfall and structure of a tropical cyclone: the sensitivity of model predictions to soil moisture parameterizations. *Bound-Layer Meteorol.*, vol. 55, No. 4, 345-380.

- David M., 1977. Geostatistical ore reserve estimation. Elsevier, Scientific Publishing Co., Amsterdam, The Netherlands.
- Delworth T., Manaba S., 1993. Climate variability and land surface processes. *Adv. Water Resour.*, vol. 16, 3-20.
- Dubois P.C., Van Zyl J.J., Engman T., 1995. Measuring soil moisture with imaging radars. *IEEE Trans. GRS*, vol. 33, No. 4, 915-926.
- Eastman J.L., Pielke R.A., McDonald D.J., 1998: Calibration of soil moisture for large-eddy simulations over the FIFE area. *J. Atmos. Sci.*, vol. 55, No. 7, 1131-1140.
- ECMWF, 2007. <http://www.ecmwf.int/en/research/projects/smos>
- ECOCLIMAP, 2010. A global database of land surface parameters at 1 km resolution in meteorological and climate models. http://www.cnrm.meteo.fr/gmme/PROJETS/ECOCLIMAP/-page_ecoclimap.htm
- Englund E., Sparks A., 1988. Geostatistical environmental assessment software. Environmental Monitoring Systems Laboratory Office of Research and Development, U.S. Environmental Protection Agency, Las Vegas, NV 89193-3478.
- ENVISAT-ASAR, 2007. <http://envisat.esa.int/handbooks/asar/>
- ENVISAT-MERIS, 2009. <http://envisat.esa.int/handbooks/meris/CNTR1.htm>
- Escorihuela M., Chanzy A., Wigneron J., Kerr Y., 2010. Effective soil moisture sampling depth of L-band radiometry: A case study. *Remote Sens. Environ.*, vol. 114, 995-1001.
- Famiglietti J.S., Rudnicki J.W., Rodell M., 1998. Variability in surface moisture content along a hillslope transect: Rattlesnake Hill, Texas. *J. of Hydrol.*, vol. 210, 259-281.
- Gamma Design Software GS+9, 2008. Geostatistics for the environmental sciences.
- Gitelson A., Buschmann C., Lichtenthaler H., 1999. The chlorophyll fluorescence ratio F735/F700 as an accurate measure of the chlorophyll content in plants. *Remote Sensing of Environment*, vol. 69. No. 3, 296-302.
- Golden Software Inc., 2011. Surfer v. 10. www.goldensoftware.com.
- Google Earth, 2012: <http://www.google.com/intl/pl/earth/index.html>.
- Google Maps, 2012: <http://maps.google.com/>.
- Gotway C., Hergert G., 1997. Incorporating spatial trends and anisotropy in geostatistical mapping of soil properties. *Soil Sci. Soc. Am. J.*, vol. 61, 298-309.
- Green T., Erskine R., 2004. Measurement, scaling, and topographic analyses of spatial crop yield and soil water content. *Hydrol. Process.*, vol. 18, 1447-1465.
- Griffith D., 1987. *Spatial Autocorrelation: A Primer*. Association of American Geographers, Washington, D.C., 1-86.
- Gruhler C., Pellarin T., de Rosnay P., Kerr Y., 2012. SMOS soil moisture product evaluation over West-Africa at local and regional scale. *Remote Sens. Environ.*, (in review).
- Haan C., 1977: *Statistical Methods in Hydrology*. Iowa State University Press, Ames, Iowa.
- Hajnsek I., 2001. Inversion of Surface Parameters using Polarimetric SAR. PhD Thesis, Friedrich-Schiller-Universität Jena.
- Houser P., 1996. Remote-sensing soil moisture using four-dimensional data assimilation. Ph.D. Thesis, Department of Hydrology and Water Resources, University of Arizona, Tucson, Arizona.
- Hu Z., Chen Y., Islam S., 1998. Multiscaling properties of soil moisture images And decomposition of large- and small-scale features using wavelet transforms. *Int. J. Remote Sensing*, vol. 19, No. 13, 2451-2467.
- Isaaks E., Srivastava R., 1989. *An introduction to applied geostatistics*. Oxford University Press, NY.
- ISMN, 2012. <http://www.ipf.tuwien.ac.at/insitu/index.php/in-situ-networks/82-swexpoland.html>

- Jackson T., Bindlish R., Cosh M., Zhao T., Starks P., Bosch D., Seyfried M., Moran S., Goodrich D., Kerr Y., Leroux, D., 2012. Validation of Soil Moisture and Ocean Salinity (SMOS) soil moisture over watershed networks in the US. *IEEE T. Geosci. Remote Se.*, vol. 50, No. 5, 1530-1543.
- Jackson T., Le Vine D., 1996. Mapping surface soil moisture using an aircraft based passive microwave instrument: Algorithm and example. *J. Hydrol.*, vol. 184, 85-99.
- Jackson T., Le Vine D., Hsu A., Oldak A., Starks P., Swift C., Isham J., Haken M., 1999. Soil moisture mapping at regional scales using microwave radiometry: the Southern Great Plains Hydrology Experiment. *IEEE Transactions on Geoscience and Remote Sensing*, vol. 37, 2136-51.
- Jaynes D., Kaspar T., Colvin T., James D., 2003. Cluster analysis of spatiotemporal corn yield patterns in an Iowa field. *Agron. J.*, vol. 95, 574-586.
- Kędziora A., 1995. Fundamentals of agricultural meteorology (in Polish). PWRiL Poznań.
- Kerr Y., Waldteufel P., Wigneron J., Martinuzzi J., Font J., Berzer. M., 2001. Soil Moisture Retrieval from Space: The Soil Moisture and Ocean Salinity (SMOS) Mission. *IEEE Transactions on Geoscience and Remote Sensing*, vol. 39, No. 8, 1729-1735.
- Koster R., Suarez M., Ducharme A., Stieglitz M., Kumar P., 2000. A catchment-based approach to modeling land surface processes in a general circulation model. 1. Model structure. *J. Geophys. Res.*, vol. 105, 24809-24822.
- Kotarba A., 2010. DGG ISEA4H9 for area of Poland (in Polish). <http://swex.cbk.waw.pl/c6/index.php/tematy/7-siatka-dgg-isea4h9-dla-obszaru-polski-wersja-0-0-23-pazdziernika-2010>.
- Koyama C., 2012. Quantitative estimation of surface soil moisture in agricultural landscapes using spaceborne synthetic aperture radar imaging at different frequencies and polarizations. PhD Thesis, Universität zu Köln.
- Ladson A., Moore I., 1992. Soil water prediction on Konza Prairie by microwave remote sensing and topographic attributes. *J. of Hydrol.*, vol. 138, 385-407.
- Leconte R., Brissette F., Galarneau M., Rousselle J., 2004. Mapping near-surface soil moisture with RADARSAT-1 synthetic aperture radar data. *Water Resources Research*, vol. 40, No. 1, 1-13.
- López-Martínez C., Ferro-Famil L., Pottier E., 2005. PolSARpro v4.0 Polarimetry Tutorial <http://earth.esa.int/polsarpro/tutorial.html>.
- Mahmoodi A., 2011. Algorithm Theoretical Basis Document (ATBD) for the SMOS Level 2 Soil Moisture Processor Development Continuation Project. Array Systems Computing Inc. Toronto, Canada.
- Malicki M., 1990. A reflectometric (TDR) meter of moisture content in soils and other capillary-porous materials. *Zesz. Probl. Post. Nauk Roln.*, vol. 388, 107-114.
- Marczewski W., Slominski J., Slominska E., Usowicz B., Usowicz J., Romanov S., Maryskevych O., Nastula J., Zawadzki J., 2010. Strategies for validating and directions for employing SMOS data, in the Cal-Val project SWEX (3275) for wetlands. *Hydrol. Earth Syst. Sci. Discuss.*, vol. 7, 7007-7057.
- Matheron G., 1971. The theory of regionalized variables and its applications. *Cahiers du Centre de Morphologie Mathématique*, Fontainebleau.
- McBratney A., Webster R., 1983. How many observations are needed for regional estimation of soil properties. *Soil Sci.*, vol. 135, No. 3, 177-183.
- McCumber M., Pielke R., 1981. Simulation of the effects of surface fluxes of heat and moisture in a mesoscale numerical model, 1. soil layer. *J. Geophys. Res.*, vol. 86, No. C10, 9929-9938.
- McGinn S., Shepherd A., 2003. Impact of climate change scenarios on the agroclimate of the Canadian prairies. *Canadian Journal of Soil Science*, vol. 83, 623-630.
- McNairn H., Brisco B., 2004. The application of C-band polarimetric SAR for agriculture: a review. *Canadian Journal of Remote Sensing*, vol. 30, No. 3, 525-542.
- McNairn H., Merzouki A., Pacheco A., 2010. Estimating Surface Soil Moisture Using RADARSAT-2. *Proceedings of ISPRS TC VIII Symposium 2010 - Networking the World with Remote Sensing*, 9-12 Aug., Kyoto, Japan.

- Mehrotra R., 1999. Sensitivity of runoff, soil moisture and reservoir design to climate change in central Indian river basins. *Climatic Change*, vol. 42, 725-757.
- Mynemi R., Hall F., Sellers P., Marshak A., 1995. The interpretation of spectral vegetation indexes. *IEEE Transactions on Geoscience and Remote Sensing*, vol. 33, No. 2, 481-486.
- Niemann K., Edgell M., 1993. Preliminary analysis of spatial and temporal distribution of soil moisture on a deforested slope. *Physical Geography*, vol. 14, No. 5, 449-464.
- Odhiambo J., Bomke A., 2007. Cover crop effects on spring soil water content and the implications for cover crop management in south coastal British Columbia. *Agricultural Water Management*, vol. 88, 92-98.
- Oliva R., Daganzo-Eusebio E., Kerr Y., Mecklenburg S., Nieto S., Richaume P., Gruhier C., 2011. SMOS Radio Frequency Interference Scenario: Status and Actions Taken to Improve the RFI Environment in the 1400–1427-MHz Passive Band, *IEEE T. Geosci. Remote Sens.*, vol. 50, No. 5, 1427-1439.
- Ookouchi Y., Segal M., Kessler R., Pielke R., 1984. Evaluation of soil moisture effects on the generation and modification of mesoscale circulations. *Mon. Wea. Rev.*, vol. 112, 2281-92.
- Pan F., 2002. Spatial and Temporal Structures of Soil Moisture Fields, PhD Thesis, Georgia Institute of Technology.
- Pannatier Y., 1994. Variowin 2.1. Program for Geostatistical Analysis. University Of Lousanne.
- Papritz A., 1993. Estimating temporal change of soil properties. Phd thesis, Swiss Federal Institute of Technology, Zurich.
- Pietroniro A., Soulis E., Kouwen N., 1994. Deriving antecedent moisture conditions from airborne SAR for input into a flood forecasting model. *IGARSS '94. International Geoscience and Remote Sensing Symposium. Surface and Atmospheric Remote Sensing: Technologies, Data Analysis and Interpretation* vol. 3, 1435-1438.
- Robinson D., Campbell C., Hopmans J., Hornbuckle B., Jones S., Knight R., Ogden F., Selker J., Wendroth O., 2008. Soil moisture measurement for ecological and hydrological watershed-scale observatories: A Review. *Vadose Zone J.*, vol. 7, 358-389.
- Rudiger C., Walker J., Kerr Y., Mialon A., Merlin O., Kim E., 2011. Validation of the Level 1c and Level 2 SMOS Products with airborne and ground-based observations. *International Congress on Modelling and Simulation (MODSIM)*, Perth, Australia.
- Schmugge T., Jackson T., Kustas W., Roberts R., Parry R., Goodrich D., Amer S., Wzltz M., 1994. Push broom microwave radiometer observations of surface soil moisture in Monsoon'90. *Water Resour. Res.*, vol. 30, 1321-1327.
- Smith J., Karr A., 1986: Flood frequency analysis using the Cox regression model. *Water Resour. Res.*, vol. 22, 890-896.
- SMOS Blog, 2012. http://www.cesbio.ups-tlse.fr/SMOS_blog/
- StatSoft, Inc. 2008. STATISTICA (data analysis software system), version 8.0. www.statsoft.com.
- Stull R., 1988. An introduction to boundary layer meteorology. *Boundary layer Meteorol.*, Kluwer Academic Publishers, 1-666.
- Topp G., Davis J., Anna A., 1980. Electromagnetic determination of soil water content: measurements in coaxial transmission lines. *Water Resources Research*, vol. 16, 574-582.
- Trangmar B., Yost R., Uehara G., 1985. Applications of geostatistics to spatial studies of soil properties. *Advances in Agronomy*, vol. 38, 45-94.
- Ulaby F., Batlivala P., Dobson M., 1978. Microwave backscatter dependence on surface roughness, soil moisture, and soil texture: Part I-Bare Soil. *IEEE Transactions on Geoscience Electronics*, vol. GE-16, No. 4, 286-295.
- Ulaby F., Bradley G., Dobson M., 1979. Microwave backscatter dependence on surface roughness, soil moisture, and soil texture: Part II-Vegetation-Covered Soil. *IEEE Transactions On Geoscience Electronics*, vol. GE-17, No. 2, 33-40.

- Usovich B., Baranowski P., Kossowski J., 1995. Spatial distribution of some physical quantities characterizing soil structure state in cultivated fields. *Polish J. Soil Sci.* vol. 28, No. 1, 19-27.
- Usovich B., Kossowski J., 1996. Distribution of soil water content in cultivated fields based on measurement by gravimetric and reflectometric methods. *Zesz. Prob. Post. Nauk Roln.*, vol. 436, 157-165.
- Usovich B., Marczewski W., Lipiec J., Usovich J.B., Sokołowska Z., Dąbkowska-Naskręt H., Hajnos M., Łukowski M., 2009. Water in soil – ground and satellite measurements in the study of climate change (in Polish). Monograph. Fundacja Rozwoju Nauk Agrofizycznych Komitet Agrofizyki PAN, 1-171.
- Vauclin M., Vieira S., Vachaud G., Nielsen D., 1983. The use of cokriging with limited field soil observations. *Soil Sci. Soc. Am. J.* vol. 47, 175-184.
- Vermeulen S., Aggarwal P., Ainslie A., Angelone C., Campbell B., Challinor A., Hansen J., Ingram J., Jarvis A., Kristjanson P., Lau C., Thornton P., Wollenberg E. 2010. Agriculture, Food Security and Climate Change: Outlook for Knowledge, Tools and Action. CCAFS Report 3. Copenhagen, Denmark: CGIAR-ESSP Program on Climate Change, Agriculture and Food Security.
- Vieira S., Hatfield J., Nielsen D., Biggar J., 1983. Geostatistical theory and application to variability of some agronomical properties. *Hilgardia*, 1-75.
- Vinnikov K., Robock A., Speranskaya N., Schlosser C., 1996. Scales of temporal and spatial variability of midlatitude soil moisture. *J. Geophys. Res.* vol. 101, No. D3, 7163-7174.
- Webster R., 1985. Quantitative spatial analysis of soil in the field. *Advances in Soil Sci.*, vol. 3, 1-70.
- Webster R., Oliver M., 1990. *Statistical methods in soil and land resource survey*. Oxford University Press, NY, 1-316.
- WIOSL, 2010. State of the Environment, Report 2010 (in Polish). Wojewódzki Inspektorat Ochrony Środowiska w Lublinie. http://www.wios.lublin.pl/tiki-download_file.php?fileId=1806.
- Zawadzki J., 2011. Geostatistical methods for natural sciences and technical faculties (in Polish). Oficyna Wyd. Politechniki Warszawskiej, 1-132.
- Zhang D., Anthes R., 1982. A high-resolution model of the planetary boundary layer-sensitivity tests and comparisons with SESAME-79 data. *J. Appl. Meteorol.* 21, 1594-1609.
- Zheng X., Eltahir E., 1998. A soil moisture-rainfall feedback mechanism, 2. Numerical Experiments. *Water Resour. Res.*, vol. 34, 777-786.
- Zumi, 2012. <http://www.zumi.pl>.

Norms and standards used during the measurements on soil samples

For soil samples examination the following norms and standards were used: ISO 12 277, PN-R-04032: 1998, PN-R-04033: 1998, PN-ISO 11461: 2003, PN-EN 13041: 2002.

6. SUMMARY

The water contained in the soil is one of the most important components of the environment. Soil moisture governs the partitioning of energy and mass fluxes on the Earth. Recognition and understanding of temporal changes and spatial distributions of soil moisture are essential to solve many fundamental scientific and utilitarian issues. Knowledge about soil moisture is very important in the management of water resources, assessment of droughts, and in the prediction of floods and surface runoffs. Without water disposed in soil any growth or devel-

opment of plants on the lands would be impossible. For those reasons, information on soil moisture is so important for applications in agriculture, such as determining the time of sowing, irrigation management and crop forecasting.

Although soil moisture is so significant and desired a parameter, its measurement raises many difficulties. Due to the fact that the soil moisture can be spatially variable, its ground-based measurements are often very time-consuming and costly, but relatively precise. On the contrary, measurements of soil moisture from satellites are cost-effective, fast and consistent, but uncertain in absolute measures, so they need to be validated using ground-based measurements. The comparison issue, connected to that, often causes the scaling problem which can be solved using statistical and geostatistical methods. These methods allow one to describe the relationship between the easily- and non-easily-measurable variables, are useful to determine the spatial dependences and are used to acquire maps of the spatial distribution of examined variables.

The study investigated the spatial distributions and time series of surface soil moisture, soil bulk density and soil particle size distribution. The distributions of soil moisture were obtained from ground-based measurements and satellite images. The time series were acquired by a network of automatic agrometeorological stations, belonging to the Institute of Agrophysics PAS in Lublin, and a series of SMOS satellite images. The effect of altitude on surface soil moisture on a local scale was examined. For the years 2010-2011, time series of soil moisture measured on the ground and from satellite in Eastern Poland were analysed, taking into account the properties of the soil. Surface soil moisture distribution maps were obtained for Poland and their properties were tested, taking into account the soils granulometric fractions. All analyses were performed using statistical and geostatistical methods.

It was concluded that locally a negative correlation between soil moisture and altitude exists. SMOS satellite measurements reflect well the trends of soil moisture observed on the ground and can be used to detect wet areas, the phenomena of drought, snow and frost. SMOS satellite indicates soil moisture content usually lower than the *in situ* measurements, although this depends on the soil properties and the environment around the ground reference. Measurements of soil moisture using ASAR satellite instrument are affected by large error due to the presence of vegetation, which underestimates the resulting soil moisture. Taking into account the soil moisture in Eastern Poland, year 2011 was drier and more variable than 2010. In the event of interference of satellite measurements, resulting in some loss of the data, geostatistical methods allow for a good interpolation of missing measurements.

Keywords: surface soil moisture, SMOS, geostatistical methods, ASAR

7. STRESZCZENIE

WILGOTNOŚĆ POWIERZCHNIOWEJ WARSTWY GLEBY. POMIARY SATELITARNE I NAZIEMNE

Woda zawarta w glebie jest jednym z najważniejszych składników środowiska. Wilgotność gleby reguluje podział strumieni masy i energii na Ziemi. Poznanie i zrozumienie zmian czasowych i rozkładów przestrzennych wilgotności gleby jest niezbędne do rozwiązania wielu podstawowych zagadnień naukowych i praktycznych. Wiedza o wilgotności gleby jest bardzo ważna w zarządzaniu zasobami wodnymi, ocenie susz, powodzi i przewidywaniu spływów powierzchniowych. Bez wody zgromadzonej w glebie niemożliwy byłby jakikolwiek wzrost czy rozwój roślin na powierzchni lądów. Z wymienionych powodów, informacja o wilgotności gleby jest tak ważna w zastosowaniach w rolnictwie, takich jak: określanie czasu siewu, zarządzanie nawadnianiem upraw i prognozowanie plonów.

Mimo że wilgotność gleby jest tak istotnym i pożądanym parametrem, jej pomiar rodzi wiele trudności. Ze względu na fakt, że wilgotność gleby może być bardzo zmienna przestrzennie, jej pomiary naziemne są często bardzo czasochłonne i kosztowne, ale za to stosunkowo precyzyjne. Satelitarne pomiary wilgotności gleby są natomiast ekonomiczne, szybkie i spójne, ale niepewne co do miar absolutnych, muszą więc być weryfikowane na podstawie pomiarów naziemnych. Związane z tym zagadnienie porównania napotyka problem skalowania, który można rozwiązać za pomocą metod statystycznych i geostatystycznych. Metody te pozwalają ponadto na opisanie relacji między zmiennymi łatwo- i trudno mierzalnymi, są przydatne do określenia zależności przestrzennych, jak również wykorzystywane do uzyskiwania map przestrzennego rozkładu badanych zmiennych.

W pracy badano rozkłady przestrzenne i szeregi czasowe powierzchniowej wilgotności gleby, gęstości gleby i jej rozkładu granulometrycznego. Rozkłady wilgotności gleby uzyskiwano z pomiarów naziemnych i zdjęć satelitarnych. Szeregi czasowe zostały otrzymane z sieci automatycznych stacji agrometeorologicznych, należących do Instytutu Agrofizyki PAN w Lublinie oraz serii zdjęć satelitarnych SMOS. Badano wpływ wysokości terenu na powierzchniową wilgotność gleby w skali lokalnej. Dla lat 2010-2011, biorąc pod uwagę właściwości gleb, analizowane były przebiegi czasowe wilgotności gleby we wschodniej Polsce, mierzonej na ziemi i z satelity. Uzyskano mapy rozkładu powierzchniowej wilgotności gleby dla Polski i badano ich właściwości uwzględniając rozkład granulometryczny gleb. Wszystkie analizy przeprowadzono z wykorzystaniem metod statystycznych i geostatystycznych.

Stwierdzono, że lokalnie istnieje ujemna korelacja pomiędzy wilgotnością gleby i wysokością terenu. Pomiary satelitarne SMOS dobrze odzwierciedlają

obserwowane na ziemi trendy wilgotności gleby i mogą służyć do wykrywania obszarów wilgotnych, zjawisk suszy oraz śniegu i przymrozków. Satelita SMOS przeważnie wskazuje wilgotności niższe niż pomiary *in situ*, choć zależy to od czynnika glebowego i otoczenia naziemnego punktu odniesienia. Pomiary wilgotności gleby przyrządem satelitarnym ASAR są obarczone dużym błędem spowodowanym obecnością szaty roślinnej, która zaniża otrzymaną wilgotność gleby. Biorąc pod uwagę wilgotność gleby na terenie wschodniej Polski, rok 2011 był suchszy oraz bardziej zmienny niż 2010. W przypadku zakłóceń pomiarów satelitarnych, powodujących utratę części danych, metody geostatystyczne pozwalają na dobrą interpolację brakujących pomiarów.

Słowa kluczowe: wilgotność powierzchniowej warstwy gleby, SMOS, metody geostatystyczne, ASAR

The view expressed herein can in no way be taken to reflect the official opinion of the European Space Agency.

Address of Authors:

Mateusz Łukowski
Bogusław Usowicz
Institute of Agrophysics, Polish Academy of Sciences
ul. Doświadczalna 4, 20-290 Lublin
e-mail: m.lukowski@ipan.lublin.pl

Adres Autorów:

Mateusz Łukowski
Bogusław Usowicz
Instytut Agrofizyki im. Bohdana Dobrzańskiego PAN
ul. Doświadczalna 4, 20-290 Lublin
e-mail: m.lukowski@ipan.lublin.pl